A Literature Study of the Arching Effect

by

Hsien-Jen Tien

B.Sc. Civil Engineering (1990)
National Taiwan University

Submitted to the Department of Civil and Environmental Engineering in Partial Fulfillment of the Requirements for the Degree of

Master of Science

at the

MASSACHUSETTS INSTITUTE OF TECHNOLOGY

February 1996

Signature of Author .....
Dept. of Civil and Environmental Engineering
February 29, 1996

Certified by .....
Prof. Herbert H. Einstein
Thesis Supervisor

Accepted by .....
Prof. Joseph M. Sussman
Departmental Committee on Graduate Studies

A LITERATURE STUDY OF THE ARCHING EFFECT

by

HSIEN-JEN TIEN

Submitted to the Department of Civil and Environmental Engineering
on Feb. 29, 1996 in partial fulfillment of the requirements for the
Degree of Master of Science in Civil and Environmental Engineering

ABSTRACT

If a portion of an otherwise rigid support of a granular mass (e.g. sand) yields, the adjoining particles move with respect to the remainder of the granular mass. This movement is resisted by shearing stresses which reduce the pressure on the yielding portion of the support while increasing the pressure on the adjacent rigid zones. This phenomenon is called the "arching effect".

The arching effect can be found widely in natural terrain as well as in man-made construction. It is an important topic for the geotechnical engineers and researchers to comprehend and recognize in their work and studies. A review of research related to the arching effect is presented. The review starts with the classical arching theories including Terzaghi's study (1936, 1943), then extends to the analytical methods, numerical analyses, empirical approaches, and experimental investigations. A new experimental approach with the application of photoelastic materials is introduced at the end of this review.

Thesis Supervisor: Dr. Herbert H. Einstein

Title: Professor of Civil and Environmental Engineering

ACKNOWLEDGMENTS

The author extends his sincere gratitude to Professor Herbert Einstein for his insightful help and encouragement throughout the development of this thesis. Thanks are owed to Professor Samuel Paikowsky of UMASS/Lowell for his precious advice and support.

The facilities of the Department of Civil and Environmental Engineering in UMASS/Lowell were used in this research work. The presented research was supported by the National Science Foundation under grant No. MSS-9358090. The use of these facilities and the assistance of the NSF are greatly appreciated.

Thanks to the entire Civil Engineering faculty in MIT with special mention to Dr. John Germaine for his help in my graduate study. Also thanks to Shun-Min Lee and Lucy Jen in MIT for their friendship and Edward Hajduk in UMASS/Lowell for his help in this thesis.

Finally, I want to thank my parents who always provided support, encouragement, and understanding. Without your help, this cannot be possible. I love you.

TABLE OF CONTENTS

LIST OF FIGURES

LIST OF TABLES

Chapter ONE
Introduction: Definition and Description of Arching

1.1 General Background

Arching effect is one of the most universal phenomena encountered in soils both in the field and in the laboratory (Terzaghi, 1943). This effect is most recognized in underground structures, for example, underground conduits. Underground openings can be built utilizing the arching action to account for the reduction in the overburden pressure. The nature of the stress redistribution influences the load that reaches the structure, whether it is from overburden soil, surface surcharge, or lateral earth pressure. The soil medium adjacent to the underground opening can increase the structure's load-carrying ability compared to an identical unburied structure. A more detailed definition of arching is presented in the following section. Arching effect can also be found in the natural landscape. For example, the arching phenomenon in karst terrain can be observed easily and widely.

Since arching affects geotechnical engineering, people have tried to understand its mechanism for decades. Much research has been done in this area, including theoretical derivations, analytical methods, numerical analyses, and experimental investigations. Researchers also applied the arching theory to practical engineering problems, for example, the soil plug problem (Paikowsky, 1989) and the sheet pile design (Rowe, 1952).

This literature study reviews past research related to the arching effect and attempts to sort the available information for future research use. The following five categories are covered in this study: (1) Relevance and Application of Arching in Soil Mechanics, (2) Classical Arching Theories, (3) Analytical Approaches, (4) Empirical Methods, and (5) Experimental Investigation. A discussion and relevant comments are provided, related to the interaction between the various categories. Conclusions and discussion concerning the existing arching studies as well as suggestions for future work are presented in Chapter 7.

1.2 Definition of Arching

Arching can be best described as a transfer of forces between a yielding mass of geomaterial and adjoining stationary members. A redistribution of stresses in the soil body takes place. The shearing resistance tends to keep the yielding mass in its original position resulting in a change of the pressure on both of the yielding part's support and the adjoining part of soil (Terzaghi, 1943). If the yielding part moves downward, the shear resistance will act upward and reduce the stress at the base of the yielding mass (Figure 1.1). On the contrary, if the yielding part moves upward, the shear resistance will act downward to impede its movement and cause increase of stress at the support of the yielding part.

Depending upon relative stiffnesses in the ground mass, arching can either be active or passive. Active arching occurs when the structure is more compressible than the surrounding soil, as illustrated in Figure 1.2 (a). When the system is subjected to loads, the resulting stress distribution across locations of equal initial elevation (Plane AA and

Plane BB) is similar to that shown in Figure 1.2 (b), where the stresses on the structure are less than those on the adjacent ground. If the structure deforms uniformly on Plane AA and BB, the stresses on it tend to be lower toward the edges due to mobilized shear stresses in the soil.

In passive arching, the soil is more compressible than the structure as illustrated in Figure 1.3 (a) As a result, the soil undergoes large displacements, mobilizing shear stresses which increase the total pressure on the structure while decreasing the pressure in the adjacent ground. Assuming the structural deformations are uniform, the stresses are highest at the edges and lowest at the centerline. The stress distributions for the passive case at Plane AA and BB are shown in Figure 1.3 (b).

If the soil medium and the structure have the same constitutive properties (i.e. load vs. deformation relationship), the stress along a plane (like Plane AA and BB shown in former figures) will be uniform. The stress along the vertical direction will be linear and increasing with depth (geostatic stresses) as no arching would be presented in this case. This condition is highly unlikely to be found in natural or man-made environments due to the differences in the mechanical properties of geomaterials (like soils or rocks) and structure components (like steel or concrete).

Underground structures normally do not have uniform deformation resulting in stress distributions more complex than those discussed above (Figure 1.2 & 1.3). An example is presented in Figure 1.4. The horizontal faces (like Plane AA) and vertical faces (like Plane BB) are more flexible towards the centers of the spans, resulting in the deformation patterns shown in Figure 1.4. The horizontal and vertical stress distributions are

also shown in this figure suggesting that the faces of the structure experience both active and passive arching at the same time.

1.3 Brief History of Arching Studies

The phenomenon of arching has been recognized for over a century. Research has generally been sporadic, usually directed toward a particular area of importance at that point in time. This section summarizes the developments in the study of arching.

Arching is present in many geotechnical problems. Nevertheless, arching was first recognized and investigated in a non-geotechnical context. During the early 1800's French military engineers were asked to design magazine silos (Feld, 1948). They found that the base of the silo only supported a fraction of the total weight of material above it, and the side walls carried far more load than anticipated. Experiments showed that if a small section of the base were detached and lowered, the resulting load that the section experienced was independent of the height of material in the silo. Hence, they concluded that an "arch" had formed above this displaced section. In the latter 1800's this knowledge of the behavior within magazine silos was utilized by Janssen (1895) in deriving an approach to the design of silos for grain and other particulate materials ("The Silo Theory").

Around 1910 considerable land drainage projects were conducted in the Midwest of the United States. Engineers found that many of the drainage pipes they specified had structural failures subsequent to installation and backfilling (Spangler & Handy, 1973). Anson Marston (1930) performed extensive research at Iowa State University into the

loads on underground conduits/pipes, finding that the loads may vary between a small fraction of the overburden and several times the overburden. Different loads on the conduits depended upon the conduit's flexibility and the installation procedure (Spangler, 1964). and this was attributed to arching.

In the 1920's and 1930's the importance of arching around tunnels was recognized. Designers found that the support loads were far less than the overburden and that considerable savings could be achieved if accurate predictions of load were possible. This gave rise to empirical relations for tunnel support loading. Some of these relations are still in use today (Széchy, 1973), including Terzaghi's design values for underground structure support loads under various ground conditions (Terzaghi, 1943; Proctor and White, 1946, 1977). The interest in tunnel support loads also led to experimental and theoretical treatment of the problem (most notable Terzaghi's research in 1936 and 1943).

In the 1950's, the decision to build an interstate highway system in America created new interest in the loads on underground conduits. Larger culverts, with fill heights and culvert loadings greater than ever before, were required. Researchers reviewed and updated Marston's recommendations in light of experience obtained in the several decades since his investigations. Particular attention was given the positive effects of load redistribution around flexible culverts, and techniques for reducing the load on a culvert through specific backfilling procedures (Spangler, 1964; Spangler & Handy, 1973).

The direction of arching-related research shifted once again in the 1960's when the Defense Department of the United States sponsored considerable research in the area of soil-structure interaction. Techniques were needed for the design of massive defense fa-

cilities and it was recognized that the arching phenomenon would allow facilities placed below ground to withstand nuclear attacks during the war, which would destroy any surface facilities (Whitman et. al., 1962, 1963). Most of the research was presented at the "Symposium on Soil-Structure Interaction" in 1964.

Starting in the 1970's, computer-based techniques have been broadly utilized in the studies of arching problems. Getzler, et. al. (1970) used the finite difference method to analyze the arching pressures in an ideal elastic soil model. Rude (1982) utilized a linear elastic finite element program to predict the behavior of a culvert installed in a laboratory testing tank. Rude's predictions based on the program had shown good agreement with experimental results. More recently, individual particle's properties and interparticle relationships are taken into account in numerical analysis. Sakaguchi and Ozaki (1992) used the "Discrete Element Method" (DEM) for computer simulations on the formation of arches plugging flow. They considered the rolling friction effect between particles and got a good agreement between the simulation outcomes and experimental measurements.

Terzaghi's trap door tests (1936) have been duplicated by several researchers, e.g. McNulty (1965), Ladanyi and Hoyaux (1969), Harris (1974), Vardoulakis et. al. (1981), Fricki and Fricker (1983), and Evans (1983). No real advances have been obtained in these research projects compared to Terzaghi's approach. Lately, some new technologies were applied in the arching studies. Iglesia, Einstein, and Whitman (1990) used centrifuge modeling to study scaling issues and arching in geomaterials. However, the stress distribution across the yielding surface and the correct shape of the sliding surfaces are still not known well. Techniques to measure the distribution of stresses within a soil body are re-

quired. The "Photogrametric Method" (Yoshida et. al., 1993) and the "Tactile Sensing Method" (Paikowsky & Hajduk, 1996) are the new techniques being investigated recently for measuring the stress distribution in granular soil. Materials like photoelastic particles can also be utilized to study the shape of the sliding surfaces related to the arching effect (Paikowsky et. al., 1996).

1.4 Scope of Study

The scope of this literature review is divided into five major categories:

(1) Relevance and Application of Arching in Soil Mechanics: (Chapter 2)

The first topic is the exploration of the natural terrain or the geologic structures relevant to the arching effect. The second one is the discussion of man-made construction which apply the arching theory. Examples for natural geological structures are Karst and Sinkholes (Beck, 1984) and examples for man-made construction are tunnel construction (Terzaghi, 1943), buried cylinders and pipes (Marston, 1930; Spangler, 1964), and soil plugging (Paikowsky, 1989).

(2) Classical Arching Theories: (Chapter 3)

The classical arching theories in soil mechanics were mostly influenced by Terzaghi (1936, 1943). Terzaghi conducted the most widely known experimental and theoretical investigations of arching. The original studies and the associated analytical derivations of the arching theories are reviewed along with the application of the theories to practical

construction. In addition to Terzaghi's research, the following studies are also reviewed: (a) Silos theory (Janssen, 1895 & Jakobson, 1958), (b) Marston/Spangler underground conduit analyses (Marston, 1930 & Spangler, 1964), (c) ground arch/dome approaches, and (d) Soil Plugging (Paikowsky, 1989),.

(3) Analytical Approaches: (Chapter 4)

These approaches include

(a) Continuum Approaches using Elasticity Theory, e.g. Finn (1963),

(b) Continuum Approaches using Plasticity Theory, e.g. Evans (1984),

(c) Discontinuum Approaches, e.g. Trollope (1957, 1963), and

(d) Numerical Methods, e.g. Finite Element Method (Selig, 1975; Rude, 1982; Einstein, 1980), Finite Difference Method (Getzler, 1970; Chelapati, 1964), and Distinct Element Method (Sakaguchi and Ozaki, 1993).

(4) Empirical Methods: (Chapter 5)

Some of the empirical methods utilize simple static analyses while others are entirely founded on the experience of the person proposing it. These methods are separated into two major areas. One area contains the methods considering the effect of overburden depth and the other area includes the methods disregarding the effect of overburden depth. For example, the methods of Bierbäumer (Széchy, 1973), Balla (1963), and Terzaghi (1946) considered the effect of overburden depth; the method of Kommerell (Széchy, 1973) neglected this effect.

(5) Experimental Investigation and Photoelasticity Methods: (Chapter 6)

All the experimental investigations are model tests which are used to examine the arching behavior

(a) McNulty's experiment (McNulty, 1965)

(b) Ladanyi and Hoyaux' experiment (Ladanyi & Hoyaux, 1969),

(c) Sandbox trap door experiments (Harris, 1974),

(d) Arching in granular soil (Evans, 1983),

(e) Centrifuge Modeling of Jointed Rock (Iglesia, et. al., 1990), and

(f) The photoelasticity method allows one to study stress distribution around structures of complex geometry. The previous study has Riley's experiment (1964) and Paikowsky and Xi's direct shear experiment (1995).

A summary and conclusions for this literature survey will be found in the last chapter (Chapter 7). Some recommendations for future researches will also be proposed in that chapter.

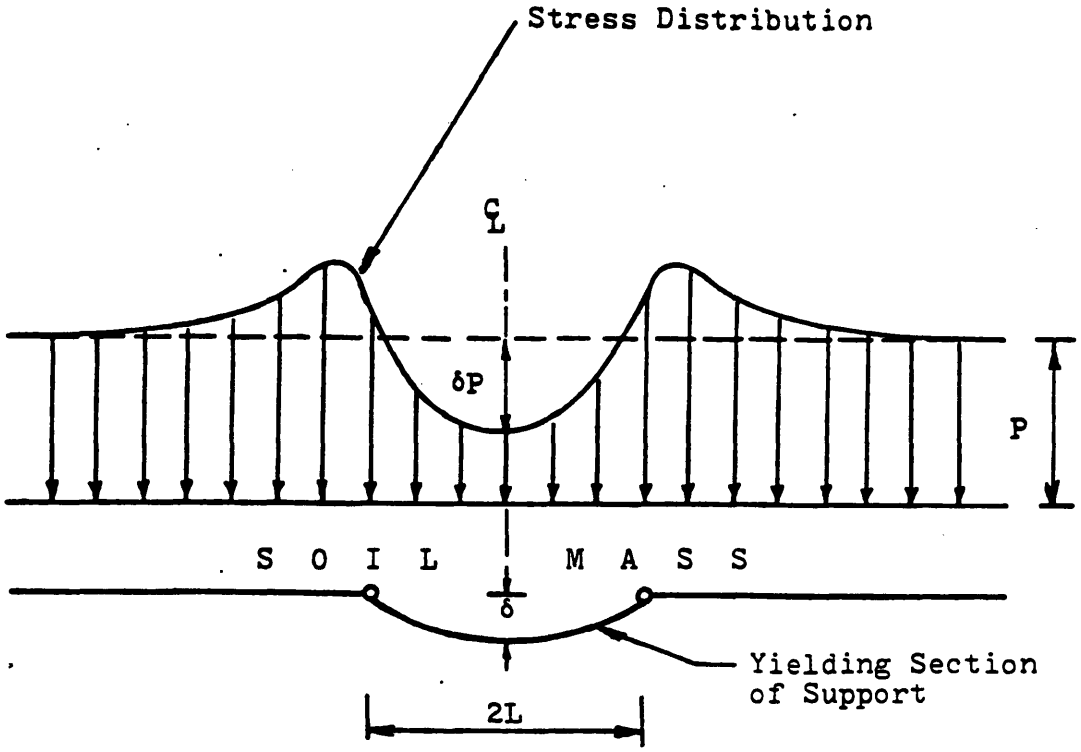

Figure 1.1 Stress Distribution in the Soil Above a Yielding Base (Bjerrum et. al., 1972; Revised by Evans, 1984)

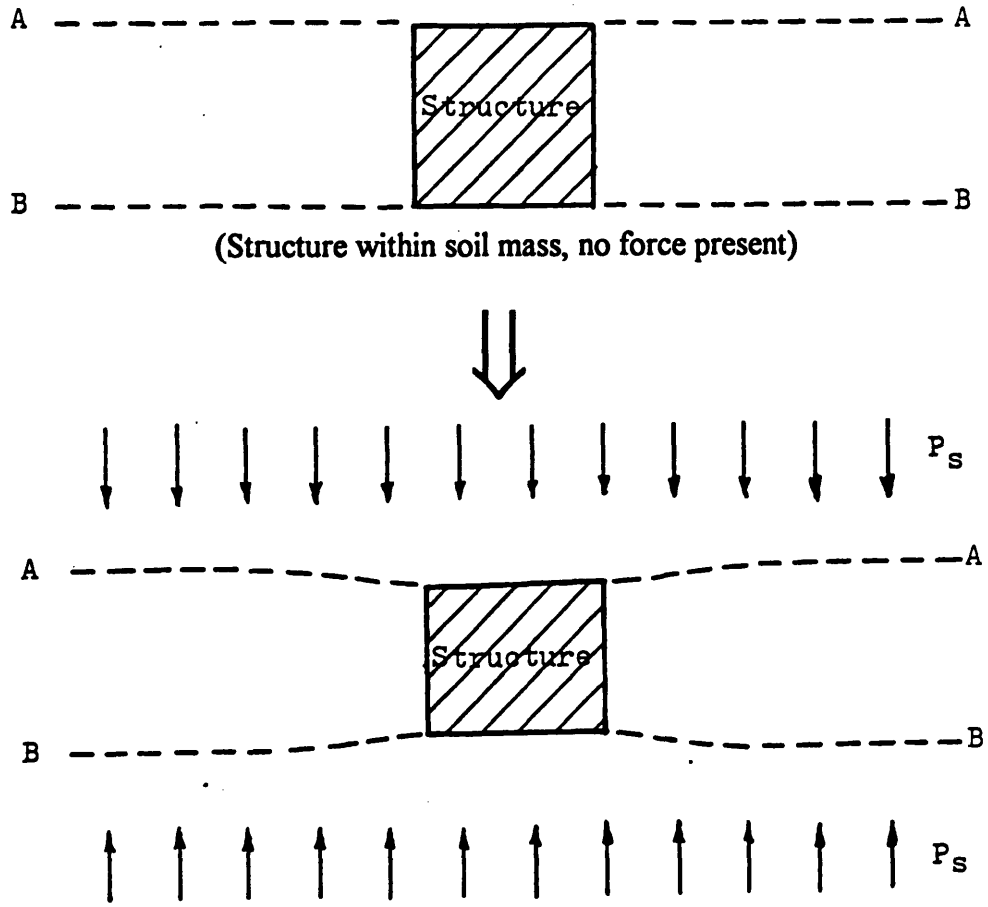

(a) Displacements under pressure Ps when structure is more compressible than surrounding soil

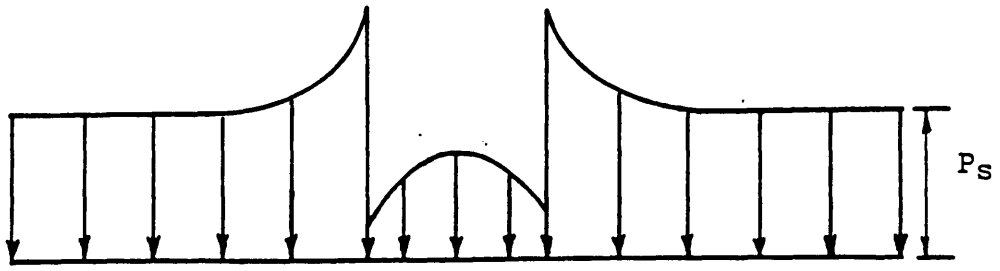

(b) Stress distribution across Plane AA or BB

Figure 1.2 Active Arching (Evans, 1984)

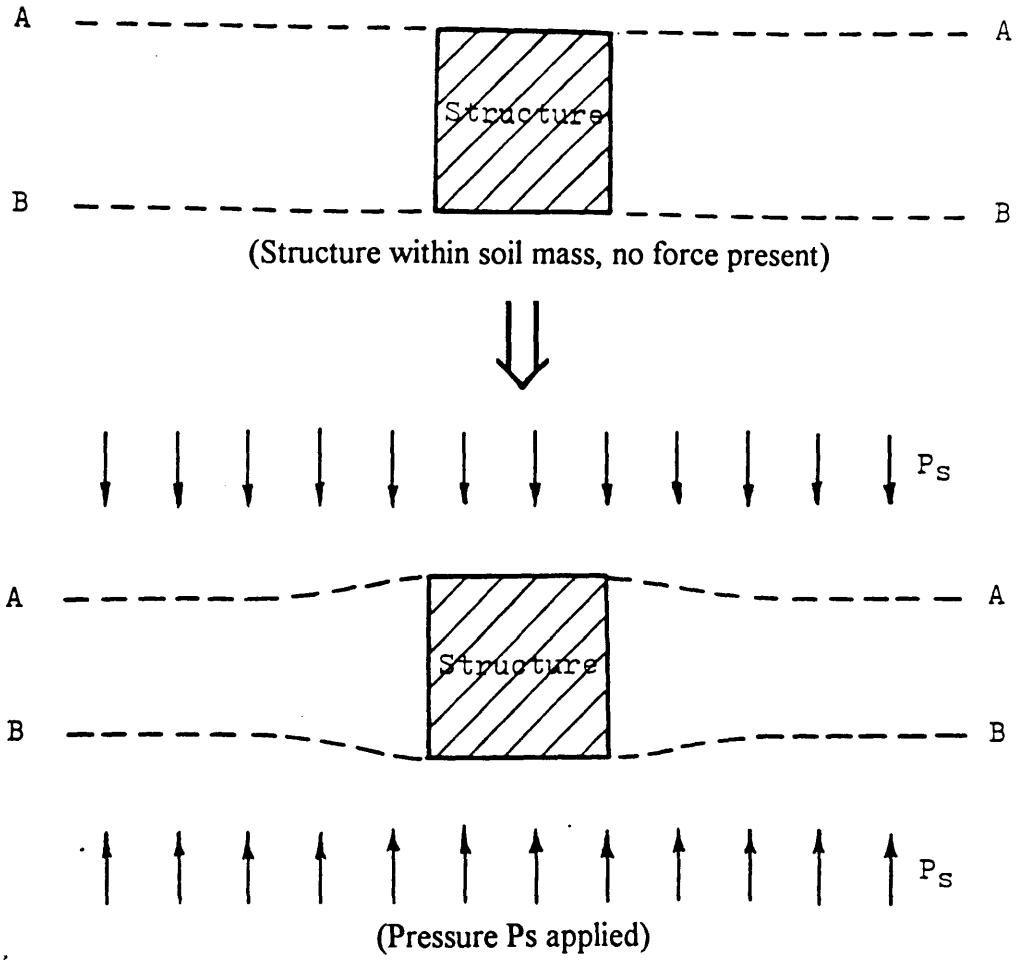

(a) Displacements under pressure Ps when structure is less compressible than surrounding soil

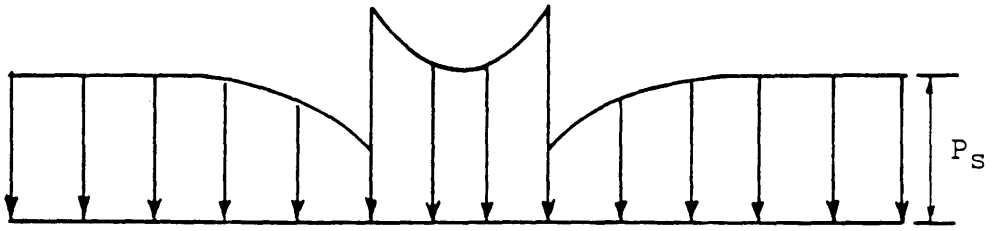

(b) Stress distribution across Plane AA or BB

Figure 1.3 Passive Arching (Evans, 1984)

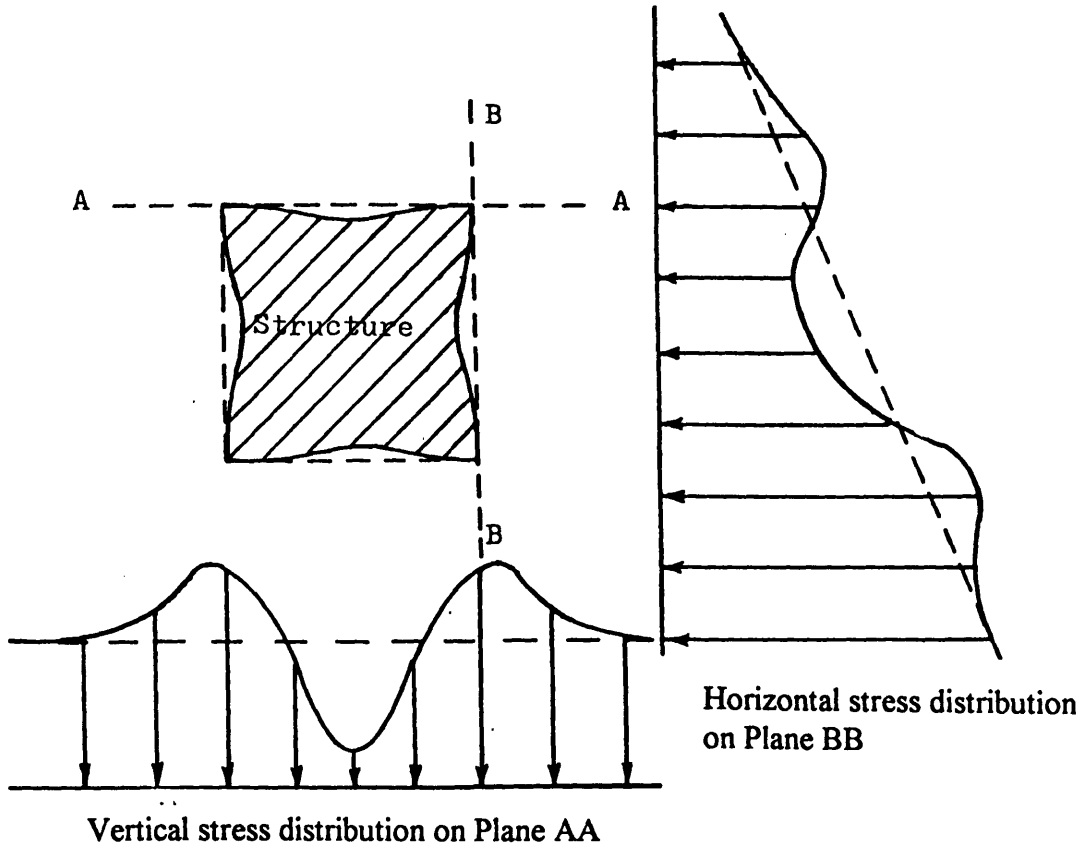

Figure 1.4 Typical deformation and stress distributions around a rectangular structure with flexible sides (Evans, 1984)

Chapter TWO
Relevance and Application of Arching in Geotechnical Engineering

2.1 Overview

The relevance and application of the arching theory in geotechnical engineering is reviewed here. In the first part of this chapter, natural terrains and geologic structures are examined in light of the arching mechanism. Man-made structures as applied to the arching theory is discussed in the later part. Examples of natural geological structures in which arching plays a role are Karst and Sinkholes (Beck, 1984). Examples for man-made structures are tunnels (Terzaghi, 1943), buried cylinders and pipes (Marston, 1930; Spangler, 1964), sheet pile designs (Rowe, 1952 & 1955), and pile plugging problems (Paikowsky, 1989).

2.2 Geological Structures

2.2.1 Review of Karst Terrain and Dolines

Karst is a complex composition of landform and subterranean materials formed by the dissolution of soluble rocks, e.g. limestone, dolomite, and gypsum. Karst terrain is quite often mantled with various surface deposits such as weathered debris, terra rosa soils, loess and alluvium. The most obvious concern of karst terrain is the development of high permeability as water travels through and dissolves the material. Unique characteristics concerning karst terrain were outlined by LeGrand (1973) as follows:

(1) A general scarcity and poor predictability of groundwater supplies,

(2) A scarcity of surface streams,

(3) Instability of surface streams,

(4) Instability of the ground, and

(5) Leakage of surface reservoirs.

There are many different factors that contribute to the formulation of karst. Not all of the conditions listed above need to be met in order for karst terrain to develop, nor does the inclusion of all these factors indispensably mean that karst terrain will emerge. Each karst terrain has particular qualities that make it unique compared to other karst terrain. An important factor to remember is that it is a land formation that is in a continuous state of change.

There are three major rock types that can be found in karst terrain. They include limestone, dolomite, and evaporites. Limestone exists in most karst terrains due to its high solubility in water, which makes it susceptible to developing pores. The chemical composition of the ground water plays an important role in karst composition. In the event that carbon dioxide is dissolved into the water, the water is transformed into a carbonic acid, increasing the dissolution rate. When water circulates through the pores due to heavy rainfall, there is the influence of both a high energy gradient and a more acidic solution to deteriorate the soil and the limestone. Figure 2.1 shows a subsidence doline in alluvium over limestone. Dolomite rock behaves in natural water in an essentially similar way to that of limestone. However, under normal air and water interface conditions, it is claimed that dolomite is usually less soluble than limestone (Douglas, 1965). The third

important karst rock is evaporite. Gypsum is an example. It is much more soluble than either limestone or dolomite (Trombe, 1952).

Dolines (also called Sinks or Sinkholes) are a special geological structure that can be found broadly in karst terrain. They are usually circular or oval in plan, with depth varying very much in relation to diameters. Several processes are responsible for sinkhole formation: surface solution, cave collapse, piping, subsidence, and stream removal of superficial covers. These processes often occur in combination. They are described individually as follows (Jennings, 1971):

(1) *Solution Dolines*: They usually form where structural control such as intersecting joints leads to infiltration of surface water. As more water flows through the defect, the depression enlarges and leads to even more inflow. Solution structural control may alter the original geometries. If sediment accumulates, the floor of a large dolines can be swamp or contain small lakes or ponds. Figure 2.2 (a) shows the diagram of a solution doline in a jointed rock mass.

(2) *Collapse Dolines*: They usually result from the collapse of a cave produced by underground solution. These dolines exhibit collapse features such as steep walls and an angular shape in plan. The depth-width ratio often is greater than for the solution dolines. If no further collapse occurs, these dolines eventually weather and appear more like a solution doline. The configuration of a collapse doline is shown in Figure 2.2 (b).

(3) *Subsidence Dolines*: They form when sinks form in karst rocks underlying a superficial deposit or thick residual soil. These dolines can also form through

continuous piping of materials through widening joints or solution pipes. Figure 2.2 (c) shows the subsidence doline.

(4) *Alluvial Stream-sink Dolines*: Dolines form in alluvium where streams sink into underlying karst rock. The processes which create subsidence dolines operate here but additionally the stream provides a good channel for mechanical removal of the insoluble alluvium. Figure 2.2 (d) shows the alluvial stream-sink doline.

(5) *Subjacent Karst Collapse Doline*: Figure 2.2 (e) shows this kind of dolines. Cave collapse occurs in karst rocks beneath overlying bedrock formations. A steep-walled, deep doline may form initially (Figure 2.2 (e)) but weathering will turn them into conical features which may be degraded into still gentler forms.

2.2.2 Relevance to Arching Effect

Sowers (1984) indicates that the most important problem in residual settlement is "the collapse of domes within the residual soils and the development of a sinkhole accompanied by catastrophic foundation subsidence, often with little warning." The formation of a sinkhole starts with the creation of a dome cavity that propagates upward until the dome can no longer support the increased load. For the most part, sinkholes collapse when the water table is lowered, and the cavern is subject to an increase in effective stress. In other words, the overburden above the cavern increases such that the dome cavern is unable to support the increased load.

Figure 2.3 shows the failure processes of the arch/cavity structure (Benson & LaFountain, 1984). In *stage I*, the total cavity system and overburden are stable. In *stage II*, the stable cavity system has some overburden instability above it. Then a moderate cavity system and more overburden instability develop in *stage III*. Finally, the considerable instability of the cavity system results in gross overburden instability and small surface displacement in *stage IV*. After this stage, the whole system fails.

As most sinkhole failures develop as a result of lowering the water table, cohesion is usually an important factor in determining the failure strength of the cavern roof. For a cohesionless granular medium, where cohesion plays no role in determining the failure stress characteristics of the cavern, it is presumed that the arching mechanism that controls lateral transmission of stresses plays the most significant role. Although arching undoubtedly contributes to the strength characteristics of cohesive medium, it's contribution is not as significant as it is for non-cohesive medium. A need for understanding the arching problems in granular material exists when one studies the strength of sinkholes comprised of non-cohesive material.

2.3 Man-made Structures

2.3.1 Pile Plugging Problems

Pile plugging problems are used in this section as an example to explain the relevance and application of arching to man-made structures. The other examples (tunnels and buried conduits) will be discussed later in Chapter Three.

Pile plugging problems are caused by soil plug behavior. Soil plug behavior happens during the installation of open pipe piles. At the initial stage of installation, soil enters the pipe pile at the same rate as the pile penetration, and the pile is called "unplugged" (Figure 2.4 (a)). As the pile is driven to the ground continuously, the inner soil body develops friction on the inner pile wall, which may prevent some of the soil in front of the opening from entering the pile. When the length of the inner soil cylinder is less than the penetration depth, the pile is considered as "partially plugged" (Figure 2.4 (b)). If a sufficient friction is developed on the inner pile wall, no more soil can enter the pile and the pile is called "plugged" (Figure 2.4 (c)). The open ended pile is then assumed to have the same penetration characteristics of a close ended pile.

Paikowsky (1989) evaluated the inner soil resistance of the pile plugging problems in his research. The behavior of a soil plug under static loads was analyzed using the "silo approach" (Jakobson, 1958) as a tool. This approach led to the conclusion that the "arching effect" controlled the mechanism of load transfer in the silo as well as in an opening pile. According to Paikowsky's study, two possible relative soil and wall movements can take place: (1) "ACTIVE" (associated with "active arching"), in which the soil settles with respect to the walls (e.g., the "standard" silo case), and (2) "PASSIVE" (associated with "passive arching"), in which the walls move downwards with respect to the soil (e.g., open pile penetration). In this section, the "PASSIVE" case related to the pile plugging problems will be presented.

Figure 2.5 (a) presents two possible principal stress trajectories in an opening pile. When the pile moves downwards with respect to the soil, the shear stresses are acting

downwards on the soil and upwards on the inner pile surface. The stresses acting on the soil and inner pile surface for this case (pile plugging) are shown in Figure 2.5 (b). If the friction angle between the soil-pile interface is assumed equal to the soil internal friction angle (ϕ), the stress state at the interface can be described by the Mohr circle diagram shown in Figure 2.5 (c). After the pole (point "P") is found, the directions of major principal stresses can be decided. These directions lead to the concave major principal stress trajectory as shown in Figure 2.5 (a). This is because in the condition of pile plugging, the soil is being pushed upwards in a "passive arching" mode, an arch made of particle contacts is oriented concave downward in the major principal stress direction. The major principal stress direction at the centerline of the pile is horizontal in this case (Figure 2.5 (a)). A real passive arching case from pile plugging samples is presented in Figure 2.6. Several concave arches can be observed in this figure. On the other hand, if the shear stresses act upwards on the soil and downwards on the inner pile surface, all the aforementioned phenomena are reversed. The soil is then in the "active arching" mode, resulting in the convex minor principal stress trajectory as shown in Figure 2.5 (a). The major principal stresses in the soil are then perpendicular to this trajectory and support the load above it. The detailed mechanism of the active arching (the silo behavior) will be depicted in the following Chapter.

Because of the passive arching effect, the open pipe piles constitute a strong foundation for land and offshore construction. They are easy to handle and splice, and more light-weight than the closed end piles.

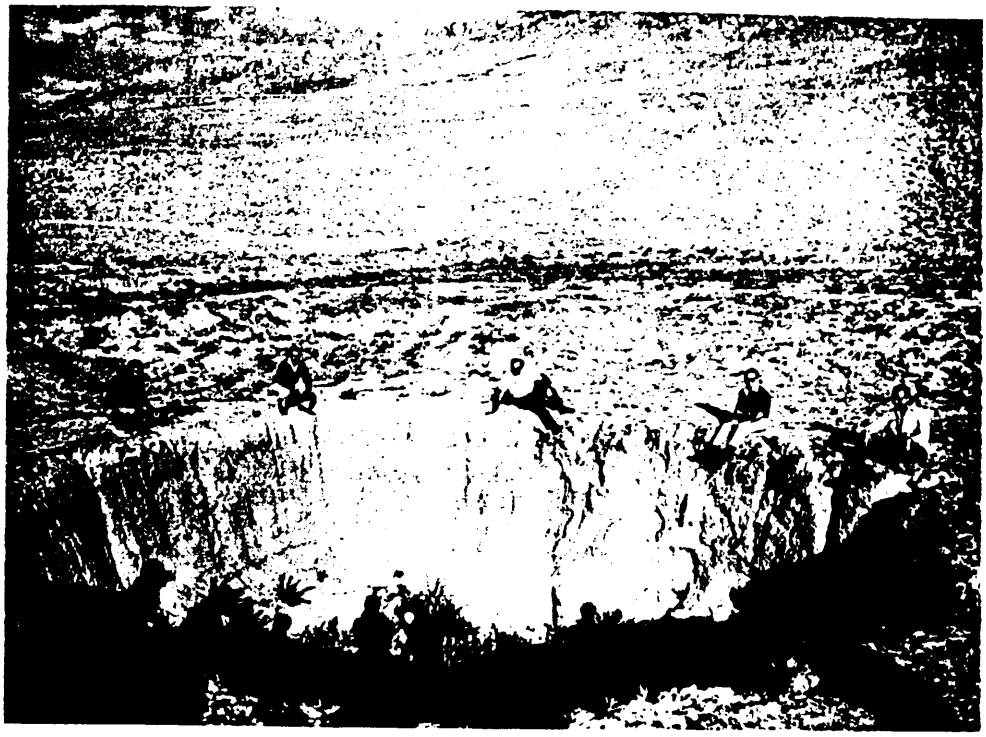

Figure 2.1 Subsidence Doline in Alluvium Over Limestone in May River Dam near Konya, Turkey (Jennings, 1971)

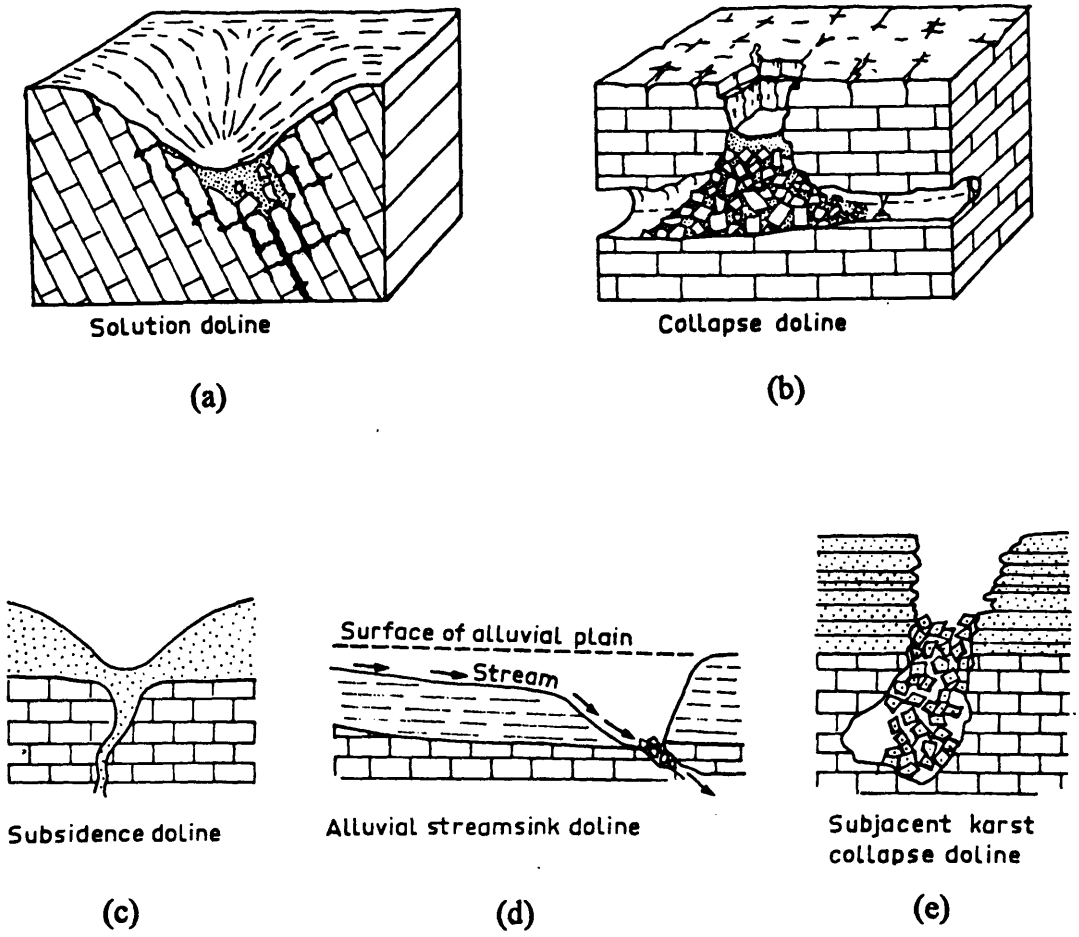

Figure 2.2 Different Types of Dolines: (a) Solution Doline, (b) Collapse Doline, (c) Subsidence Doline, (d) Alluvial Stream-sink Dolines, and (e) Subjacent Karst Collapse Doline. (Jennings, 1971)

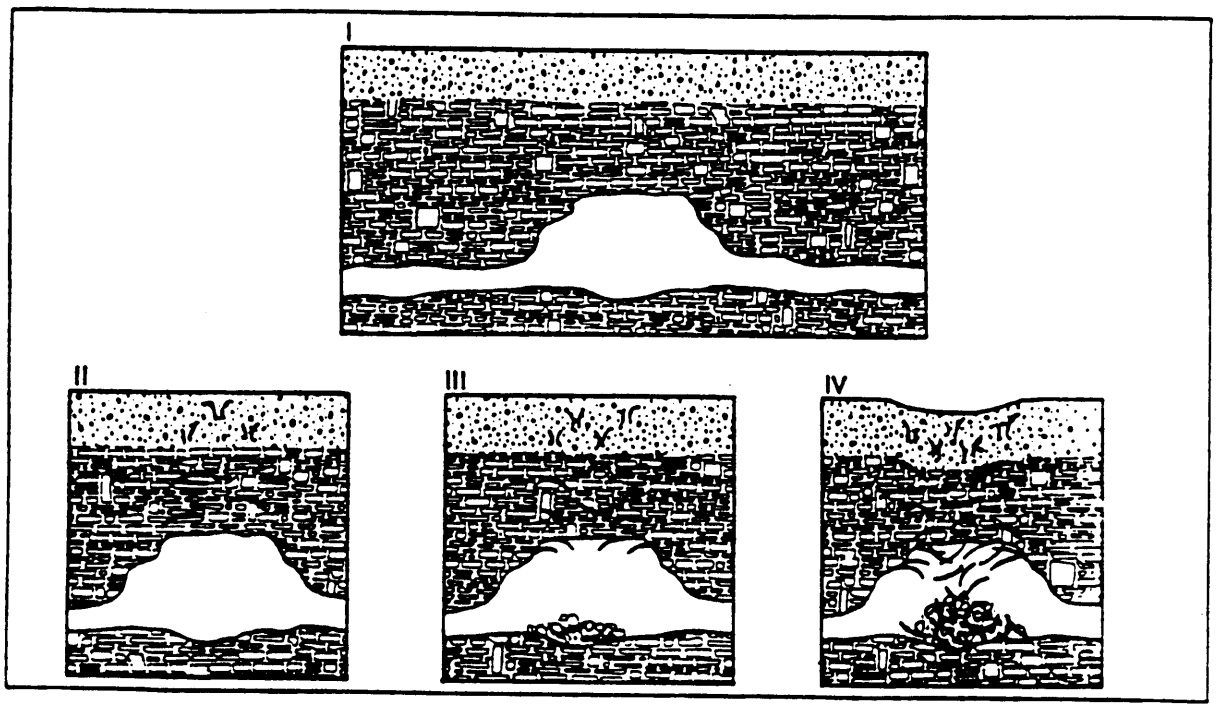

Figure 2.3 Failure Processes of the Cavity Structure: *Stage I* - Stable Cavity and Overburden System, *Stage II* - Stable Cavity System with Some Overburden Instability, *Stage III* - Moderate Cavity System with unstable Overburden, *Stage IV* - Failure of Cavity System (Benson & LaFountain, 1984)

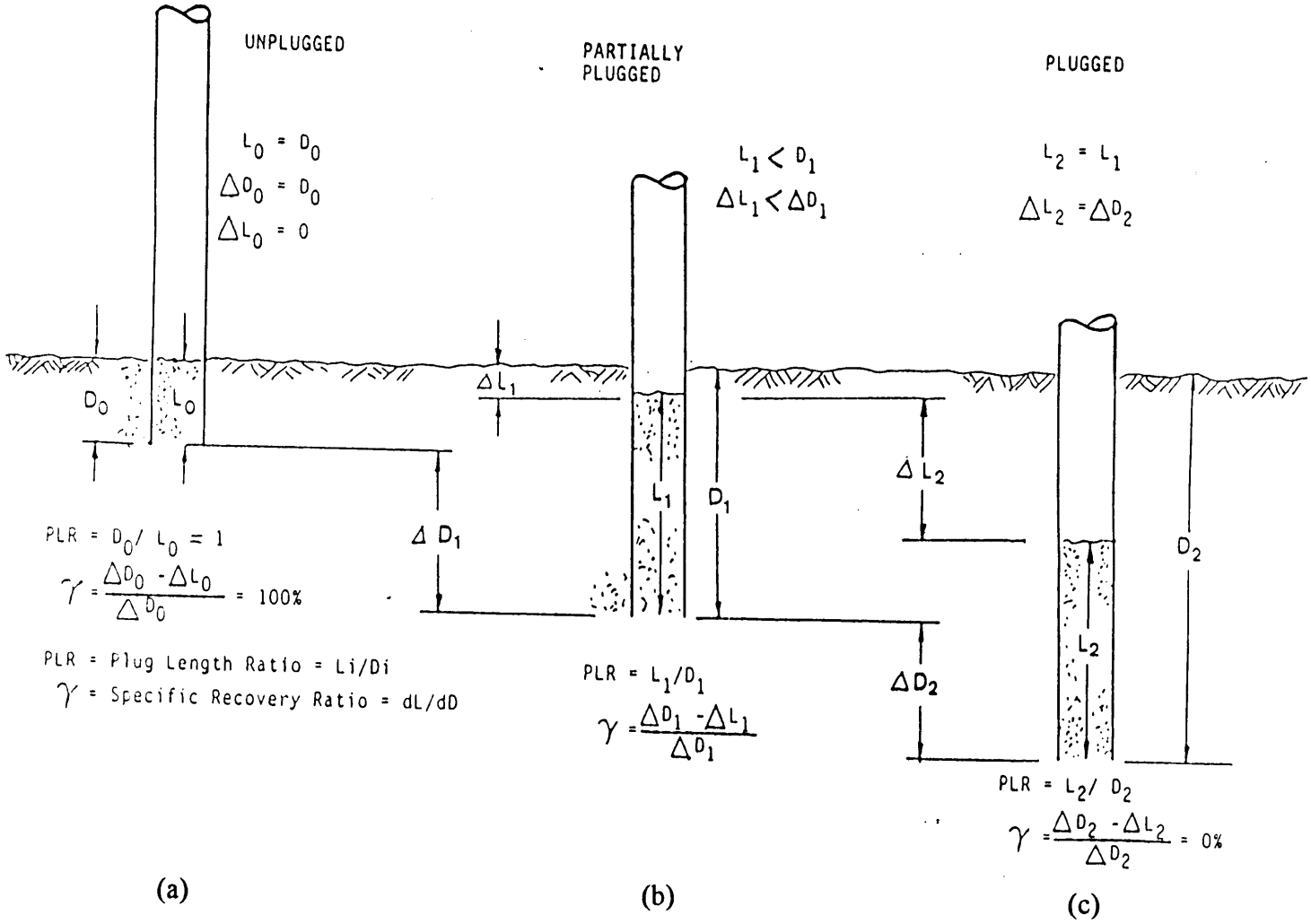

Figure 2.4 Penetration States of the Open Pipe Pile: (a) Unplugged — Free Soil Intrusion, (b) Partially Plugged — Limited Soil Intrusion, and (c) Fully Plugged — No Soil Intrusion (Paikowsky, 1989)

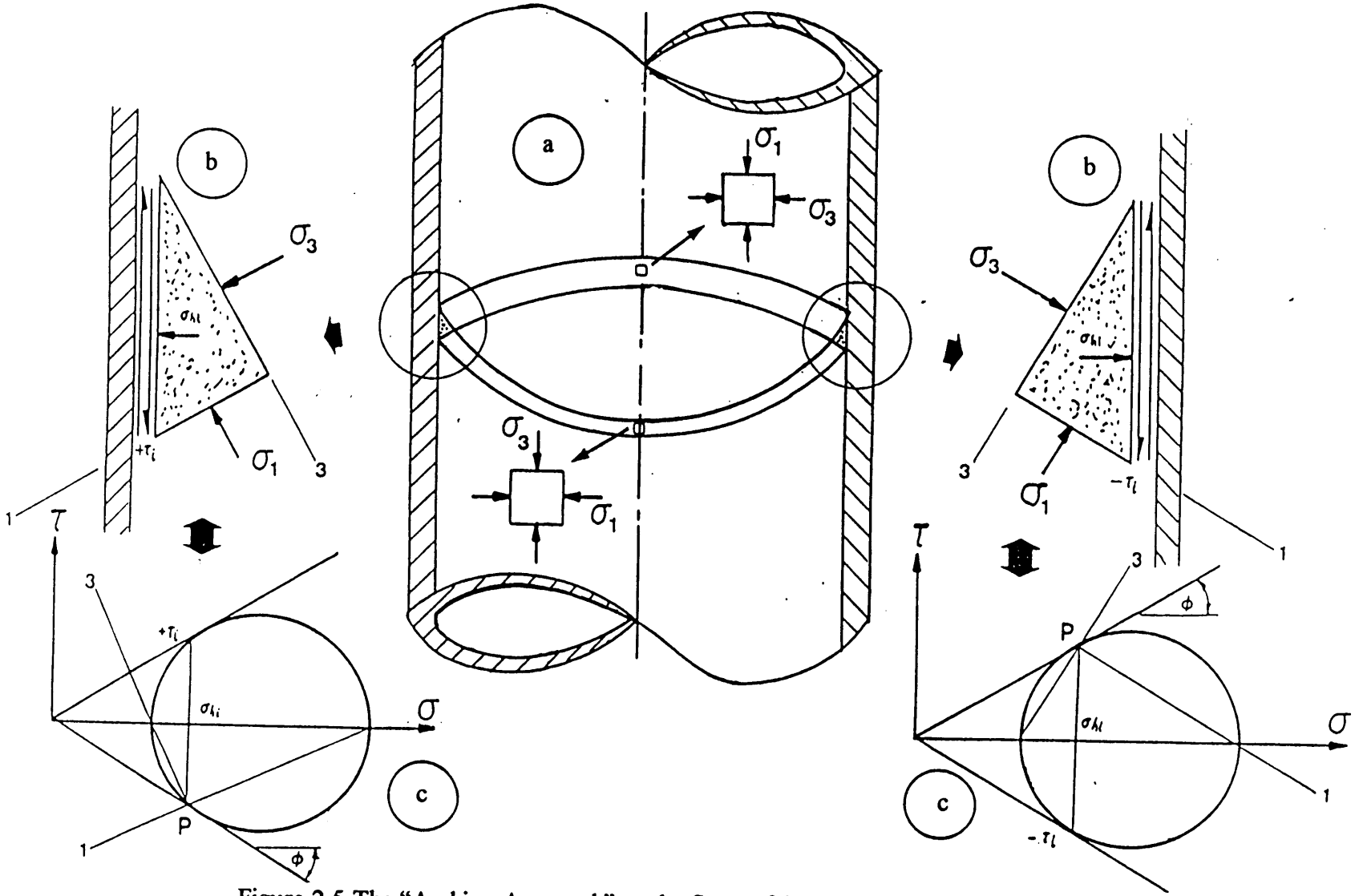

Figure 2.5 The "Arching Approach" to the State of Stress in the Inner Soil Plug: (a) Continuous Possible Arches Defined by the Principal Stress Trajectory, (b) Free Body Diagram, and (c) Mohr Circle for the Stress State Along the Interface (Paikowsky, 1989)

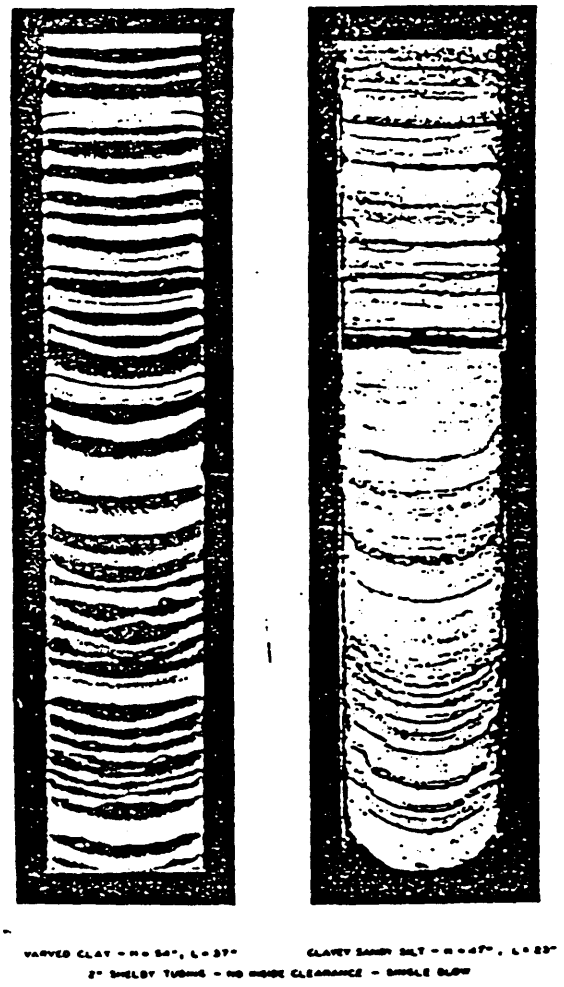

Figure 2.6 Distortion of Soil Due to Sampler Plugging — Passive Arching
(Paikowsky, 1989)

Chapter THREE
Classical Arching Theories

3.1 General

Classical arching theories combining experimental observation and theoretical derivation are introduced and discussed in this chapter. The theories presented here served as the foundation to the development of many additional arching studies. They play an important role in exploring the arching effect.

The most widely known experimental and theoretical investigations of arching were conducted by Terzaghi (1936, 1943). These studies are introduced at the beginning of this chapter. In addition to his studies, the analyses of loads on buried conduits (Marston, 1930; Spangler & Handy, 1973), the silo theory (Janssen, 1895; Jakobson, 1958), and ground arch (& dome) approach will be discussed consecutively.

3.2 Terzaghi's Investigations of Arching

3.2.1 Background

In order to improve understanding of the arching phenomenon in general, and specifically the stress distribution around tunnels, experimental investigations were made by K. Kienzl in Terzaghi's laboratory in Vienna (Terzaghi, 1936). From these results, the theories of arching were derived in 1943. Terzaghi (1943) described the arching effect as "the transfer of pressure from a yielding mass of soil onto adjoining stationary parts" and the soil is said to "arch over the yielding part of the support". He also combined the

knowledge which was obtained in these studies and information from many underground construction projects to generate the design values for underground structure support loads under various ground conditions (Proctor and White, 1946 & 1977). Some of Terzaghi's recommendations are still applied in underground construction practice at present.

3.2.2 Terzaghi's Trap Door Experiment (Terzaghi, 1936)

In Terzaghi's experiment a trap door, which was mounted flush with the base of a box containing sand, was translated downward while the total load on the door and its displacement were monitored. Horizontal and vertical stresses at various heights above the door were indirectly measured using the friction tape method. Terzaghi's experimental set-up is shown in Figure 3.1. The trap door has a width (2B) of 7.3 cm and a length of (L) 46.3 cm (out of the figure plane).

Figure 3.2 shows the typical results presented by Terzaghi (1936). The force on the trap door was normalized by its initial value, i.e. the force acting on the trap door before the trap door was lowered. In Figure 3.2, the normalized force decreased rapidly as displacement begun and the minimum value of this normalized force occurred at a displacement of only about 1% of the trap door width. These minimum values were less than 10% of the overburden sand weight and had the tendency to be lower for dense sand (6%) than for loose sand (9.6%). As displacement continued, the "structure" developed within the sand was believed to have disintegrated somewhat, causing the load to increase until a constant value which was still only a small fraction of the overburden (≈12.5%). This constant value was obtained for trap door displacements greater than about 10% of the

door's width. In addition, dense and loose sand showed an ultimate trap door force of the same magnitude.

Figure 3.3 shows measured vertical and horizontal stresses within the soil profile above the trap door. The vertical stresses decreased as soon as the trap door was moved downward. The horizontal stresses increased a little in a part of the soil profile above the trap door (at the position about H/3) but it decreased to a small value after the augment. Figure 3.4 shows values for the coefficient of lateral stress (K) obtained from the experiments. For the case of 1% deflection, K was approximately 1.0 directly above the trap door and increased to about 1.6 at about one trap door width (2B) above the door. At a distance of 5B above the trap door, K was essential equal to K_0. Terzaghi thought this result meant that lowering the trap door seemed to have no effect at all on the state of stress in the sand above this height, i.e. no arching effect outside this range. He suggested the value of K to be approximately unity, based on experiments and experience (Terzaghi, 1943).

Terzaghi noted that arching does not necessitate the crushing of soil particles to support the arch formation. It is a temporary circumstance dependent on the shear stresses in the soil. Vibration is the primary mechanism capable of disturbing the arching phenomena. Experimental results reported here are cases of "active" arching, which has upward shear stresses acting at the sides of the soil prism above the trap door. Because of the upward shear stresses, the normal stresses acting on the trap door were smaller than the overburden stresses at the top of the trap door.

3.2.3 Terzaghi's Arching Theory (Terzaghi, 1943)

According to the experimental results presented in the last section, Terzaghi proposed a theoretical approach for the arching problems in sand under plane strain condition (Terzaghi, 1943). He defined the arching effect as the pressure transfer between a yielding mass of soil and adjoining stationary parts. The relative movement in the soil is opposed by a shearing resistance within the contact zone of the yielding and stationary masses. Hence, the pressure transfer is possible through the shearing resistance which plays an important role in the arching theory.

The real surfaces of sliding, as observed by Terzaghi in 1936, are curved and at the soil surface their spacing is greater than the width of the yielding strip. The yielding strip **ab** at the solid base is presented in Figure 3.5, and the real sliding surfaces are curve **ac** and curve **db** in the same figure. Several assumptions are used in the arching theories based on the experimental observations. The sliding surfaces are assumed to be vertical. The vertical sections **ae** and **bf** through the outer edges of the yielding strip in Figure 3.5 represent surfaces of sliding. The pressure on the yielding strip is thus equal to the difference between the weight of the sand located above the strip (**ab**) and the shear resistance along the vertical sections. The free body diagram for a slice of soil in the yielding zone above strip **ab** is presented in Figure 3.6. In addition to the vertical sliding surface assumption, Terzaghi also assumed that the normal stress is uniform across horizontal sections and the coefficient of lateral stress (K) is a constant. Cohesion (c) was assumed to exist along the sliding surfaces. The vertical equilibrium for the free body in Figure 3.6 is:

$$2B\gamma dz = 2B(\sigma_v + d\sigma_v) - 2B\sigma_v + 2cdz + 2\sigma_h dz \tan\phi \qquad \text{(Eq. 3.1)}$$

in which

2B = width of the yielding strip (**ab**),

z = depth,

γ = unit weight of soil,

σ_v = vertical stress,

σ_h = horizontal stress = $K\sigma_v$,

K = the coefficient of lateral stress,

c = cohesion,

ϕ = friction angle.

The boundary conditions are $\sigma_v = q$ (surcharge) at $z = 0$. Solving Equation 3.1, leads to:

$$\sigma_v = \frac{B(\gamma - c/B)}{K \tan\phi}(1 - e^{-K \cdot \tan\phi \cdot z/B}) + q \cdot e^{-K \cdot \tan\phi \cdot z/B} \qquad \text{(Eq. 3.2)}$$

in which

q = surcharge at the soil surface.

The experimental investigations regarding the state of stress in the sand located above a yielding strip (see Section 3.2.2) have shown that the arching effect only extends to a height of 5B. In other words, at elevations of more than 5B above the center line the lowering of the strip has no effect at all on the state of stress in the sand (Terzaghi, 1936 &1942). Terzaghi assumed therefore that the shear resistance of the sand was active only on the lower part of the vertical boundaries **ae** and **bf** in Figure 3.5. With this assumption, the upper part of the soil prism ($\mathbf{ee_1f_1f}$) is treated as a surcharge q on the lower part

($\mathbf{e_1abf_1}$). If $z_1 = n_1B$ is the part of prism which acts like surcharge, and $z_2 = n_2B$ is the part of prism with shear resistance at the vertical boundaries, then Eq. 3.2 becomes:

$$\sigma_v = \frac{B(\gamma - c/B)}{K\tan\phi}(1 - e^{-K\cdot n2\cdot\tan\phi}) + \gamma B n_1 \cdot e^{-K\cdot n2\cdot\tan\phi} \qquad \text{(Eq. 3.3)}$$

when we substitute $q = \gamma n_1 B$ and $z = n_2 B$ to Eq. 3.2. When n_2 is very large, the vertical stress $\sigma_{v(\infty)}$ is equal to $B(\gamma\text{-}c/B)/K\tan\phi$. This means below certain depth, the vertical stress on the yielding strip will be a constant.

Finally, several limitations of Terzaghi's arching theory are presented: (1) the vertical stresses on the horizontal yielding surface are assumed to be uniform, (2) the trap door or yielding strip is assumed rigid, and (3) the assumed sliding surfaces are not true. For the arching studies in the following sections, researchers have tried to modify these assumptions in order to make the predictions of their theories closer to the physical conditions.

3.2.4 Application in Tunnel Design

Terzaghi applied the aforementioned theory to tunnel design (Terzaghi, 1943). The stress state in the soil above the top of a tunnel is similar to the stress state in the soil above a yielding strip. Terzaghi assumed the soil adjacent to the tunnel yields laterally toward the tunnel during construction. This creates an active earth pressure condition with the boundaries of the yielding zone inclined at about $(45° + \phi/2)$. The yielding zones at the sides of the tunnel and the assumed yielding prism ($\mathbf{e_1b_1b_1e_1}$) are shown in Figure 3.7 (a).

At the level of the tunnel roof, the width of the yielding strip ($2B_1$) for a rectangular tunnel is:

$$2B_1 = 2[B_0 + H \cdot \tan(45^\circ - \frac{\phi}{2})] \qquad \text{(Eq. 3.4)}$$

If the tunnel roof is located at a depth D in the ground, the vertical stress on the roof is:

$$\sigma_v = \frac{B_1(\gamma - c/B_1)}{K \tan\phi}(1 - e^{-K \cdot \tan\phi \cdot D/B_1}) \qquad \text{(Eq. 3.5)}$$

Figure 3.7 (b) shows the vertical stresses in the soil above the tunnel.

If a tunnel is located at a great depth below the surface, the arching effect cannot extend beyond a certain elevation D_1 above the tunnel roof (like z_2 in the last section, see Figure 3.5). Also the soil located above this elevation has a depth D_2 (like z_1 in Figure 3.5). Figure 3.8 (a) shows the configuration of the tunnel at a great depth. The vertical stress on the roof is then expressed as:

$$\sigma_v = \frac{B_1(\gamma - c/B_1)}{K \tan\phi}(1 - e^{-K \cdot \tan\phi \cdot D1/B1}) + \gamma D_2 \cdot e^{-K \cdot \tan\phi \cdot D1/B1} \qquad \text{(Eq. 3.6)}$$

When D_1 is very large, the vertical stress $\sigma_{v(\infty)}$ will reach a limit value:

$$\sigma_{v(\infty)} = \frac{B_1(\gamma - c/B_1)}{K \tan\phi} \qquad \text{(Eq. 3.7)}$$

If the tunnel is constructed in sand, then cohesion (c) is equal to 0. However, for safety reasons, c = 0 is assumed and Eq. 3.7 can be simplified to:

$$\sigma_{v(\infty)} = \frac{B_1\gamma}{K \tan\phi} \qquad \text{(Eq. 3.8)}$$

Figure 3.8 (b) shows the vertical stress profile at the top of a tunnel at a great depth. The arching effect only exists within a distance D_1 above the tunnel roof (Figure 3.8). There is no arching effect outside this range, i.e. no shear resistance within D_2.

3.3 Loads on Buried Conduits (Spangler and Handy, 1973, 1982)

3.3.1 Background

In 1913, Anson Marston developed a theory to explain the characteristics of a soil column above a buried conduit. Marston found that the load due to the weight of the soil above a buried conduit does not fully act on the conduit; part of the weight is undertaken by the arching action in which load is transferred to the adjacent side material (e.g. soil). Buried conduits can be grouped according to their installation procedures. The two major categories are those installed in a ditch excavated through existing soil, i.e. ditch conduit (Figure 3.9 (a)), and those placed at existing ground level above which an embankment is subsequently constructed, i.e. projecting conduit. If the top of the structure projects above the ground surface, it is a "positive" projecting conduit (Figure 3.9 (b)). If it is placed in a shallow trench and the top lies below the ground surface, it is a "negative" projecting conduit (Figure 3.9 (c)).

Arching action and the equal and opposite arch support play a tremendously important role in the development of earth load on a structure. In some cases, such as the case of a pipe in a trench (a ditch conduit), its effect is favorable; that is, it reduces the load as compared to the dead weight of the prism of soil lying above the structure (Figure 3.10 (a)). In other cases, such as some installations of culverts under embankments,

arching action may be inverted and the load on the structure may be considerably greater than the weight of the overlying prism of soil (Figure 3.10 (b)). In this section, the various aspects of the Marston theory (Marston, 1913) are reviewed. Then a new method named "Imperfect Ditch Method of Construction" (Spangler, 1964) are discussed. The imperfect ditch method utilizes the principles of arch action and arch support to minimize the load on a buried structure. Figure 3.9 (d) shows the layout of an imperfect ditch conduit.

3.3.2 Assumptions

Loads on a conduit equal the overburden if no relative motion occurs within the soil or between soil and conduit; however, this is seldom the case. Marston assumed that sufficient movement occurs to mobilize shearing resistance on sliding planes. After the movement has been activated, it continues to be effective because of the tendency for movement, even though the actual finite movements have ceased. The above assumption was verified by Spangler and Handy (1973) with their in-situ test data. The other assumption that Marston used in his derivations was that cohesion between the backfill material and the sides of the ditch was negligible. This assumption yields the maximum probable load on the conduit and offers a safer estimate for our design purpose.

3.3.3 Design of Buried Conduits

In the development of load on an underground structure, arch action is considered to be the resultant of lateral thrust and vertical shearing forces which are mobilized on certain vertically oriented planes in the soil overburden. The magnitude of arch support

can be evaluated by means of the Marston Theory. It represents the algebraic difference between the dead weight of the overburden soil and the earth load to which the structure is subjected, as indicated by Eq. 3.10. The derivations of the formulas in this section can be found in Spangler and Handy's book — "Soil Engineer" (1982). They are not shown in details here.

For *ditch conduits*, this load formula is derived by considering the forces acting on a thin horizontal slice of backfill material. The layout of a ditch conduit is shown in Figure 3.11. Equating the upward and downward vertical forces on the horizontal slice, the following equation is obtained:

$$V + dV + 2K\mu' \frac{V}{B_d} dh = V + \gamma B_d dh \qquad \text{(Eq. 3.9a)}$$

in which

V = vertical pressure on the top of the horizontal slice,

dV = vertical press increment,

γ = unit weight of backfill,

K = the coefficient of lateral stress (generally, the Rankine's active ratio : $K_a = \tan^2(45^\circ - \phi/2)$ is applied),

$\mu' = \tan \phi'$ = coefficient of friction between fill material and sides of ditch,

B_d = width of ditch at top of conduit.

This is a linear differential equation, the solution is:

$$V = C_d \times \gamma \times B_d^2 \qquad \text{(Eq. 3.9b)}$$

in which

$$C_d = \frac{1 - e^{-2K\mu'(H/B_d)}}{2K\mu'}, \qquad \text{(Eq. 3.9c)}$$

H = the distance from the ground surface to the top of the conduit,

e = base of natural logarithms.

Hence, for the case of a rigid ditch conduit with relatively compressible side fills, the load on the conduit (W_c) will be:

$$W_c = C_d \times \gamma \times B_d^2 \qquad \text{(Eq. 3.9d)}$$

C_d is a coefficient which can be calculated from Eq. 3.9c.

The magnitude of arch support is the algebraic difference between the weight of backfill and the load on the structure. For the case of ditch conduits, this difference is:

$$A_s = \gamma \times B_d \times (H - C_d \times B_d) \qquad \text{(Eq. 3.10)}$$

in which A_s = arch support (support derived form both sides of the ditch). The thin slice of backfill material in the free body diagram of Figure 3.11 will look like an arch shape slice when the arching effect is activated in the backfill over a ditch conduit.(Figure 3.10 (a))

The case discussed above is when an underground conduit is stiffer relative to the soil medium (i.e. a rigid conduit) and the load distribution at the top level of the conduit would be like that in Figure 3.12. In other words, the stiff conduit takes almost all of the load from overburden soil. When this occurs, Eq. 3.9d is valid. However, for the case of a flexible pipe conduit and thoroughly tamped side fills having essentially the same degree of stiffness as the pipe itself, the value of W_c given by Eq. 3.9d might be multiplied by the

ratio B_c/B_d, where B_c is the outside width of the conduit. The load from the overburden is distributed uniformly on the conduit and the soil beside it. Therefore, the load on the flexible pipe would then be:

$$W_c = C_d \times \gamma \times B_c \times B_d \qquad \text{(Eq. 3.11)}$$

It's emphasized that for Eq. 3.11 to be applicable, the side fills must be compacted sufficiently to have the same resistance to deformation under vertical load as the pipe itself. The equation can't be used merely because the pipe is a flexible type. In the actual condition, it's probable that the load on a pipe lies somewhere between the results in Eq. 3.9 and Eq. 3.11, depending upon the relative rigidity of the pipe and the sidefill columns of soil.

As to *projecting conduits*, there are two types of them, the *positive* projecting conduits and the *negative* projecting conduit. When a conduit is installed as a positive projecting conduit, shearing forces also play an important role in the development of arch action and the resultant load on the structure. In this case the planes along which relative movements are assumed to occur and on which shearing forces are generated, are the imaginary vertical places extending upward form the sides of the conduit as indicated in Figure 3.13 (a) and 3.13 (b). The width factor in the development of an expression for load is the outside width of the conduit, designated as B_c.

The magnitudes and directions of relative movements between the interior prism ABCD of Figure 3.13 (a) and (b), and the adjacent exterior prisms are influenced by the settlement of certain elements of the conduit and the adjacent soil. Marston combined these settlements into an abstract ratio, called the settlement ratio,

$$r_{sd} = \frac{(s_m + s_g) - (s_f + d_c)}{s_m} \qquad \text{(Eq. 3.12)}$$

in which

r_{sd} = settlement ratio,

s_m = compression strain of the side columns of soil of height pB_c,

p = projection ratio,

pB_c = the vertical distance from the natural ground surface to the top of the structure,

B_c = outside width of the conduit,

s_g = settlement of the natural ground surface and adjacent to the conduit,

s_f = settlement of the conduit into its foundation,

d_c = shortening of the vertical height of the conduit.

Marston also defined a critical plane, which is the horizontal plane through the top of the conduit when the fill is level with its top, i.e. when H = 0. During and after construction of the embankment, this plane settles downward. If it settles more than the top of the pipe, as illustrated in Figure 3.13 (a), r_{sd} is positive; the shearing forces on the exterior prisms move downward with respect to the interior prism. The shearing forces on the interior prism are directed downward, and the resultant load on the structure is greater than the weight of the prism of soil directly above it. This case is called "projection condition" and the arching effect increases the load on the conduit. If the critical plane settles less than the top of the conduit, like the one shown in Figure 3.13 (b), r_{sd} is negative; the interior prism moves downward with respect to the exterior prisms. The shearing forces on the interior prism are directed upward, and the resultant load on the structure is less

than the weight of the soil above the structure. This case is called the "ditch condition" and the arching effect decreases the load on the conduit.

Using the aforementioned parameters, if the shear stresses at the sides of the interior prism are developed to the top of the embankment, which is called the "complete condition", the load on the positive projecting conduits derived by Marston is:

$$W_c = C_c \times \gamma \times B_c^2 \qquad \text{(Eq. 3.13a)}$$

in which

$$C_c = \frac{e^{\pm 2K\mu(H/B_c)} - 1}{\pm 2K\mu}, \qquad \text{(Eq. 3.13b)}$$

$\mu = \tan \phi$ = coefficient of friction of fill material.

The plus signs are used for the projection condition and the minus signs are used for the ditch condition.

The two different results in the analyses of positive projecting conduits are caused by the stiffness of the buried conduit. If the conduit is rigid relative to the refilled soil, the projection condition exists like Figure 3.13 (a). If the conduit is flexible relative to the refill soil, the ditch condition exists like Figure 3.13 (b). Figure 3.14 presents the difference of the loads on conduits which have different stiffness while under the same situation. The load on the concrete pipe (rigid pipe) is consistently greater by about 50% than that on a parallel corrugated steel pipe of approximately the same diameter, i.e. the concrete pipe can take more load than the corrugated steel pipe.

In order to reduce the load on the conduit under the projection condition. Marston proposed the idea of the *imperfect ditch conduits* in 1920. Spangler provided the

analysis of loads on imperfect ditch conduits later in 1950. In the imperfect ditch conduit construction procedure, illustrated in Figure 3.9 (d), the conduit is first installed as a positive projecting conduit. Then the soil backfill at the sides and over the conduit is compacted up to some specified elevation above its top. Next, a trench of the same width as the outside horizontal dimension of the pipe is excavated down to the structure and refilled with very loose, compressible material, e.g. loosened soil, straw, or hay. The purpose of this method is to insure that the interior prism of soil will settle more than the exterior prisms, thereby generating friction forces which are directed upward on the sides of the interior prisms. The resultant load on the conduit is then reduced.

The load formula for an imperfect ditch conduit is :

$$W_c = C_n \times \gamma \times B_c^2 \qquad \text{(Eq. 3.14)}$$

where C_n is a load coefficient which is a function of the ratio of the height of fill to the width of ditch, H/B_c, the projection ratio p', and the settlement ratio r_{sd}. Spangler and Handy provided several sets of C_n diagrams with different parameter values (Spangler & Handy, 1973 & 1982). The settlement ratio, r_{sd}, is always a negative quantity in the imperfect ditch conduit case, which means the arching effect will always transmit the load at the top of conduit to the side soil media.(The direction of shear forces at the sides of the interior prism is always upward.)

The negative projecting conduit has the same function as the imperfect ditch conduit. The analysis of loads on negative projecting conduits follows the same procedures as that for imperfect ditch conduits, but uses a different width factor, B_d, instead of the width of the imperfect ditch, B_c. B_d is the width of the shallow ditch in which the pipe is in-

stalled (see the layout at Figure 3.9 (c)). The same load coefficient diagrams are applicable to both case.

3.3.4 Discussion of the Coefficient of Lateral Stress (K)

In the original formulation, Marston suggested K to be the active Rankine ratio (K_a) in his design of underground conduits. However, the other researchers, such as Krynine (1945), Ladanyi and Hoyaux, and Handy (1985) found that since K_a was derived from the assumption that the horizontal and vertical stresses are principal stresses, using K_a is only valid when there is no friction (shear stress) between the fill material and the sides of the ditch. However, Figures 3.10, 3.11, and 3.13, present that there is friction existing at the sides of the ditch. Soil arches formed in the ditch are caused by this friction. Therefore, the active Rankine ratio (K_a) cannot be used.

If the vertical sides of the ditch are where the friction of the soil is mobilized, then a new value of K can be determined from Figure 3.15 (Iglesia et. al., 1990). In this figure, the distance from the point of origin in the τ-σ coordinate to the center of the Mohr circle is $OC = 1/2 \cdot (\sigma_h + \sigma_v)$. If the stress at the vertical sides of the ditch lie tangent to the failure envelope, the radius of the Mohr circle is $R = OC \cdot \sin\phi$. Since the radius R can also be expressed as $\frac{(\sigma_v - \sigma_h)}{2\sin\phi}$, therefore:

$$\frac{(\sigma_v - \sigma_h)}{2\sin\phi} = \frac{1}{2}(\sigma_h + \sigma_v)\sin\phi \qquad \text{(Eq. 3.15)}$$

Eq. 3.15 can be rearranged to:

$$\sigma_h = K_K \cdot \sigma_v \qquad \text{(Eq. 3.16)}$$

in which

$$K_K = \frac{1-\sin^2\phi}{1+\sin^2\phi} = \frac{\cos^2\phi}{1+\sin^2\phi} \qquad \text{(Eq. 3.17)}$$

3.4 Silo Theory

The formula for computing the pressure/force acting at the bottom of a silo was first developed by Janssen in 1895 (Jakobson, 1958). Using the layout in Figure 3.16 (Evans, 1983), a silo full of granular material with diameter B and height H, one can determine F, the vertical force on the base. Consider the forces acting on the horizontal differential element of height *dh*, diameter B, and at depth h. Vertical forces on the element are the downward directed force on the top (V), the upward force on the bottom (V+dV), and the element's self weight ($W = \gamma\pi B^2 dh/4$). The lateral stress, $\sigma_h = 4KV/\pi B^2$, is symmetric about the centerline, producing no net force on the element (where K is the coefficient of lateral stress).

The silo theory is based on two assumptions: (1) The coefficient of lateral stress (K) has the same value at all depths, and (2) the material settles with respect to the side walls sufficiently to develop shear stresses over the full depth of the silo. Therefore, if the element is assumed to move downward with respect to the rigid walls of the silo, the upward acting shear stresses developed will be:

$$\tau = \frac{4KV\tan\phi'}{\pi B^2} \qquad \text{(Eq. 3.18)}$$

in which $\tan\phi'$ = the coefficient of friction between the granular material and the silo's walls. These shearing stresses contribute to an upward acting vertical force on the element which is equal to $\tau \times dh \times \pi B$. The vertical equilibrium is therefore:

$$V + dV + \frac{4KV\tan\phi' dh}{B} = V + \frac{\gamma\pi B^2 dh}{4} \qquad \text{(Eq. 3.19)}$$

Solving this linear differential equation:

$$V = \frac{\gamma\pi B^3}{16K\tan\phi'}\left(1 - e^{-4K\tan\phi'(h/B)}\right) \qquad \text{(Eq. 3.20)}$$

The force acting on the base of the silo (F) is obtained by substituting H (height of the silo) for h in the above equation.

The arching effect decreases the force exerted on the base of a silo since all the shear stresses between the side wall of the silo and the granular material in the silo are upward. It was also assumed that the vertical normal pressure was uniformly distributed. But in fact, according to the experiments performed by later researchers, this assumption was incorrect. Hence, Jakobson proposed a new method to find out silo pressure. He assumed that every point of the contained mass settles vertically when the load increases, which means that the ratio between the horizontal normal pressure and the vertical pressure at every point is equal to the coefficient of earth pressure at rest (Jakobson 1958). Under this condition, uniform vertical normal pressure distribution is unnecessary. He used the equilibrium equations in a cylindrical coordinate to find the normal force at the base of a silo:

$$\frac{\partial\tau_{r\theta}}{\partial r} + \frac{1}{r}\frac{\partial\sigma_\theta}{\partial\theta} + \frac{\partial\tau_{\theta z}}{\partial z} + \frac{2\tau_{r\theta}}{r} = 0 \qquad \text{(Eq. 3.21a)}$$

$$\frac{\partial \tau_{rz}}{\partial r}+\frac{1}{r}\frac{\partial \tau_{\theta z}}{\partial \theta}+\frac{\partial \sigma_z}{\partial z}+\frac{\tau_{rz}}{r}=\gamma \qquad \text{(Eq. 3.21b)}$$

$$\frac{\partial \sigma_r}{\partial r}+\frac{1}{r}\frac{\partial \tau_{r\theta}}{\partial \theta}+\frac{\partial \tau_{rz}}{\partial z}+\frac{\sigma_r-\sigma_\theta}{r}=0 \qquad \text{(Eq. 3.21c)}$$

,in the case here:

$$\sigma_r=\sigma_\theta=\sigma_h=K\cdot\sigma_z \qquad \text{(Eq. 3.21d)}$$

$$\tau_{r\theta}=\tau_{\theta z}=0 \qquad \text{(Eq. 3.21e)}$$

$$\tau_{rz}=\tau \qquad \text{(Eq. 3.21f)}$$

where

τ = the vertical and (horizontal) shear stress,

r = the distance from the center of the silo,

σ_z = vertical normal pressure at the depth z,

K = the coefficient of lateral stress,

γ = unit weight of the contained mass.

Substitute the parameters in Eq. 3.21a to Eq. 3.21. Then, Eq. 3.21 can be rearranged as follows:

$$\frac{\partial \tau}{\partial r}+\frac{\partial \sigma_z}{\partial z}+\frac{\tau}{r}=\gamma \qquad \text{(Eq. 3.22a)}$$

$$K\cdot\frac{\partial \sigma_z}{\partial r}+\frac{\partial \tau}{\partial z}=0 \qquad \text{(Eq. 3.22b)}$$

,with the boundary conditions:

$\tau=\sigma_z=0$, for $z=0$, (Eq. 3.22c)

$\tau=\tan\phi'\times K\times\sigma_z$, for $r=R$ (the radius of silo) (Eq. 3.22d)

The solution of these equations is very complicated. Jakobson found the solution by the use of expansion series. Some values of the vertical normal pressure close to the wall (r=R) and in the center (r=0) were calculated. The calculated vertical normal pressure at r=R agreed with the result from Janssen's method ($\sigma_z = V/\pi R^2$), which assumed the vertical normal pressure was uniformly distributed. This suggested that Janssen's method still could be utilized under some situations, although his assumption of normal stress distribution was inappropriate.

Jakobson (1958) also discussed the ratio between the horizontal normal pressure and the vertical pressure (K). He believed that this ratio must amount to a certain minimum value which is greater than the ordinary coefficient of active pressure (K_a), even when the silo walls yield a lot.

3.5 Ground Arch Approach and Ground Dome Approach

3.5.1 Background

Some general principles about underground conduits were outlined by Marston and his associates (Spangler, 1964). However, there was little information pertaining to predicting the collapse loading for a soil-structure system involving a flexible tube, arch, or dome. Some of the important questions left unanswered were as follows: If the structure yields suddenly, can an arch "immediately" form in the surrounding earth, and also what strength and stiffness is necessary in the surrounding soil to ensure that a thin arch will fail by compressive yielding rather than by buckling or bending? In order to find the answers, Whitman, et. al. (1962 & 1963) made observations from small-scale tests on thin

metal domes buried within a coarse dry sand (static loading). They found that the level of pressure required to cause failure of the buried dome was several times that required for failure of an unburied dome. They postulated that a sand dome had developed above the structure, assuming some of the load which had previously acted upon the structure. This explained the reason that higher pressure was needed to cause the failure of a buried dome.

3.5.2 Ground Arch/Dome Approach

After Whitman et. al. (1962 & 1963), several researchers proposed a similar "structural" hypothesis to explain the load redistribution around a yielding structure. In the planar condition, they suggest that when the adjacent soil deforms or yields, an arch or ring will form within the soil. In the spatial condition, a dome or sphere will develop in the soil. Once these "ground-structures" are developed, they will redistribute loads away from the actual buried structure and only part of the original overburden pressure will be transmitted to the structure itself.

Figure 3.17 shows some examples. These soil arches and domes were proposed by Nielson in 1966. The differential soil arch in Figure 3.17 (a) was used to determine arching over a buried conduit. The arch was assumed to be circular, with supports located on the surfaces of maximum shear stress (these surfaces are determined by the elasticity theory). Then the problem was solved using numerical procedures and a computer solution (code) was presented. Later on, Nielson extended this approach to some non-circular structures. A rectangular underground structure is shown in Figure 3.17 (b). He also

applied the approach to a three-dimensional structure(Figure 3.17 (c)). In the three-dimensional case, a differential soil shell was formed. This was accomplished by putting a soil dome above the underground structure to assume part of the overburden pressure at the top of the structure. However, no attempt was made to formulate the solutions for the rectangular case and the three-dimensional case (Evans, 1983).

As to the increased load-carrying capacity of the buried structure, Luscher and Höeg (1964 & 1965) attribute it to three types of action by soil around the buried structure: pressure redistribution, deformation restraint, and arching. They proposed a study to analyze the aforementioned interactions between a buried cylindrical tube and the surrounding soil under large applied loads. These three types of action are briefly explained as follows:

(1) The restrain against tube deformations in the second mode (that is, counteracting the deformation from the originally circular shape into a horizontal ellipse, see Figure 3.18) by mobilization of lateral passive earth pressures is called "pressure redistribution" (Luscher & Höeg, 1965). In the other words, this restrainment causes stresses to redistribute to a more uniform configuration as the crown deflects vertically and the springlines horizontally.

(2) The action against deformations in the third and higher modes (see Figure 3.18) enhances the resistance of the tube against buckling failure by forcing it to buckle in higher modes rather than in an unsupported situation: this action is called "deformation restrain" (Luscher & Höeg, 1965). The buckling resistance of the

tube is increased dramatically here, i.e. the load-carrying ability of the tube is increased greatly at this process.

(3) The reaction of the surrounding soil to tube deformations in mode one (pure compression) or mode zero (rigid body motion) is called "arching". Redistribution of pressure away from or onto the tube, depending on the relative compliances of tube and soil surrounding, is defined as active or passive arching, respectively (Luscher & Höeg, 1965).

The distinction between these three actions was somewhat artificial and arbitrary. Because the effects operate simultaneously, they influence each other. In Luscher and Höeg's experiments on buried flexible tubes, they concluded that a sand ring, as shown in Figure 3.19 formed around the tube when deflection occurred. They believed that the vertical-sliding-surface concept (Figure 3.5 and Figure 3.6) from Terzaghi (1943) should be replaced by the concept of thrust-ring action, i.e. structural arches or domes forming in the soil. Only dry, cohesionless soils were specifically considered in their research. However, Luscher and Höeg believed their conclusions apply in a general way to any soil.

There are also numerous field data supporting the contention that buried structures have a much higher load-carrying capacity. These data were presented by Davis and Bacher (1968) in their California's Culvert Research Program. They gave magnitudes of actual loads experienced and ultimate capacities of culverts installed using several different backfills and backfilling techniques as well as load capacities of unburied culverts.

Another structural analogy for arching was also proposed by Getzler, et. al. (1968) in experiments which they conducted with structures having various roof shapes. Their

experimental setup is shown in Figure 3.20. The analytical model they utilized is shown in Figure 3.21. They proposed a soil arch on the top of the buried structure. This arch sits on the soil abutments, which are the soil bodies at the side of the structure. However, in their study, no theoretical formulation was presented. They reached a conclusion in their experiments about the effect of different roof shapes of buried structures. They summarized that buried structures with triangular or arch shape peak roofs, experienced greater load reduction from arching than structures with flat roofs. Similar experimental results from Whitman et. al. were found in 1962. In Whitman's tests a flat roof experienced approximately 50% higher total load than a hemispherical roof at the same depth of soil cover. Luscher and Höeg (1964) also discussed this problem in their study. They believed the roof shape was an important factor to be considered when the stress acting on a buried structure was analyzed. The vertical-sliding-surface analysis does not take into account the geometric configuration of a buried structure but the trust ring method (Figure 3.19) takes into account the shape of the buried structure.

The above soil structural approaches provided explanations for the increase of the load-carrying capacity of the buried structures and also showed the interaction between the structure and soil body. Nevertheless, these approaches are rarely used in actual application. Selig (1975) released a paper to summarize the basic concepts of soil-structure interaction and the nature of the stresses and deflections associated with buried structures. He used the large corrugated-metal buried structures, which are commonly referred to as "flexible' structures, to verify different approaches of the "soil-structural" analysis. He pointed out that the aforementioned approaches have never been fully developed. In order

to obtain the results, engineers have to make a lot of assumptions such as the shape of the arch or dome, locations of the supports, conditions at the supports ,and interference behavior between elements. However, with different assumptions, the results may vary a lot. These assumptions give the risk and inconvenience to the engineers when they use these approaches.

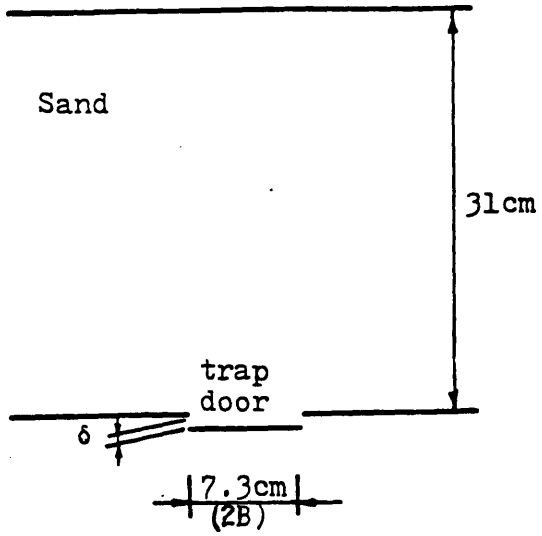

Figure 3.1 Terzaghi's Experimental Set-up (Terzaghi, 1936)

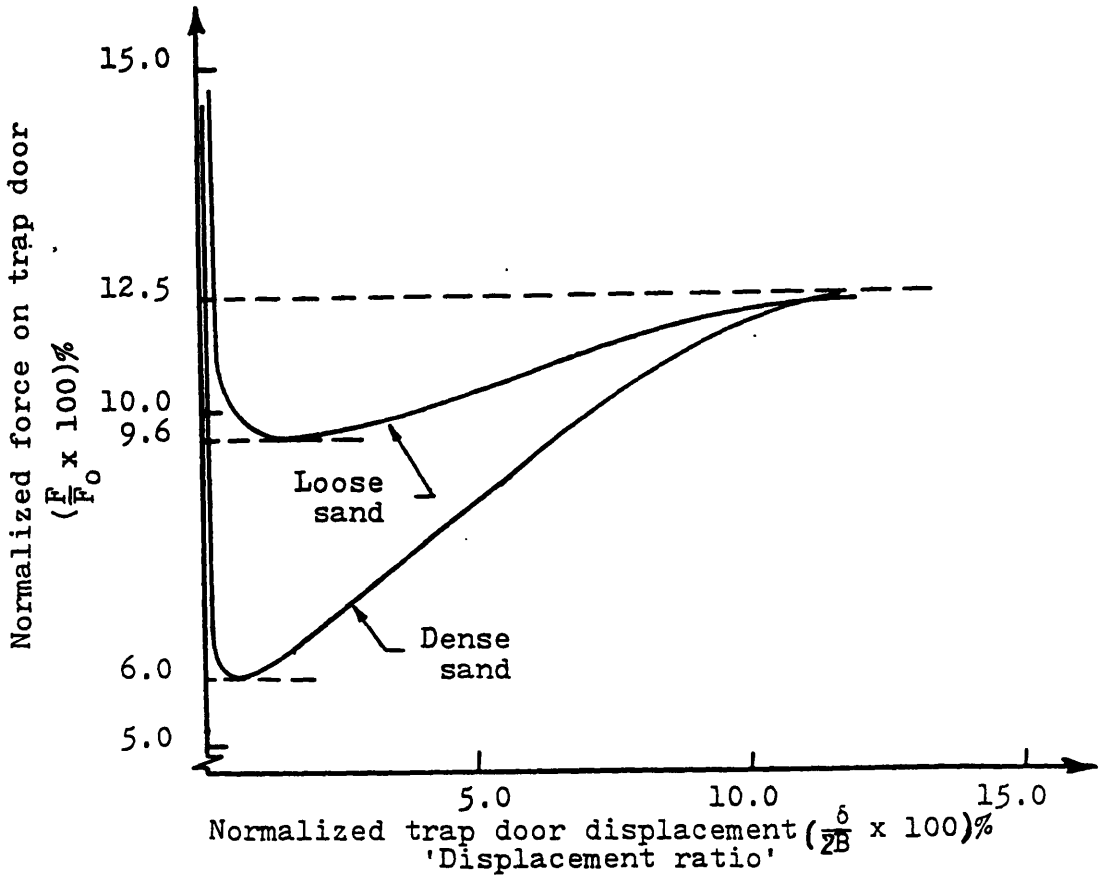

Figure 3.2 Terzaghi's Experimental Results: Vertical Force on Trap Door *vs.* Displacement of Trap Door (Terzaghi, 1936; Revised by Evans, 1984)

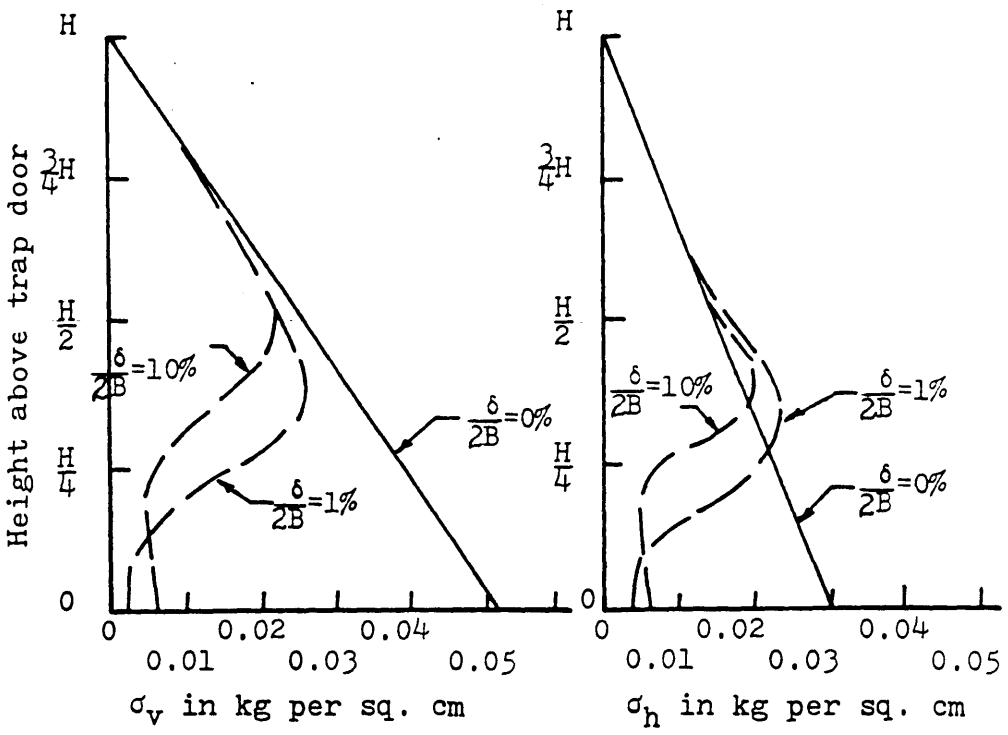

Figure 3.3 Terzaghi's Experimental Results: Vertical and Horizontal Stresses in Soil Body *vs.* Depth (Terzaghi, 1936; Revised by Evans, 1984)

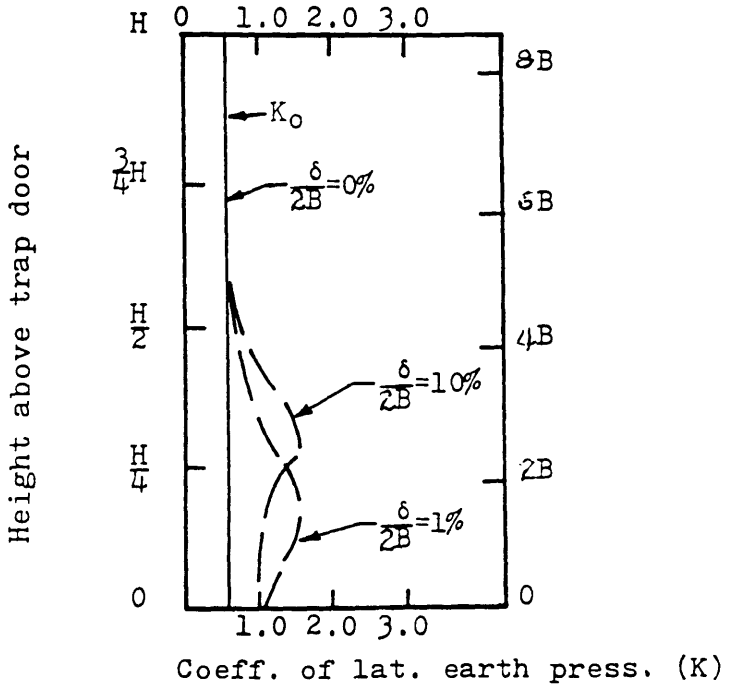

Figure 3.4 Terzaghi's Experimental Results: Coefficient of Lateral Earth Pressure (K) *vs.* Depth (Terzaghi, 1936; Revised by Evans, 1984)

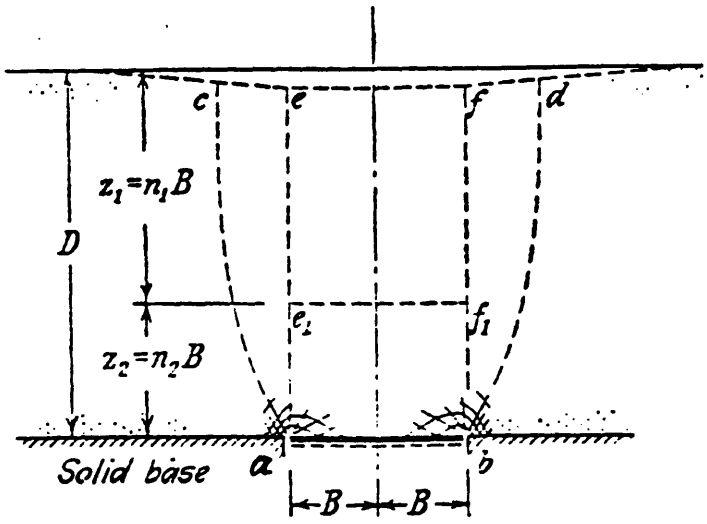

Figure 3.5 Yielding in Soil Caused by Downward Movement of a Long Narrow Section (**ab**) at the Base; Curve **ac** & **bd**: Actual Sliding Surfaces, Line **ae** & **bf**: Assumed Sliding Surfaces (Terzaghi, 1943)

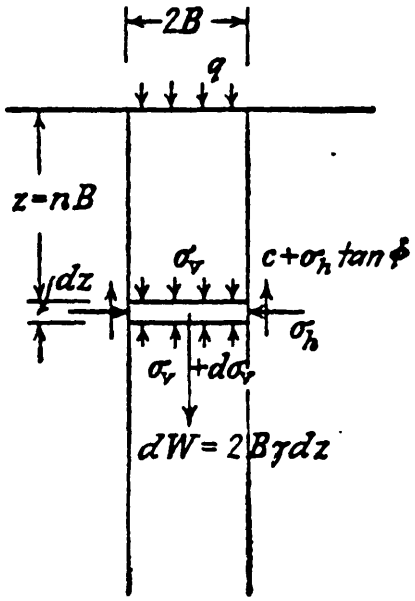

Figure 3.6 Free Body Diagram for a Slice of Soil in the Yielding Zone (Terzaghi, 1943)

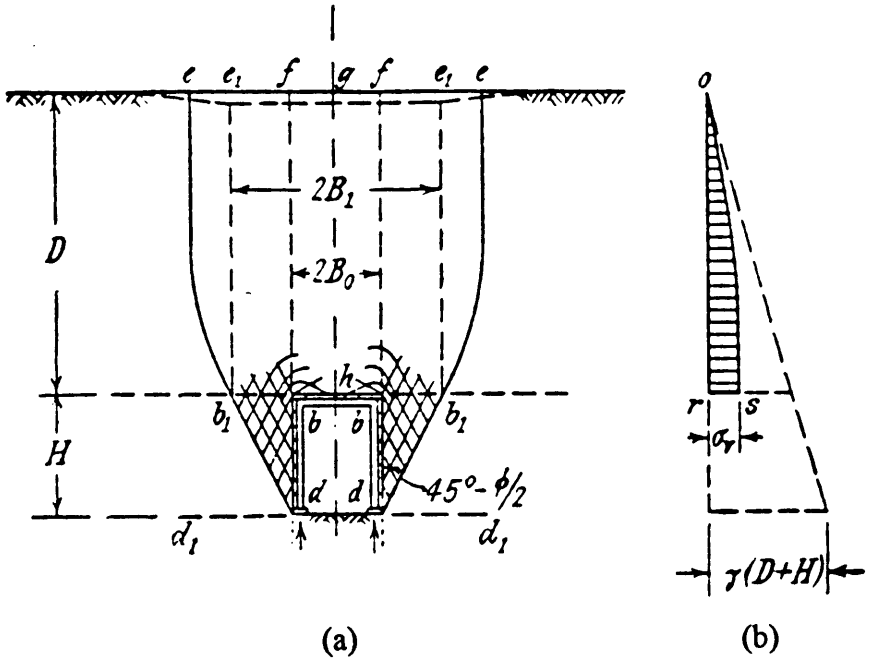

Figure 3.7 (a) Flow of Soil Toward Shallow Tunnel When Yielding Happened in the Soil Body; Curve $\mathbf{eb_1}$: Actual Sliding Surface, Line $\mathbf{e_1b_1}$: Assumed Sliding Surface, (b) Vertical Stress Profile in Soil Located above the Tunnel (Terzaghi, 1943)

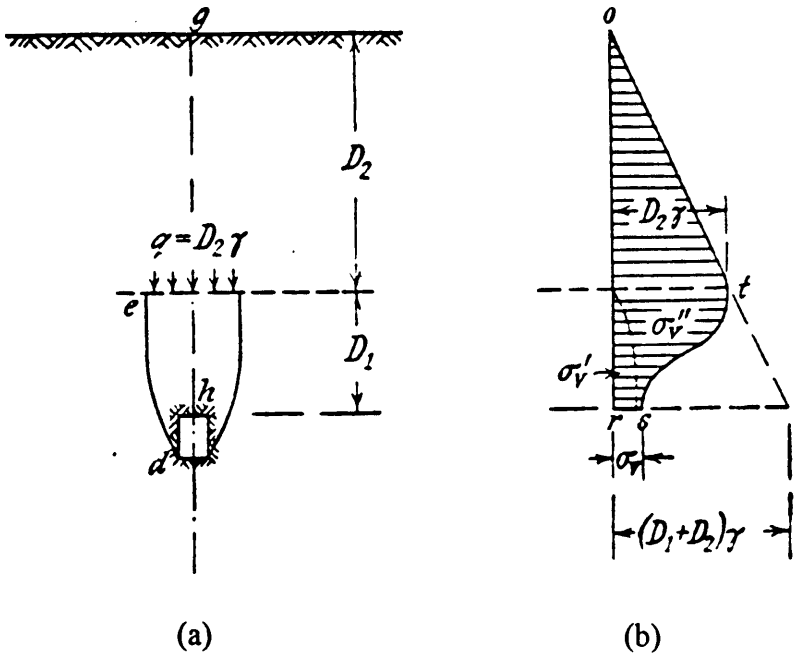

Figure 3.8 (a) Yielding Zone in Soil When Tunnel Located at Great Depth, (b) Vertical Stress Profile in Soil Located above the Tunnel (Terzaghi, 1943)

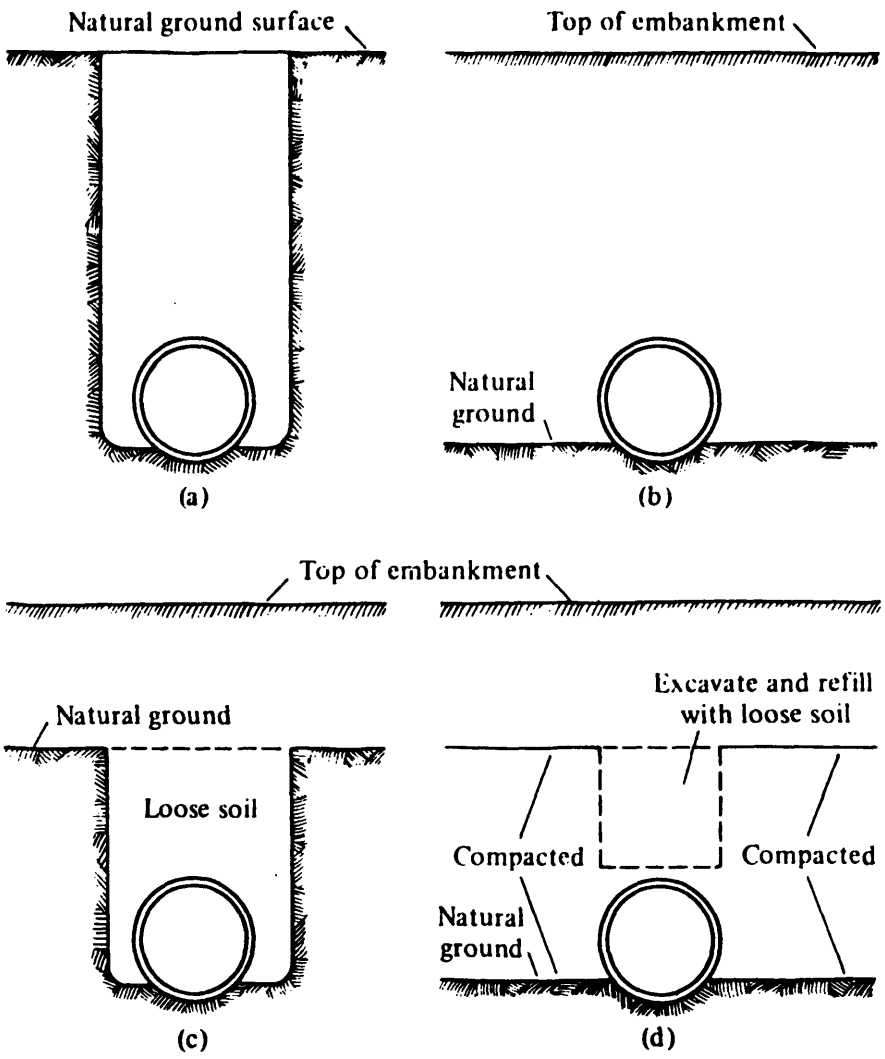

Figure 3.9 Various Classes of Conduit Installations: (a) Ditch Conduit, (b) Positive Projecting Conduit, (c) Negative Projective Conduit, and (d) Imperfect Ditch Conduit (Spangler & Handy, 1973)

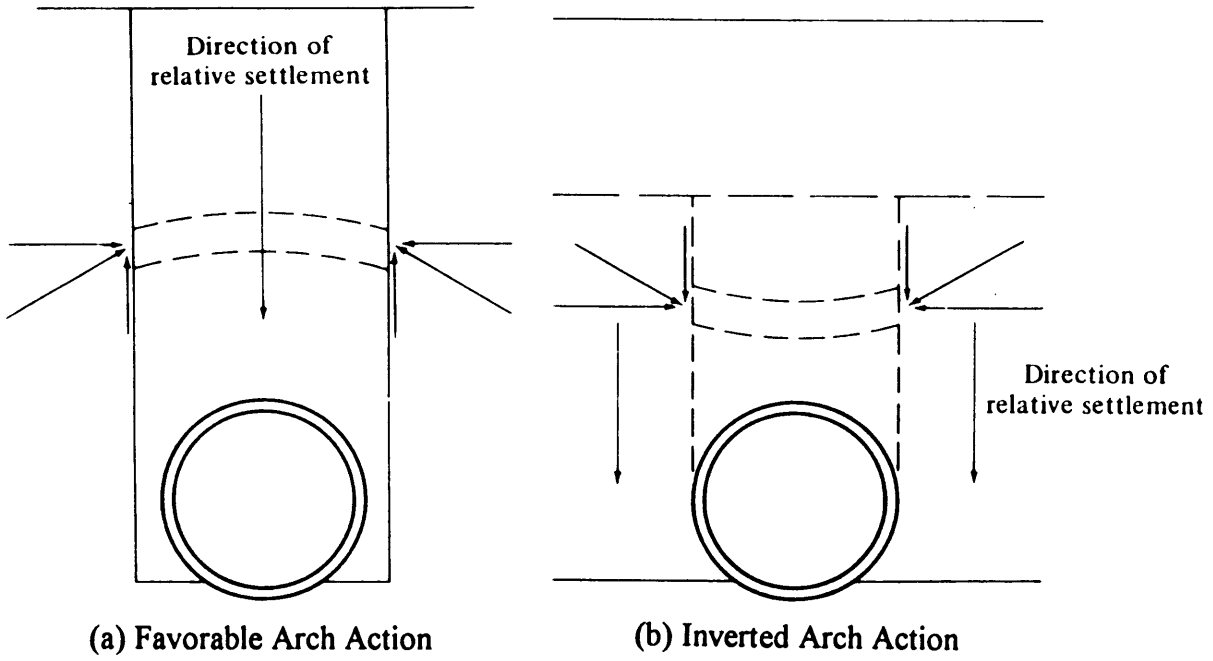

Figure 3.10 Arching Effect in Underground Conduits: (a) Favorable Arch Action, (b) Inverted Arch Action (Spangler & Handy, 1973)

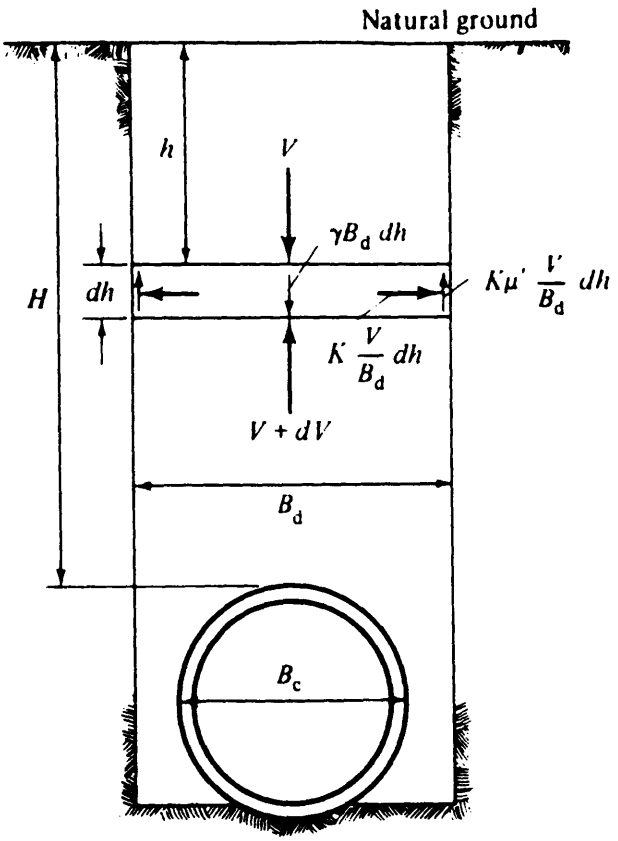

Figure 3.11 Free Body Diagram for Ditch Conduit (Spangler & Handy, 1973)

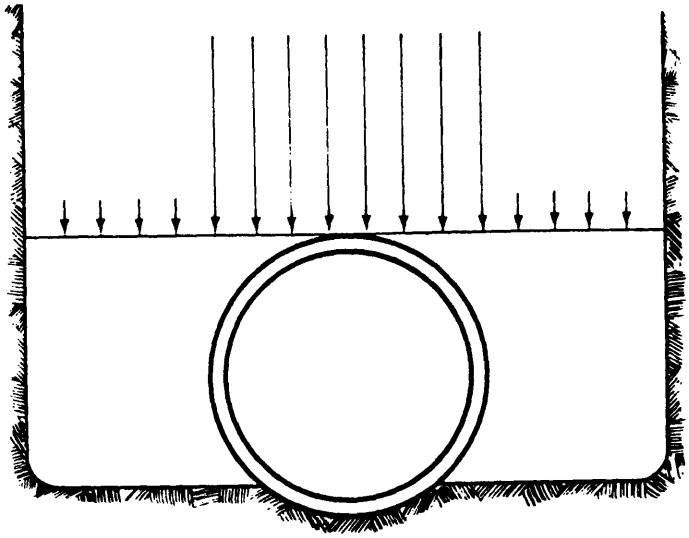

Figure 3.12 Load Distribution at Level of Top of Pipe (when sidefill soil columns are more flexible than the pipe, from Spangler & Handy, 1973)

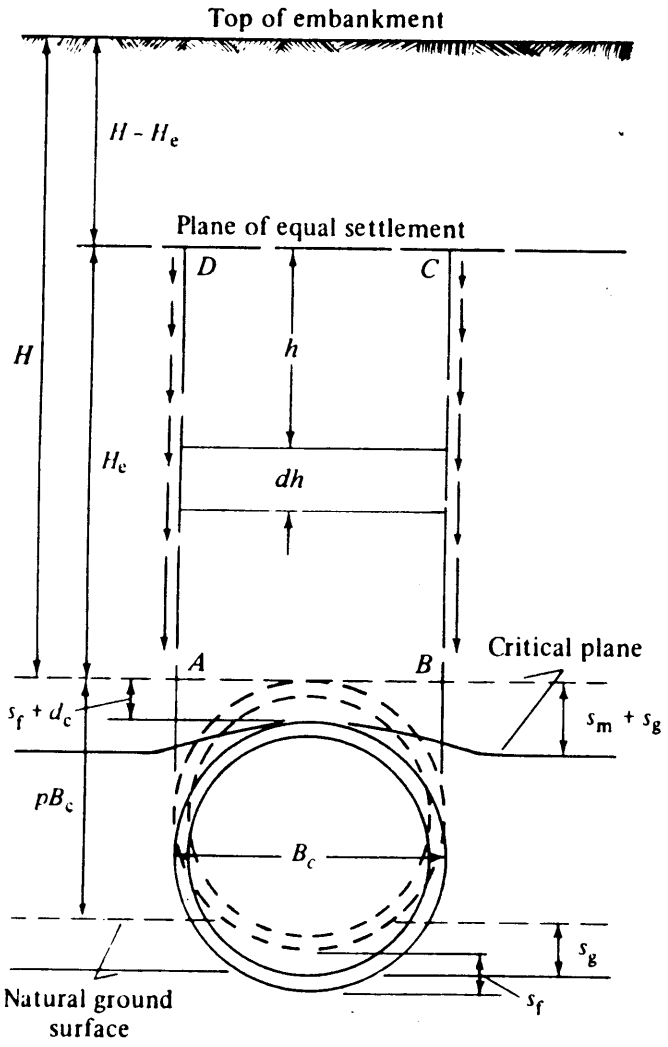

(a) Rigid Conduit/ Projection Condition

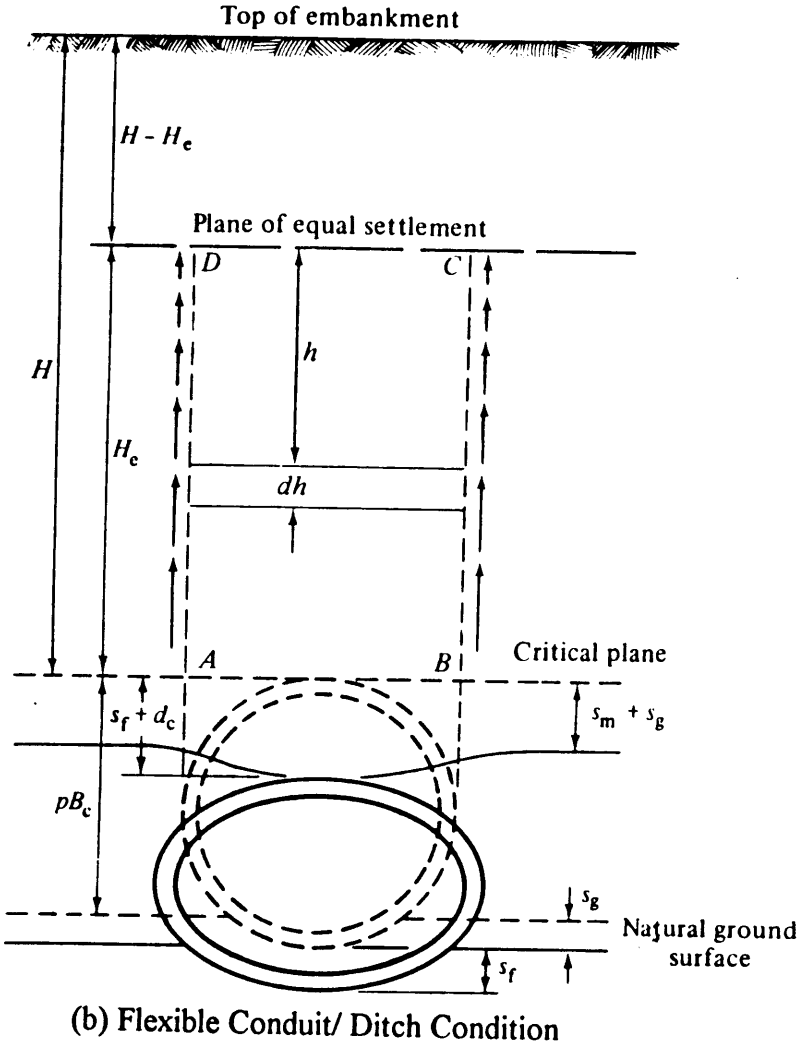

(b) Flexible Conduit/ Ditch Condition

Figure 3.13 Settlements Which Influence Loads on Positive Projecting Conduits
(Spangler & Handy, 1973)

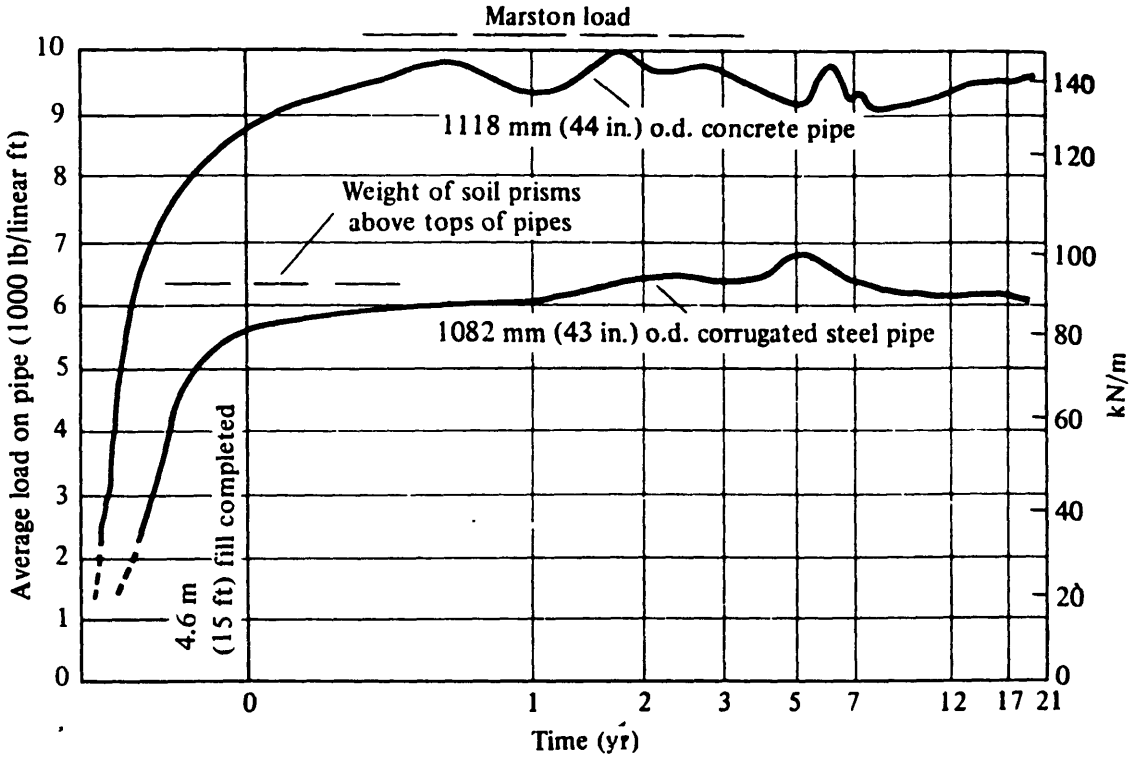

Figure 3.14 Comparison of Measured Loads on Rigid Pipe and Flexible Pipe (Spangler & Handy, 1973)

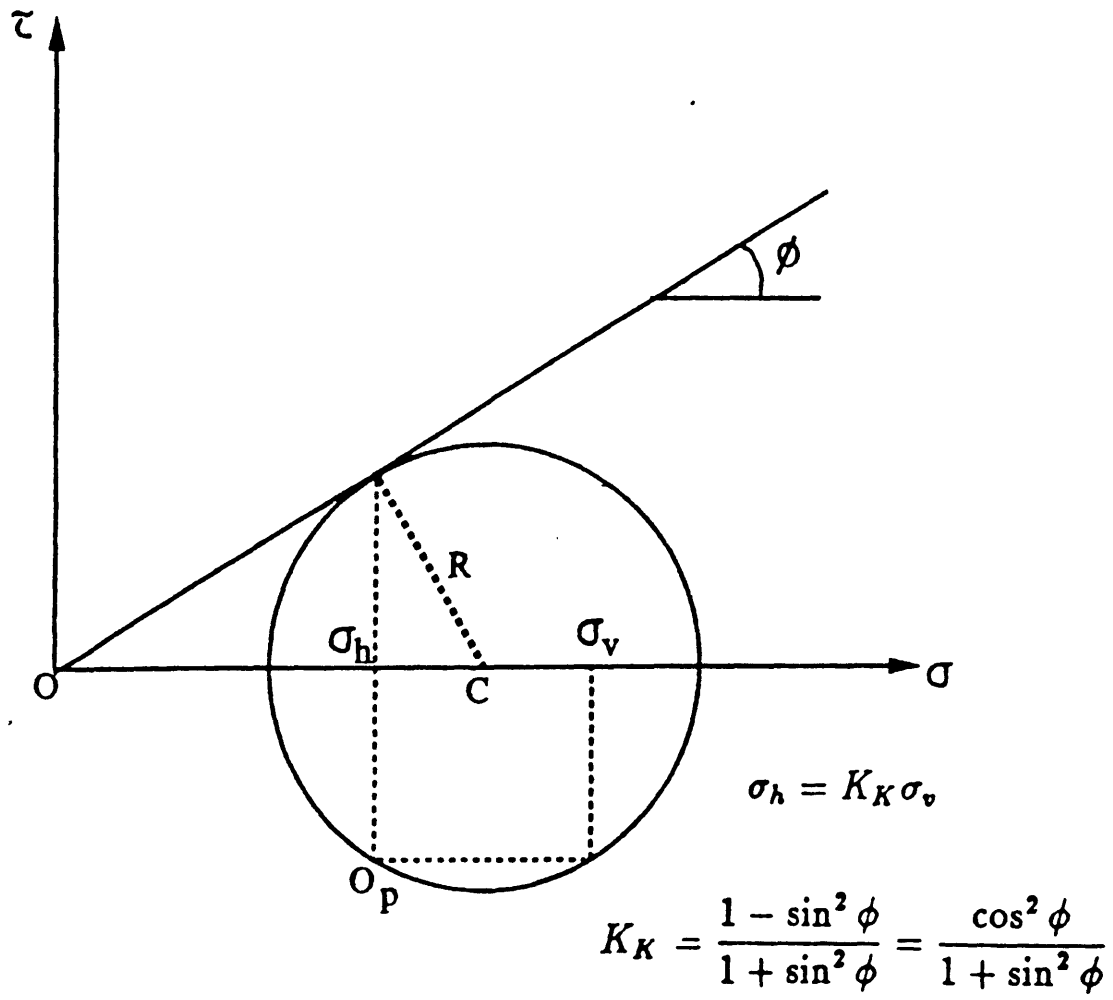

Figure 3.15 The Coefficient of Lateral Stress (K) for the Design of Underground Conduits (Iglesia et. al., 1990)

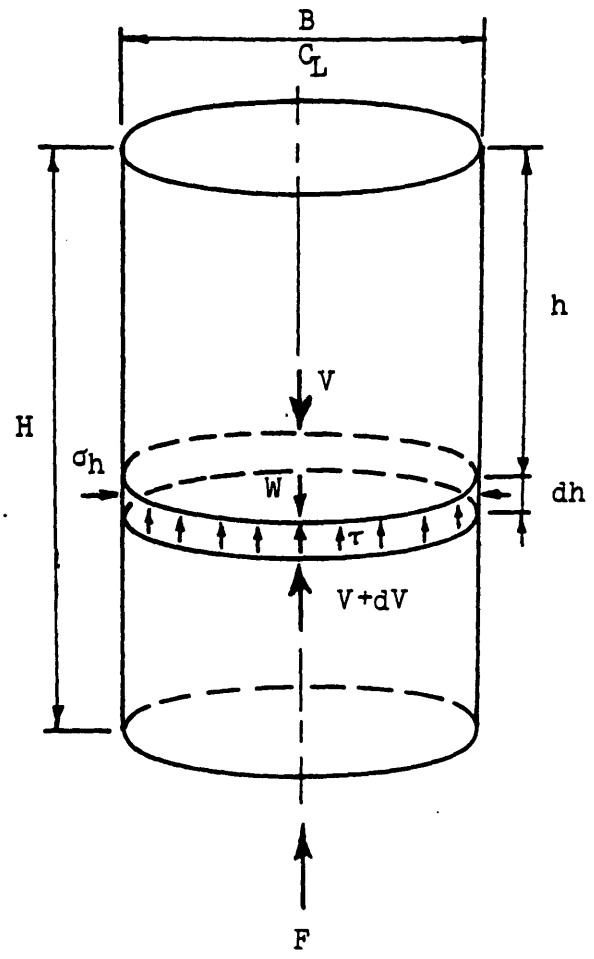

Figure 3.16 Free Body Diagram for Silo Theory (Origin form Janssen (1895), the picture shown here is the revised plot from Evans (1984).)

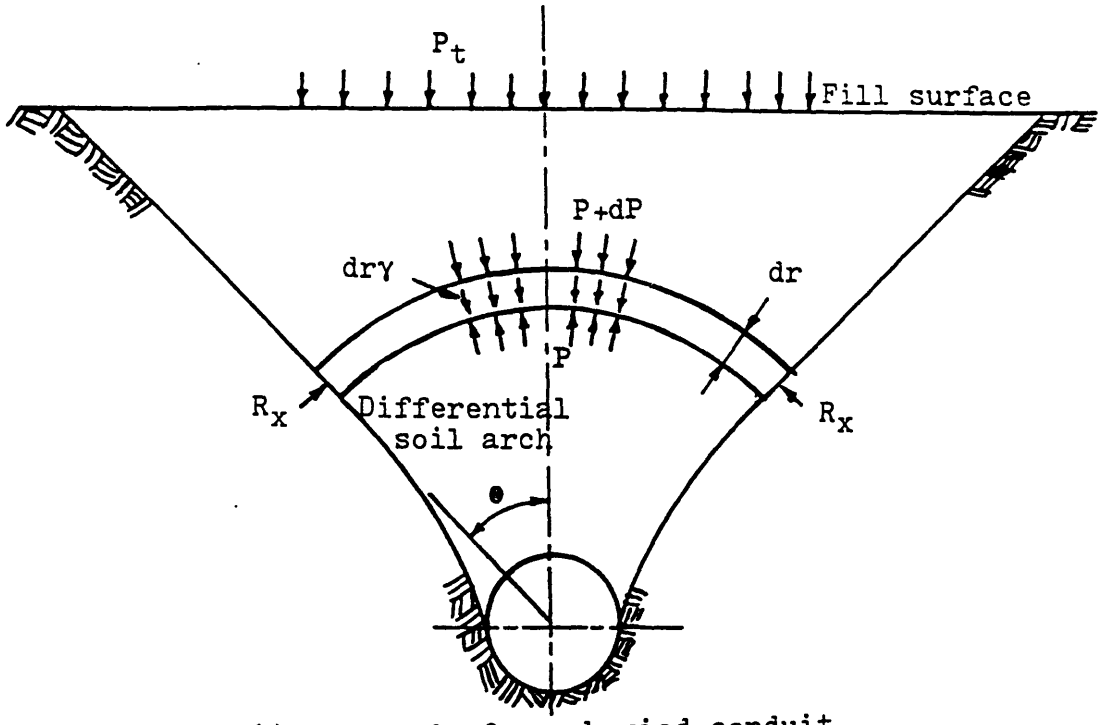

(a) Free body for a buried conduit

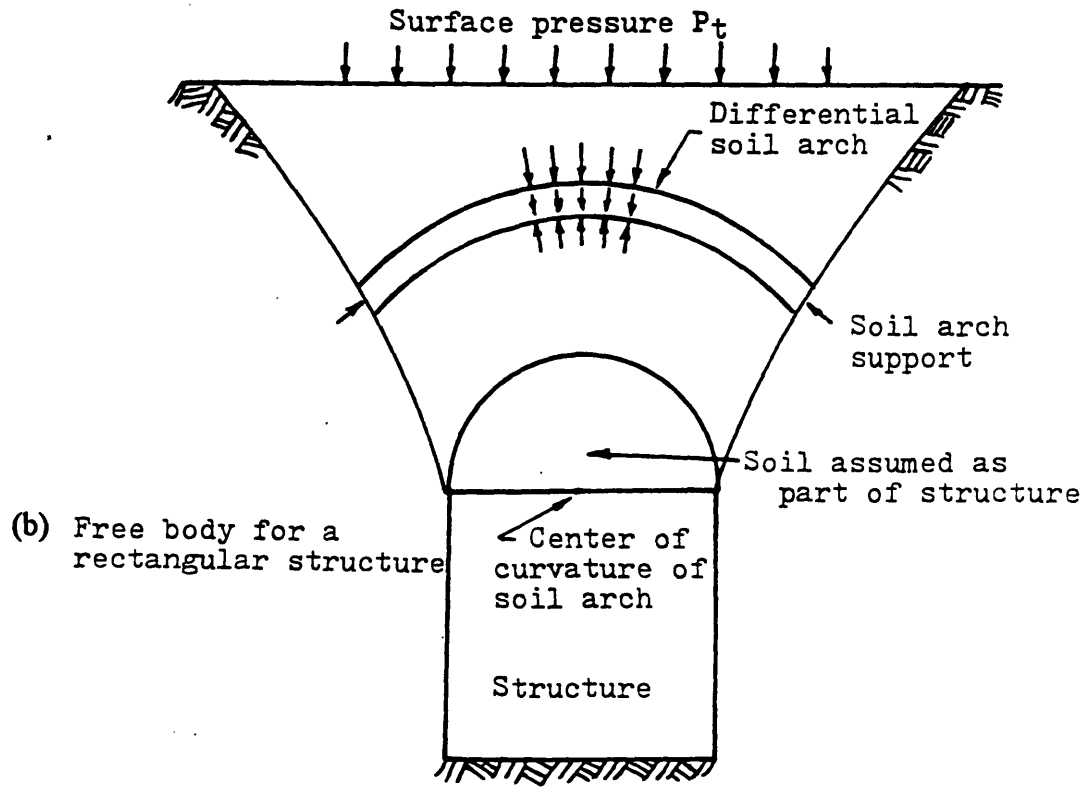

(b) Free body for a rectangular structure

Figure 3.17 Free Body Diagram for Nielson's Arching Analysis (Nielson, 1966)

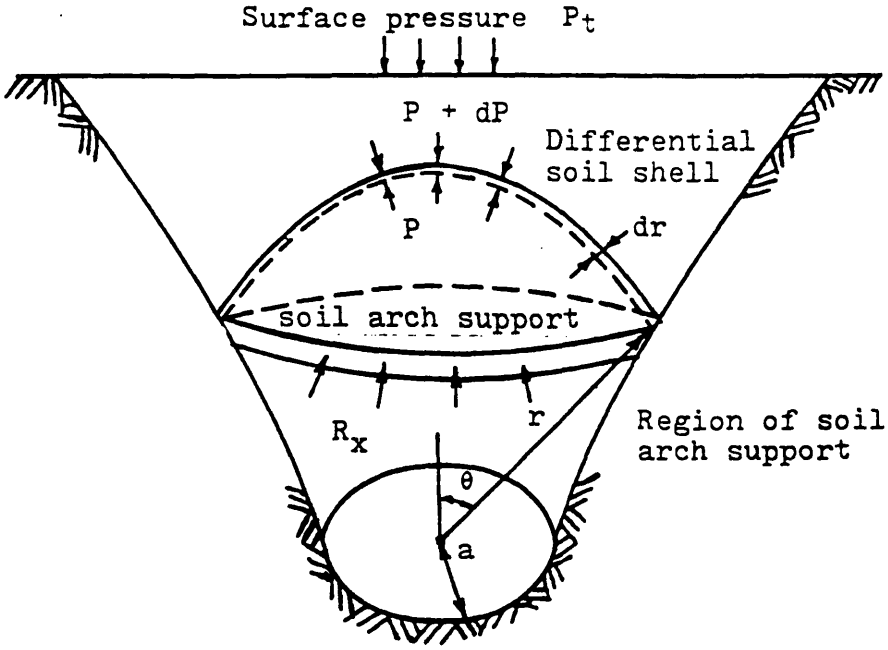

(c) Free body for a three-dimensional structure

Figure 3.17 (cont'd) Free Body Diagram for Nielson's Arching Analysis (Nielson, 1966)

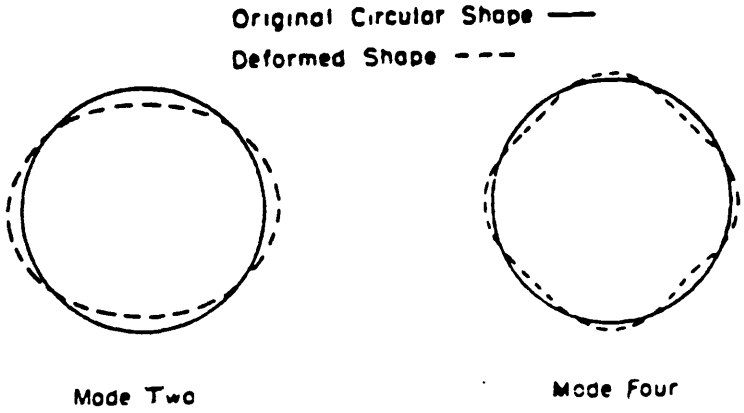

Figure 3.18 Deformation of Tubes: Mode Two and Mode Four (Luscher & Höeg, 1964)

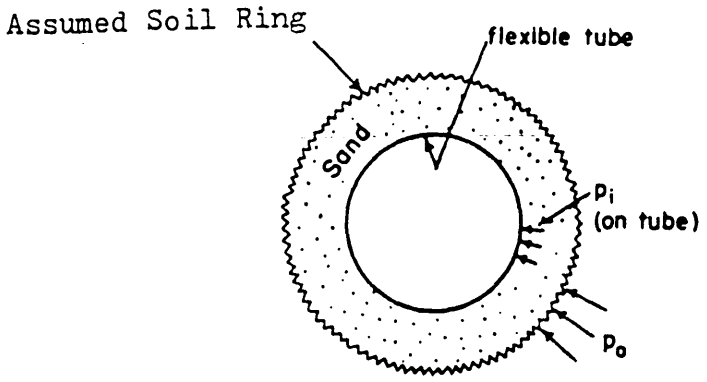

Figure 3.19 Soil Arching as A Thrust Rings About the Structure (Luscher & Höeg, 1964)

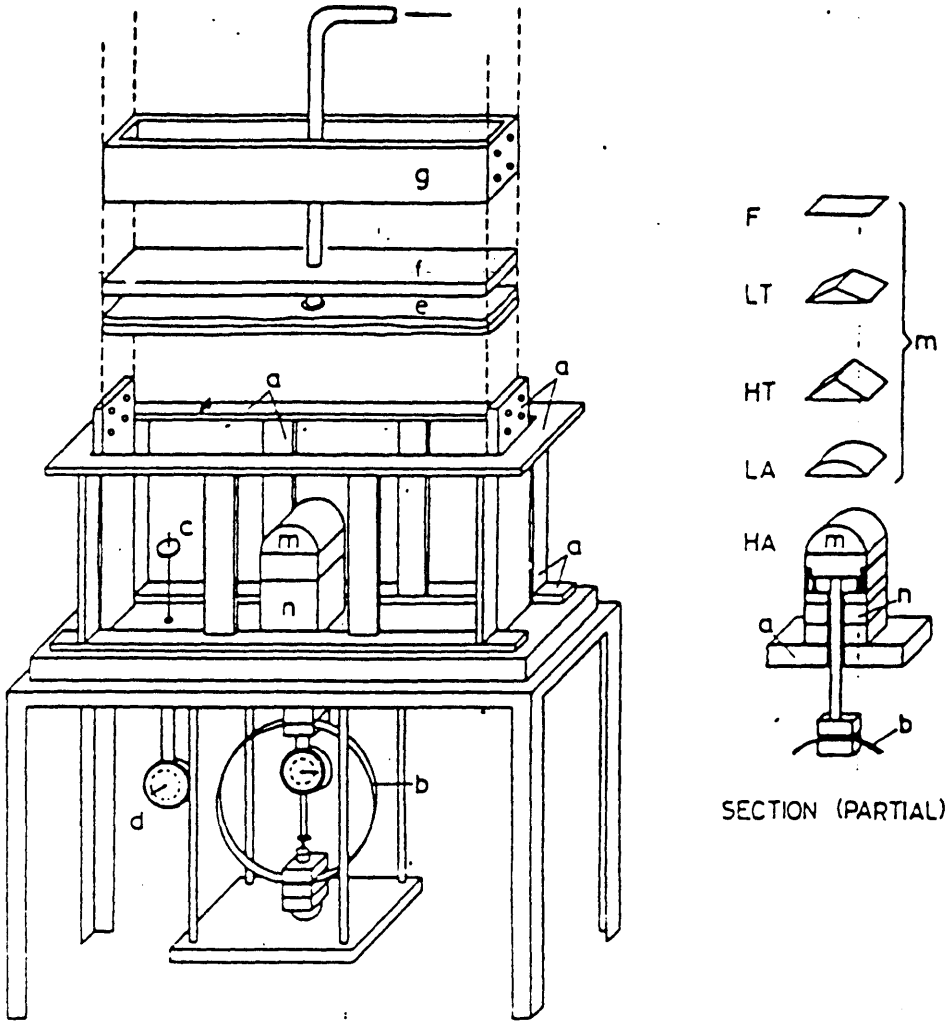

Figure 3.20 Trap Door Test Instrument with Various Roof Shapes (Getzler et. al., 1968)

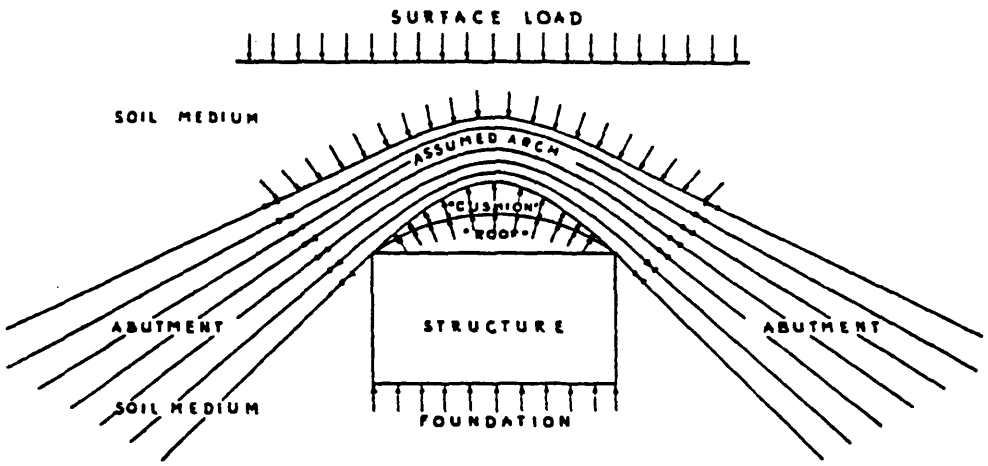

Figure 3.21 Soil Arching as An Arch Above the Structure (Getzler et. al., 1968)

Chapter FOUR
Analytical Approaches

4.1 Introduction

In this chapter, several theoretical solutions will be discussed. First are the continuum approaches which use the elasticity theory and the plasticity theory to study the stress redistribution in the trap door experiment and arching in underground construction. Second, several discontinuum methods will be illustrated for comparison with the continuum methods. There is, however, little research dealing with the discontinuum approaches because of their complexity and because continuum approaches can generally describe soil behavior quite well.

Numerical analyses utilized to study underground openings are also examined in this chapter. These analyses are perhaps the most comprehensive methods available for the analysis of stress redistribution around buried structures. Numerical analyses allow one to analyze problems with complications such as involved geometries, concentrated loads, non-homogeneity, and anisotropic behavior. Theoretical solutions will have limitations due to their assumptions which are used to simplify problems. Numerical analyses are more flexible regarding their assumptions and, therefore, can generate solutions closer to the real situations. Several numerical analyses used to study arching will be introduced in this chapter. They include the analyses by the finite different method and finite difference method. A new numerical simulation using the distinct element method (Sakaguchi & Ozaki, 1992) is also presented.

4.2 Continuum Approaches Using Elasticity Theory

An underground structure is normally treated with continuum approaches to simplify the analysis of its mechanical behavior. Determination of the stress distribution in continua is usually based on elasticity theory. In other words, the mechanical behavior of the geomaterial and of the underground structure are assumed elastic. Some researchers, however, do not believe solutions based on elasticity theory can describe the real mechanical behavior of ground-structure systems, since most of the deformations caused by the ground-structure systems are inelastic. This is especially prevalent, when we try to describe arching phenomena in the ground, since arching effects occur mostly in a ground-structure system which deforms plastically. This section introduces the elastic solutions.

Finn (1963) presented closed form solutions for the change in vertical stress resulting from translation or rotation of a trap door. Figures 4.1 (a) and (b) show the two boundary conditions in his analysis. Figure 4.1 (a) is the pure translation case and Figure 4.1 (b) is the pure rotation case. In these figures, the vertical displacement (v) and the vertical stress (σ_y) on the ground surface are both assumed to be equal to zero. A plane strain condition is assumed with the soil treated as an elastic medium with unit weight (γ) resting on a rigid horizontal boundary with a trap door located in it. The rigid base is considered frictionless ($\tau_{xy} = 0$) initially (Figure 4.1 (a) (b)) but is then treated as frictional and cohesive later. The trap door has a width equal to $2b$. The depth of soil is assumed to be infinite ($h \rightarrow \infty$). The displacement of the trap door is d. Finn restricted his analysis to problems where displacement of the soil was very small and entirely elastic.

A typical distribution of the change in vertical stress across the base for a downward translating door is shown in Figure 4.2. Infinite tensile stresses develop near the edges of the trap door, while infinite compressive stresses occur on the base next to the door. The results obtained by the theory of elasticity from Finn (1963) were checked against available published experimental and field results. The stress distributions, the approximate location of the force resultants, and the influence of the various types of displacements predicted by the analysis were in reasonable agreement with the published results (Finn, 1963). However, one big obstacle to the determination of these values was the displacement of the trap door, *d*. These predicted results were only good for very small d values.

Finn also applied his solution based on elasticity theory to the analysis of retaining walls. Figure 4.3 shows the layout of a retaining wall which is similar to the set-up in Figure 4.1 (a). But the trap door is changed (erected) to be a retaining wall. The horizontal displacement of the retaining wall is equal to the vertical translation movement of the trap door. The pressure on the wall due to this displacement, however, will only be the pressure on one half of the trap door because the displacement is modified by the effect of removing the stresses on the line corresponding to the free surface of backfill (Figure 4.3). Based on the aforementioned method, Finn found that the resulting pressure distribution against a translating wall corresponded to the results of Taylor's method (1948). He suggested a combination of his translation and rotation solutions could be used to predict the stress distribution of a general retaining wall.

In Finn's study, the depth of the soil was always taken as infinite which imposed restrictions in adapting the solution to practical problems of finite soil depth. Chelapati (1964) presented a study using Finn's model but dealt with the stresses in a soil field of finite depth, h. The soil mass was again assumed to be a homogeneous, elastic, isotropic medium but subjected to high overburden pressure, i.e. $\sigma_y = P_0$. The geometry and boundary conditions of Chelapati's analysis is shown in Figure 4.4. Basically, it is the same as Finn's analysis in Figure 4.1 (a), except in the finite depth (h) and large overburden pressure (P_0).

Using the model in Figure 4.4, Chelapati superimposed stresses caused by the yielding trap door onto those due to surcharge load. The problem of infinite stresses at the trap door edges still existed. Since he considered granular soils in his study, and granular soils cannot sustain tension, the stress on the door was assumed to be zero wherever tensile stresses were indicated. The vertical stress distribution across the base for a downward translating door is shown in Figure 4.5. In the figure, H is the depth of soil and B is the width of the trap door. Compressive stresses on the base adjacent to the door were then reduced to produce no net change in total vertical force on the boundary (the boundary includes the trap door and the base), as shown in Figure 4.5. Chelapati used the method of series expansion to find the solutions in his study. All results were presented graphically in terms of h (the depth of soil), b (the trap door width), P (soil self weigh, P_0 , plus overburden pressure, γh), E (Young's modulus) , and μ (Poisson's Ratio). Chelapati concluded from the results that arching for the cases in his study was dependent on

three parameters, *b/h*, *Ph/dE*, and μ. For practical purposes, however, the effect of Poisson's ratio, μ, can be neglected over a wide range of the other parameters.

Bjerrum, Frimann Clausen, and Duncan (1972) believed that Chelapati's elastic solution can be further extended to give approximate values for the change in vertical pressure (Δp) at the center of a flexible section located within a rigid horizontal boundary. The layout of the model from Bjerrum, Frimann Clausen, and Duncan is shown in Figure 4.6. The variation of vertical pressure at the center was expressed as:

$$\Delta p \approx \alpha \times (\delta/l) \times E \qquad \text{(Eq. 4.1)}$$

in which,

δ : the deflection of the trap door,

l : half width of the trap door,

δ/l : the deflection ratio,

E : Young's modulus,

α : a coefficient whose value varies from 0.3 to 1.0 depending on the factors, *h*, *l*, δ, and μ,

h : soil depth,

μ : Poisson's ratio.

The above equation shows that the pressure changes due to arching increase with E (Young's modulus). Therefore, the pressure change is greater in dense sand than in loose sand, and it is greater in sand than in silt or clay. This result agrees with the observations in real engineering cases. In addition, this formula is restricted to those cases which have

small Δp values. Hence, the accuracy of this formula is questionable when large stress reductions are observed in the laboratory and field.

This kind of approach was taken one step further by Burghignoli (1981) when investigating stress redistribution around rectangular underground openings with flexible roofs (crowns). In his analysis, he assumed linear elastic behavior both for the soil and for the roof. Using the arching model from Bjerrum et. al. (1972), Burghignoli treated the tunnel crown as a flexible part in a rigid base (Figure 4.6). In other words, he incorporated the elastic property of the flexible section (the roof) within the rigid boundary into the arching analysis. All of Burghignoli's results were presented in graphical form. He used the relevant results in the analysis of the interaction between the crown of the tunnel and the overlying soil. Some appropriate estimates was given in Burghignoli's study to demonstrate the validity of his approach. Iteration is necessary when using his method to analyze a tunnel structure, because a deformation (δ) at the centerline has to be assumed first (see Eq. 4.1).

4.3 Continuum Approaches Using Plasticity Theory

Visual observations and pressure measurements show that many of the previously derived analytical and experimental methods are not correct. For example, soil does not behave elastically, nor does it shear along vertical planes progressing from trap door edges. Peck (1975) doubted the applicability of arching analyses which assumed elastic behavior. He stated "The ground movements associated with construction, particularly in soft soil, are so large that the soil is likely to be stressed far beyond the limits of elasticity"

(Peck, 1975). Evans (1984) also mentioned the inappropriateness of the elasticity assumption. He believed this assumption would result in predicted thrusts and moments larger than those actually measured in field and laboratory installations (Evans, 1984).

Since the elasticity theory cannot describe the arching behavior well, Evans (1984) provided an approach which used plasticity theory to solve the problem of a translating trap door within a granular soil. Figure 4.7 shows the idealized model for his analysis. The soil was represented by a frictional granular material which was cohesionless, isotropic, and homogeneous. A layer of this material with finite thickness (H) and unlimited lateral extent rested on a base containing a trap door. This door which might be raised or lowered, had width B and an infinite length perpendicular to the plane of the figure, i.e. plane strain conditions were assumed. His model is similar to those using elasticity theory where the traditional stress-strain equations from elasticity theory govern the soil's behavior in the elastic zones. However, here the failure criteria and plastic flow rules define the behavior within the plastic zones. Evans utilized the Coulomb failure criterion and the associate flow rule in his development of plastic solutions for the trap door problem.

In the plastic solutions of Evans, two major factors govern the deformation of a soil body with a trap door at the bottom. The first factor is the direction of the trap door movement. If the trap door moves downward away from the soil body, then this is the active case. If the trap door moves upward into the soil body, then this is the passive case. The other factor is the variable called the "angle of dilation (ν)". The angle of dilation is the angle of the plastic potential with respect to the horizontal. The "plastic potential" is a curve defined as being perpendicular to all plastic strain increment vectors. Hence, the

flow rule forms vectors in the $\delta\varepsilon_{vol}^{plastic}$ —$\delta\varepsilon_{shear}^{plastic}$ space as shown in Figure 4.8. "δ" in Figure 4.8 represents the changes of these two strains. ν also defines the direction of the plastic strain increment vector and is therefore a convenient variable to use for expressing a plastic flow rule. When ν is 0, no volume change occurs, while for $\nu > 0$, the material will dilate or expand.

By using the plasticity theory, Evans discovered different theoretical results. In active arching, when the angle of dilation (ν) is larger than zero, a prism of soil above the trap door will move downward and the shape of the soil prism is triangular, like Figure 4.9 (a). However, when ν is equal to zero in the case of active arching, the shape of the soil prism is rectangular (Figure 4.9 (b)), like the result from Terzaghi (1943). The similar condition happens in passive arching. When ν is larger than zero, a trapezoidal prism of soil moves upward (Figure 4.10 (a)). When ν is equal to zero, a rectangular soil prism is used to analyze the arching problem. Evans expanded his theoretical solutions to three-dimensional cases after these two-dimensional studies. He considered different geometries of the trap door in his three-dimensional cases. The shapes of the soil prism used in his three-dimensional solutions are shown in Figure 4.11 to Figure 4.14. Figure 4.11 and Figure 4.12 present the cones of soil above a circular trap door. The active case is a cone (Figure 4.11) and the passive case is a truncated cone (Figure 4.12). Figure 4.13 and Figure 4.14 show the soil prisms above a rectangular trap door.

Evans assumed a perfect plastic soil model in his arching analysis. However, the real soil is not a perfect plastic material. Therefore, his plastic solutions for arching are not very rigorous but these solutions do provide insight into what is actually occurring

within the soil when a trap door is lowered or raised. Most of the theories derived by Evans assumed plane strain behavior (like Figure 4.9 and Figure 4.10). These derived theories were compared with the experimental results in Evans' study. The comparison proved that plasticity theory could give a better description of the ground deformation behavior and the arching effect in granular soil. More details are discussed in Chapter Six. As to the three-dimensional case, since preceding literature contains little information on the three-dimensional behavior of particulate matter, it is difficult to evaluate the appropriateness of Evans' extensions for the circular and rectangular trap doors.

4.4 Discontinuum Approaches

The ideal approach to arching in granular soil is to solve the equilibrium of individual soil particles. This kind of method is called the discontinuum approach. The discontinuum approach is not practically applicable in the study of arching in granular soils, because of the vast amount of soil particles. However, Trollope (1957 & 1963) derived a solution for arching beneath a triangular embankment on a flexible base by this kind of approach. He believed that the stress distribution induced by body-force within granular masses could be evaluated from an analysis of the static equilibrium of a systematically packed system of mono-sized, smooth, rigid spheres. Trollope postulated a "systematic arching theory" in two dimension. In this theory, soil was represented by single sized discs in a regular packing. Figure 4.15 shows the packing. Each particle was acted upon by six normal forces from adjacent particles (Figure 4.15). The whole soil body was then

solved as a static equilibrium system with the assumptions that horizontal forces were zero and no tensile forces existed.

The results from Trollope's solution showed close agreement with the measured values in his experiment of the laboratory scale and full size embankments. Butterfield (1968) utilized Trollope's concept in his studies on the stresses developed within silos. He produced results which were similar to those from the silo theory (Section 3.4), but he failed to give enough information as to how his model was set up.

Maeda et. al. (1995) utilized the discontinuum approach to study the deformation and failure mechanism in granular materials. They used a microstructure composed of granular particles aligned as an ellipse as a basic unit (Figure 4.16). When they modeled the elliptic microstructure, the shape, size, and number of constituent particles were not taken into account; only the shape of the elliptic structure was considered as an essential parameter controlling the mechanical properties of the structure.

The mechanical properties of this elliptic structure were developed in two dimensions. Interparticle contact forces in the elliptic structure were found by the static equilibrium in each microstructure. As shown in Figure 4.16, the contact force (f_c) can be decomposed to normal component (f_n) and tangential component (f_t). The relation between these two force components is:

$$f_t = f_n \times \tan\phi_c \qquad \text{(Eq. 4.2)}$$

in which ϕ_c is the mobilized interparticle friction angle.

Each elliptic microstructure was subjected to the external contact forces generated at interface with adjacent elliptic structures. The external contact forces between elliptic

microstructures were calculated. Then these contact forces were "homogenized" to the "equivalent stresses" as shown in Figure 4.17. Maeda et. al. used this idealization (homogenized) to develop the macroscopic mechanical models of granular materials. With this elliptic structure model, Maeda et. al. found that the stability of the soil body could be presented as a function of the shape of the elliptic structure and the stress condition surrounding the structure. They also believed that the characteristic mechanical properties of a granular material, such as deformation anisotropy and dilatancy, could be explained by the elliptic structure, where the rotation of the constituent particles played an important role. However, there were not many analysis results available at the present time. The applicability of their model to different types of granular materials is still unsure.

4.5 Numerical Methods

Due to the simplified assumptions, the aforementioned theoretical approaches are usually limited in the application of practical engineering. Compared to the theoretical approaches, numerical methods are more flexible, and may be the most comprehensive methods available for the analysis of stress redistribution when dealing with arching problems. Several kinds of numerical methods were used by engineers and researchers, including: Finite Difference Method (FDM), Finite Element Method (FEM), Boundary Element Method (BEM), and Distinct Element Method (DEM; also called "Discrete Element Method"). These methods allow for analysis of problems with difficult boundary condi-

tions or complicate material properties, such as irregular geometries, non-homogeneity, and anisotropic behavior.

Getzler, et. al. (1970) performed a finite difference analysis of plane strain trap door problem. The soil was assumed to be linear elastic and Chelapati's theoretical solution (Section 4.2) was used as the formulation in their analyses. Figure 4.18 presents their computational model. The roof of the underground structure is a trap door located in a rigid layer. Figure 4.19 shows the superposition of two different modes in their model. Mode (a) is no settlement of the trap door relative to the medium, in which the external surcharge and overburden stress are taken into account. Mode (b) has the differential settling of the structure, with no external surcharge or overburden stress. From the numerical analysis results, Getzler et. al. found the principal compressive stress trajectories produced by the differential settling indicate that a soil arch was formed in the overlying soil, abutting on both sides of the structure and transferring part of the load to those zones. These discoveries agree with the theory which interprets the arching effect as a "structure-like" action of the overlying soil, for example, an arch in plane strain case (Whitman, et. al., 1962 & 1963; Nielson, 1966) and a dome in three dimensional case (Nielson, 1966).

Ranken and Ghaboussi (1975) used an axisymmetric finite element program to simulate an advancing tunnel in isotropic, homogeneous, and continuous soil. Again, the soil was treated as a linear elastic material. Several cases were run in their analysis using combinations of the following conditions: (1) lined and unlined tunnel, and (2) linear elastic soil, elasto-plastic soil with strength independent of mean stress and angle of friction,

and elasto-plastic soil with strength dependent on the aforementioned parameters. They obtained reasonable data from their finite element program and suggested various values for different tunnel designs in their paper.

Stone (1988) performed non-linear finite element analyses of the trap door tests to help explain his experimental outcomes. He reproduced the characteristics of his physical model tests with numerical analyses which resulted in a correct prediction of an initial soil localization propagating from the edge of the trap door into the overlying soil. The strain distributions simulated numerically were seen to form an arch at small door displacements. However, the discrete nature of the formation of the soil localizations observed in his physical model did not show in the numerical analysis result.

Koutsabeloulis and Griffiths (1989) considered the soil as a perfectly plastic material and ran a finite element analysis of the trap door problem. The Coulomb failure criterion was used with the non-associate flow rule. The soil body was discretized to fifteen-node iso-parametric triangular elements, as shown in Figure 4.20. Figure 4.21 presents the predicting results of their analyses for active and passive arching, in which H is the depth of overburden soil and D is the width of the trap door. In the active arching case, the load on the trap door drop down as the trap door is lowered. However, after the load drops down, instead of an increase, the load just stays at a constant value. This phenomenon is different from most of the trap door test results. As to the passive case, the curves show a similar tendency as physical test results. The parameter H/D shows the same effect in these numerical results as the former testing results. As the value of H/D increases,

the arching effect is more apparent (i.e. the load on the trap door decreases more in active arching and increases more in passive arching).

A new numerical method called "Distinct Element Method" (or "Discrete Element Method") considers granular material as a constitution of many individual particles. The distinct element method can give a better description of the discrete characteristic of a granular material due to its special capability of modeling each particle as a separate entity. Sakaguchi and Ozaki (1992) used this method to analyze the formation of arches plugging the flow of granular materials. Their analyses were applied when the granular particles discharging out of a silo due to the gravity. The granular particle was modeled as an elastic disc which size is 10 mm in diameter. A concept called "rolling friction" which allowed the effective development of geometrical interference among particles, was introduced in their analyses. Figure 4.22 presents their simulation results: the upper plots are the transforming configurations of particles in a silo, and the lower plots are the pictures showing the velocity vector fields. The arches were formed in the final stage (1.28 sec) and plugged the particle flow. Sakaguchi and Ozaki also ran several tests to compare their numerical results. The comparison showed that the prediction from the distinct element method was in good agreement with the experimental measures not only in the flow pattern but also in the formation of arches.

Numerical methods are recently applied widely in engineering study and practice, because they are flexible and because confronting problems are more and more complicated. However, there are still some shortcomings in numerical methods. One is that these analyses require appropriate selection of input parameter values, and sometimes, a

constitutive model (e.g. Cam Clay Model) to obtain good results. The second is that these methods are usually time-consuming and expensive, especially when one uses trial and error method to adjust the input data. Hence, a simple and quick method is necessary for rough estimation and preliminary design in complicated engineering problems. This kind of method is called empirical method which is discussed in next chapter.

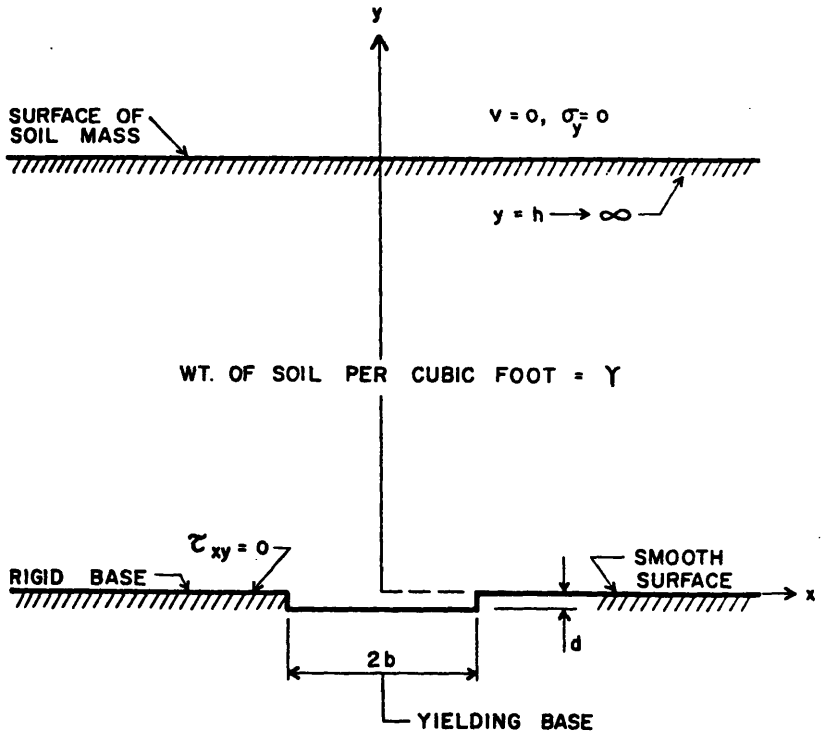

(a) Translational Yielding Base

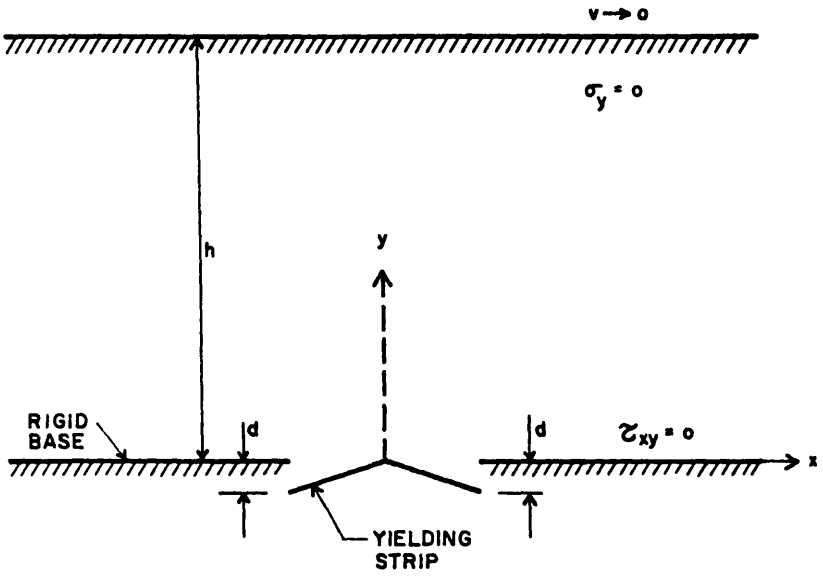

(b) Rotational Yielding Base

Figure 4.1 Boundary Conditions for Soil Mass with Yielding Base (Finn, 1963)

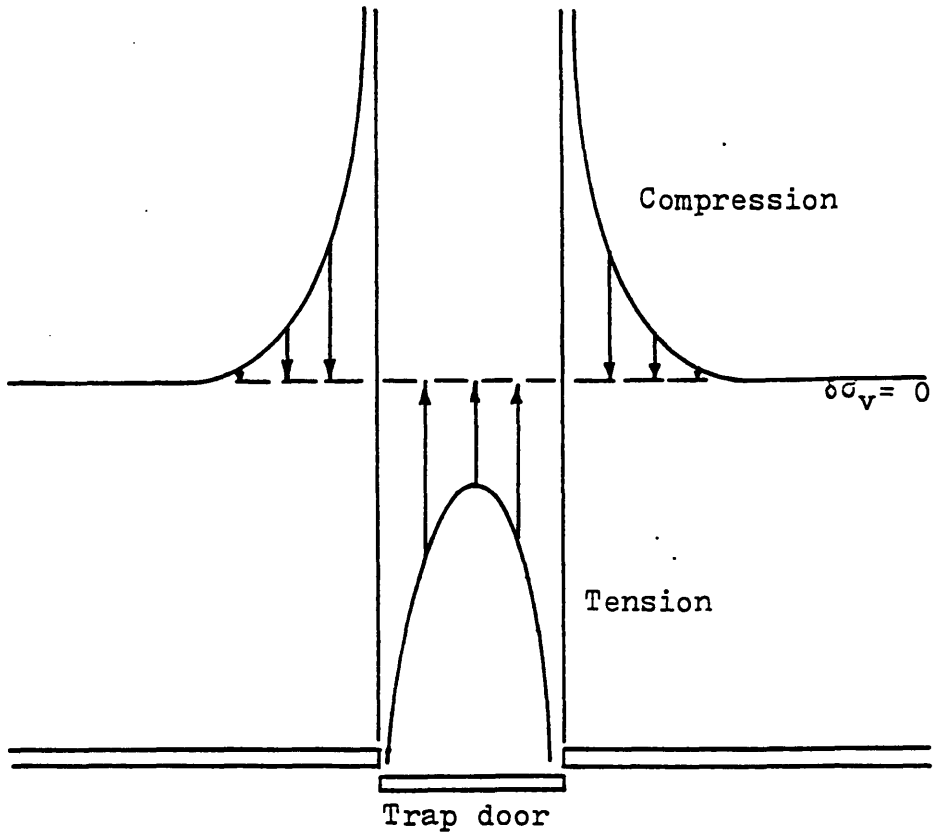

Figure 4.2 Typical Distribution of Change in Vertical Stress for Downward Translating Trap Door (Finn, 1963; Revised by Evan, 1984)

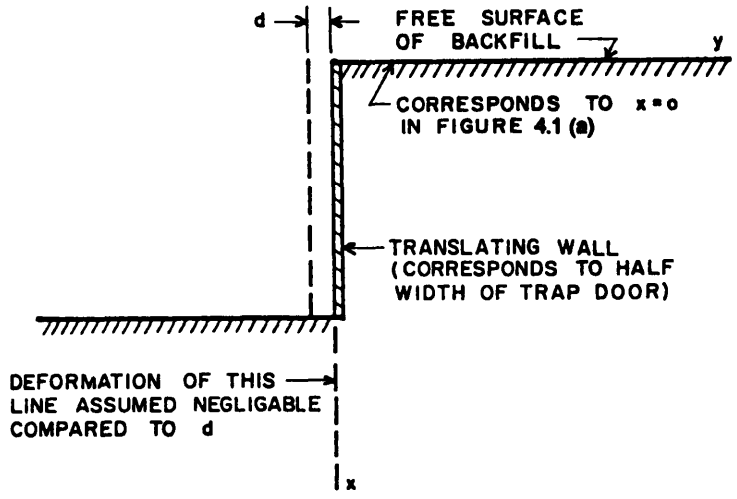

Figure 4.3 Translating Retaining Wall (Finn, 1963)

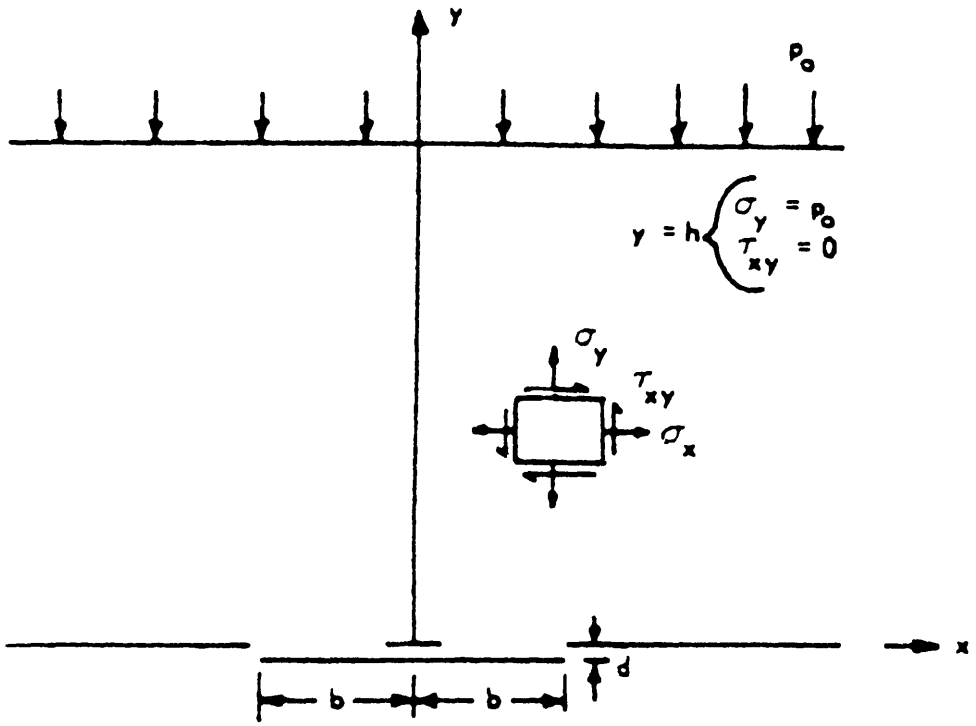

Figure 4.4 Boundary Condition for Chelapati's Analysis of Arching in Granular Material (Chelapati, 1964)

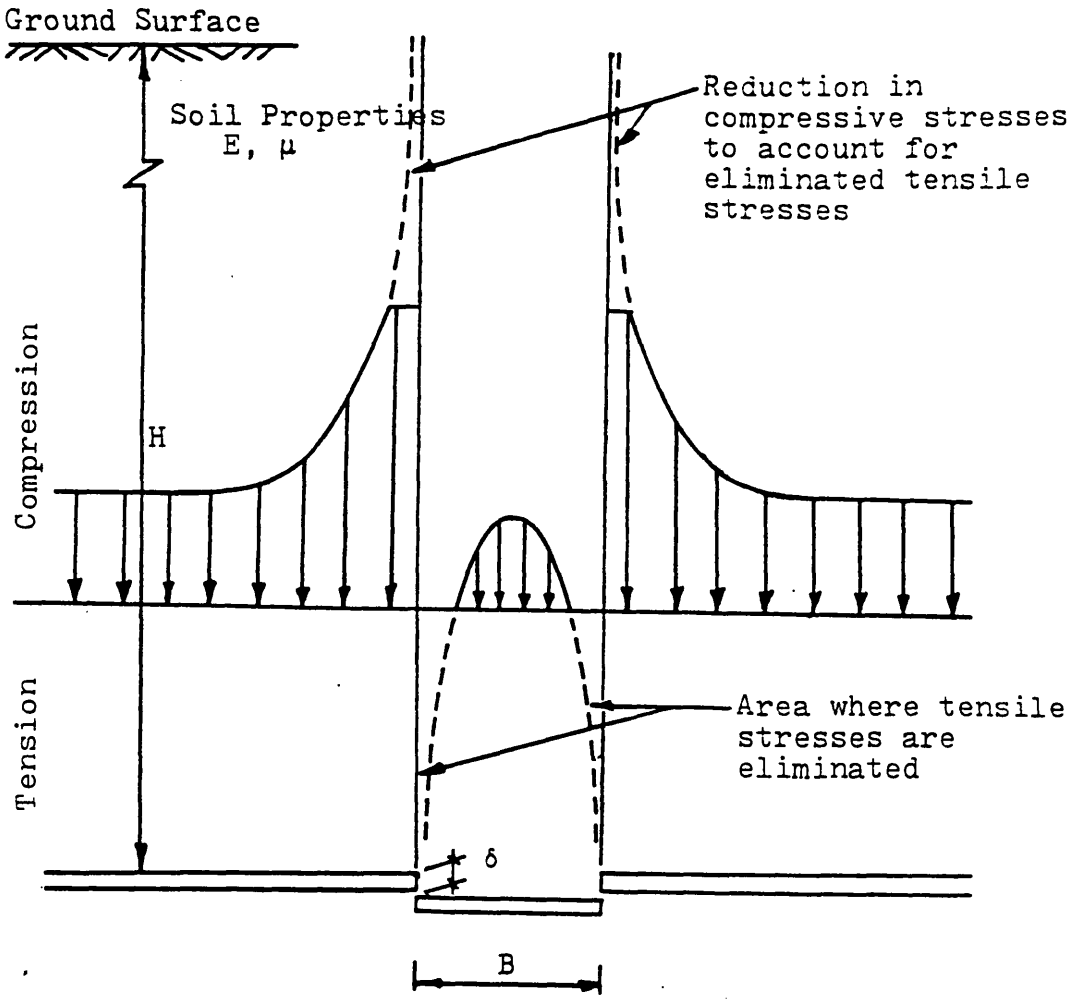

Figure 4.5 Chelapati's Technique for Elimination of Tensile Stresses using an Elastic Solution for Arching (Chelapati, 1964; Revised by Evans, 1984)

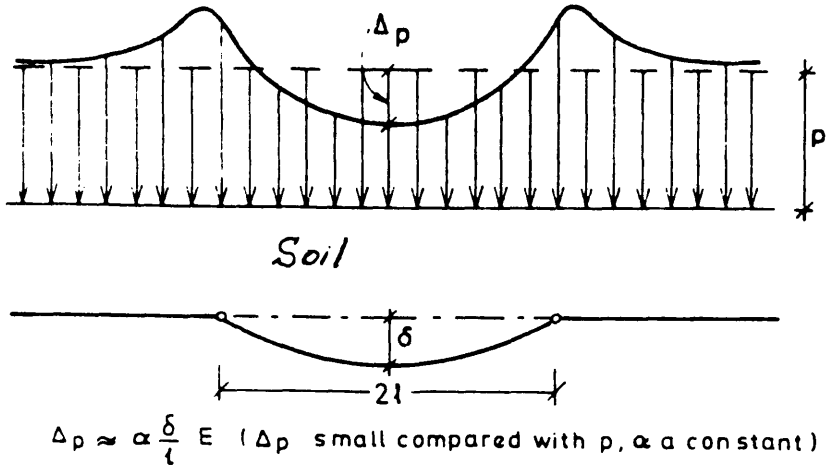

Figure 4.6 Arching Model in the study of Bjerrum et. al. (Bjerrum et. al., 1972)

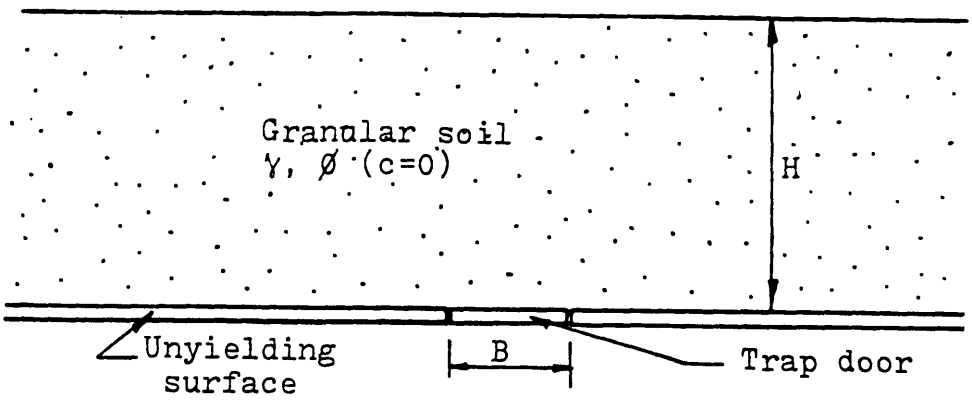

Figure 4.7 Idealized Model for Trap Door Problems (Evans, 1984)

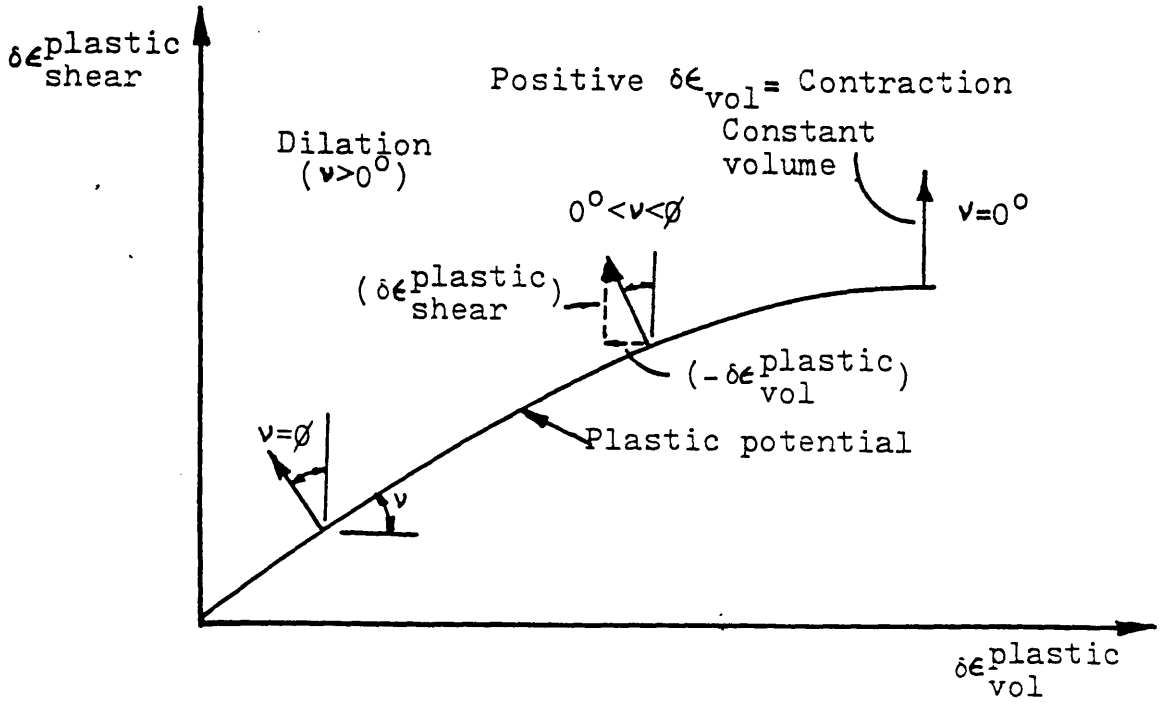

Figure 4.8 Plastic Flow Rule (Evans, 1984)

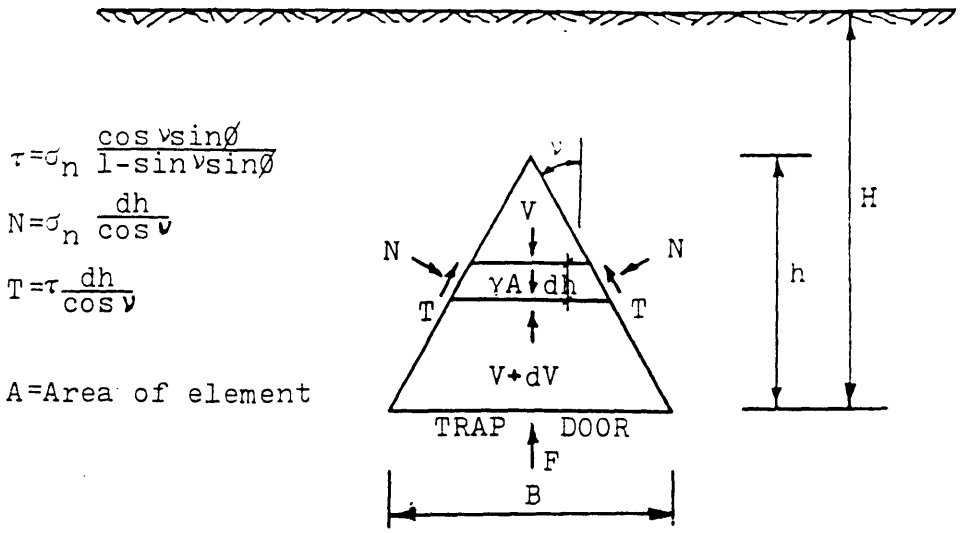

A. Free Body Diagram for $\nu>0^{\circ}$

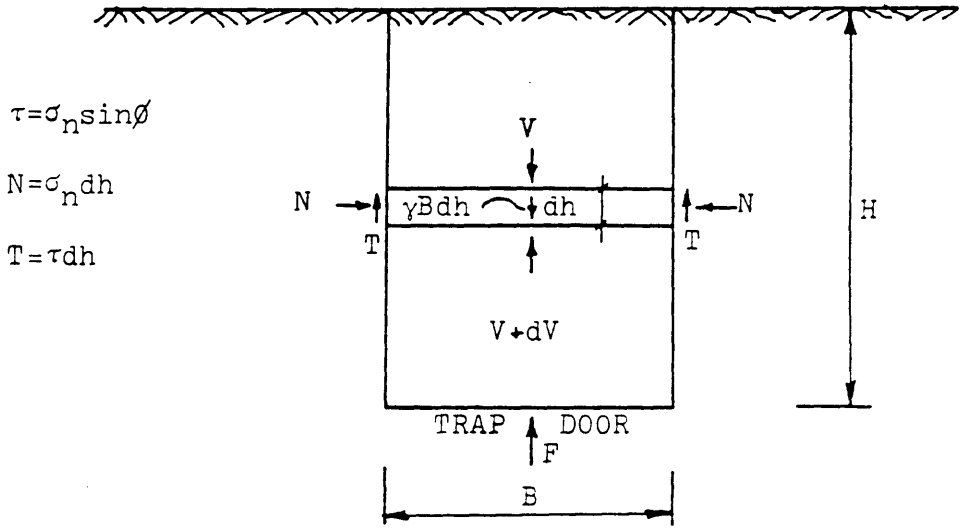

B. Free Body Diagram for $\nu=0^{\circ}$

Figure 4.9 Free Body Diagrams for Active Arching in the Two-Dimensional Case (Evans, 1984)

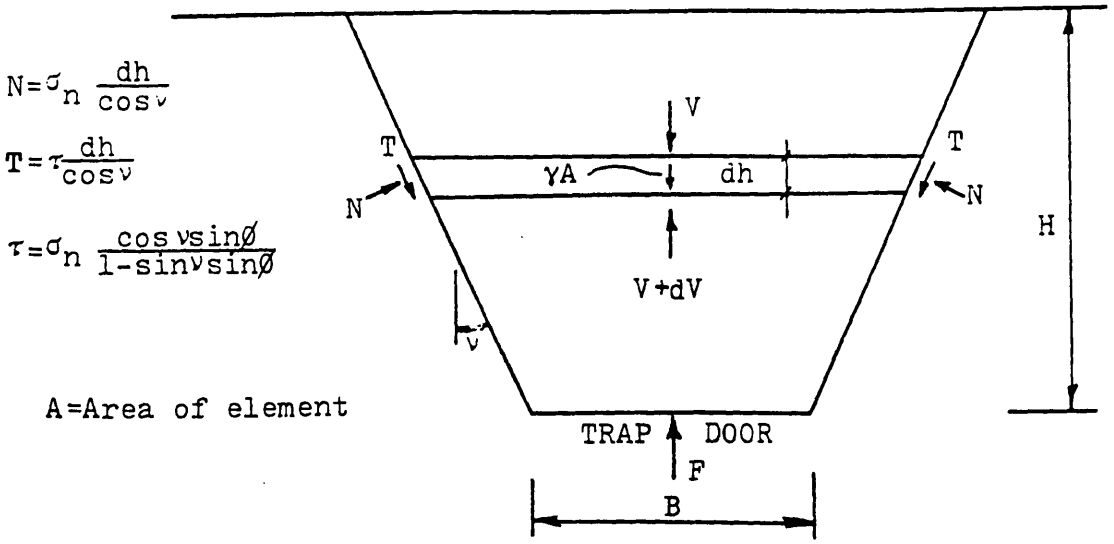

A. Free Body Diagram for $\nu>0^o$

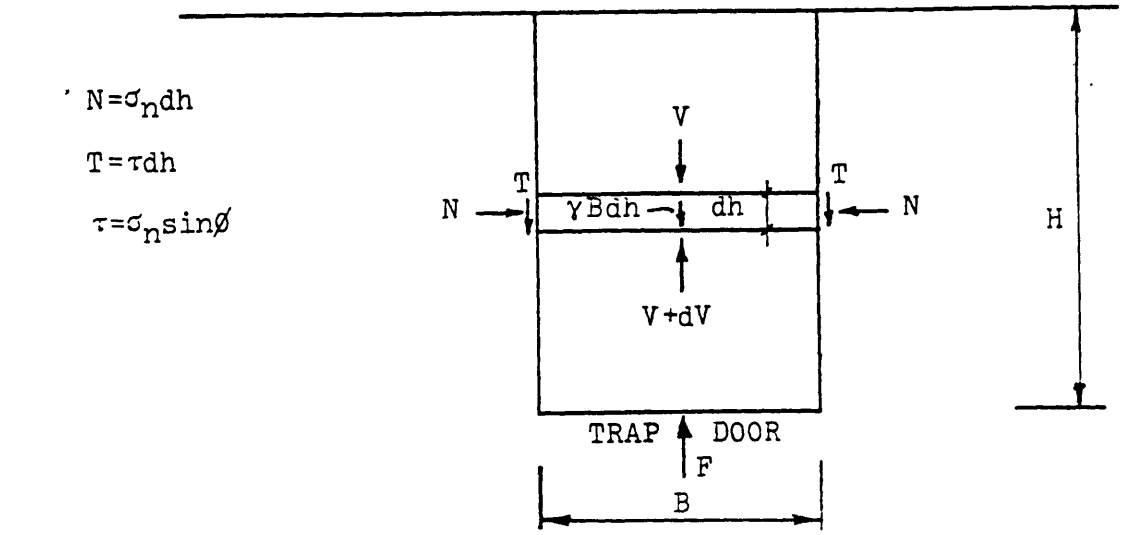

B. Free Body Diagram for $\nu=0^o$

Figure 4.10 Free Body Diagrams for Passive Arching in the Two-Dimensional Case (Evans, 1984)

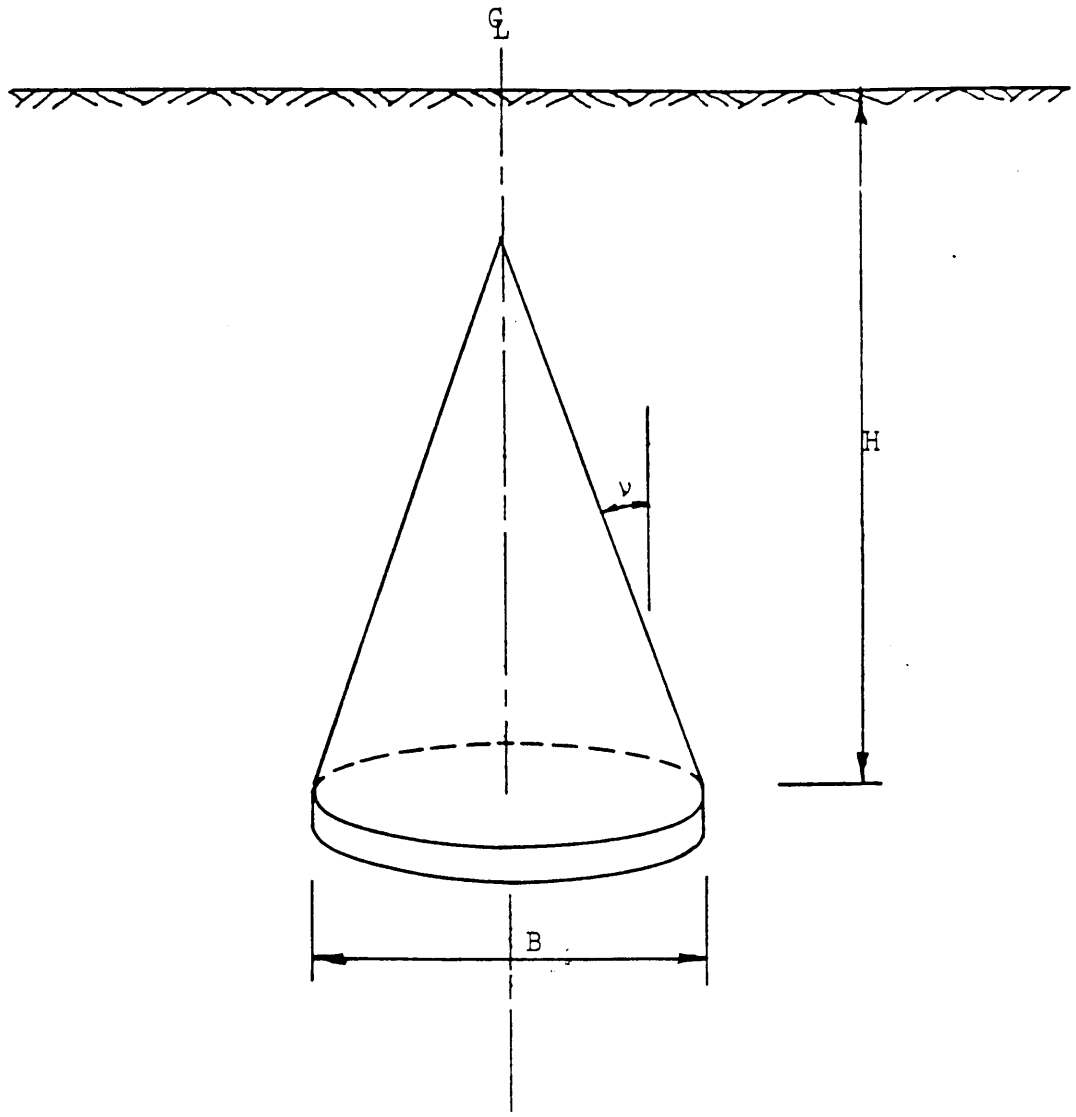

Figure 4.11 Soil Cone for Active Arching Above a Circular Trap Door (Evans, 1984)

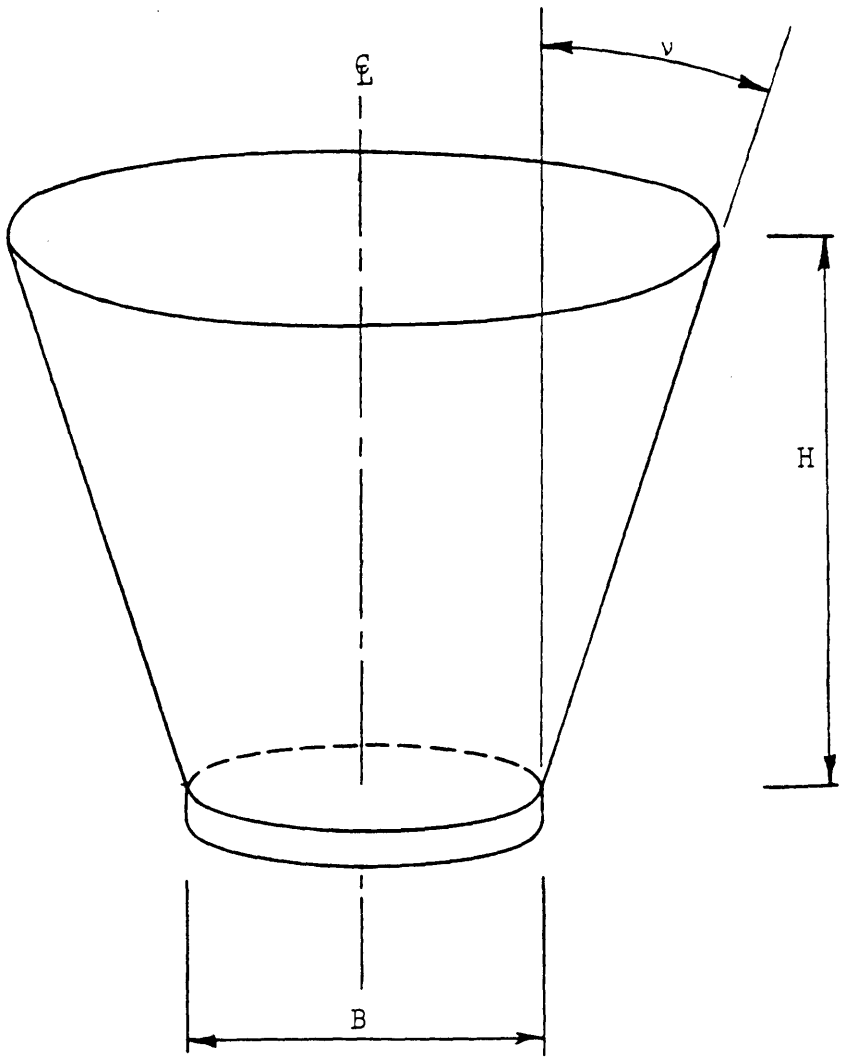

Figure 4.12 Soil Cone for Passive Arching Above a Circular Trap Door (Evans, 1984)

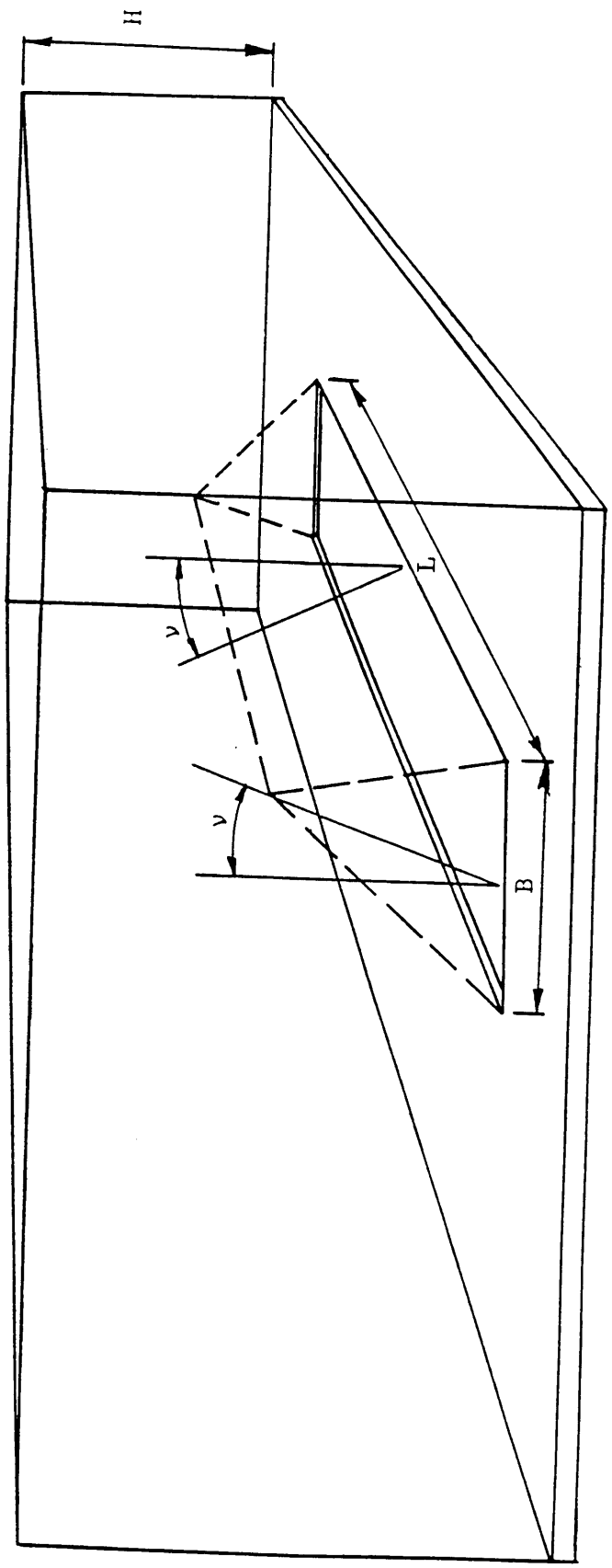

Figure 4.13 Soil Prism for Active Arching Above a Rectangular Trap Door (Evans, 1984)

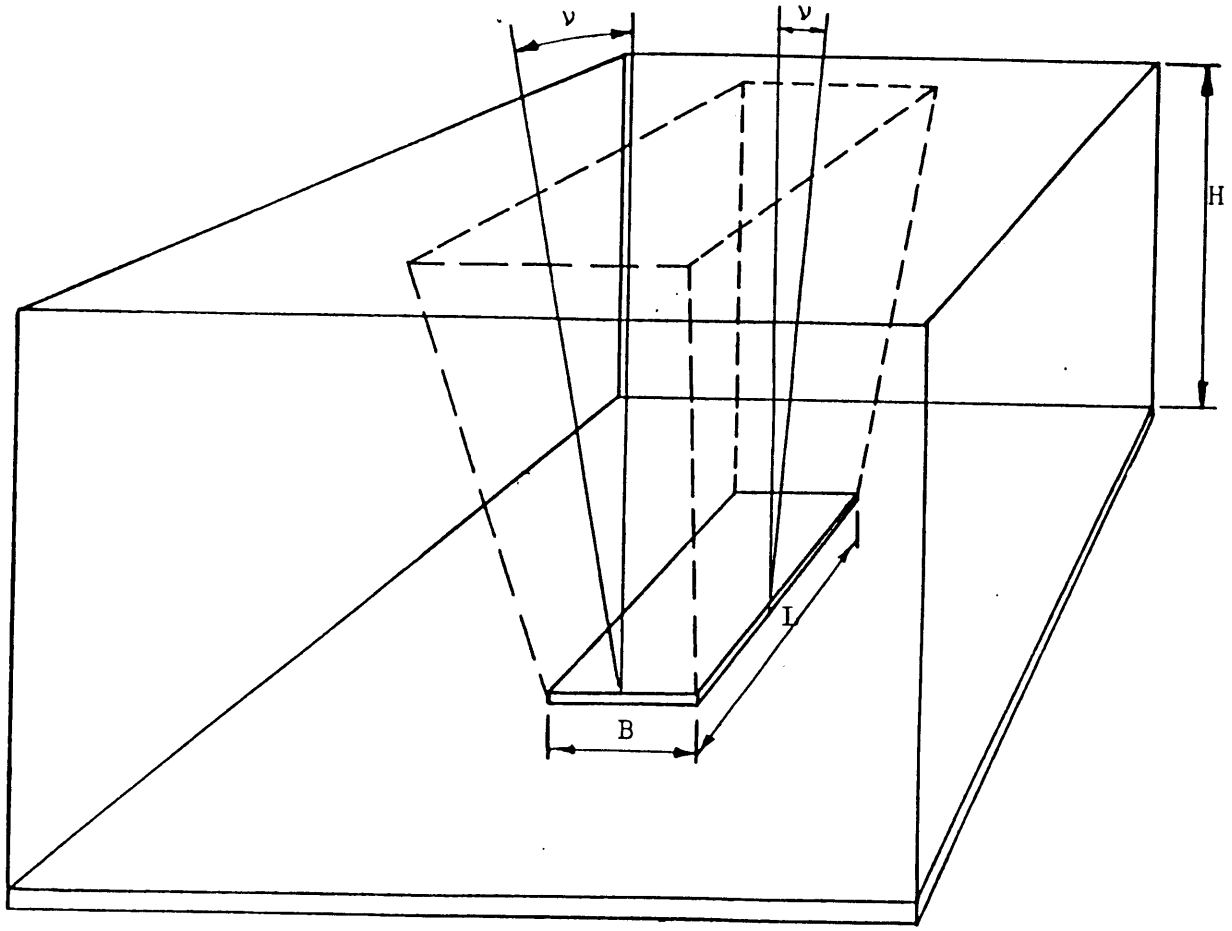

Figure 4.14 Soil Prism for Passive Arching Above a Rectangular Trap Door (Evans, 1984)

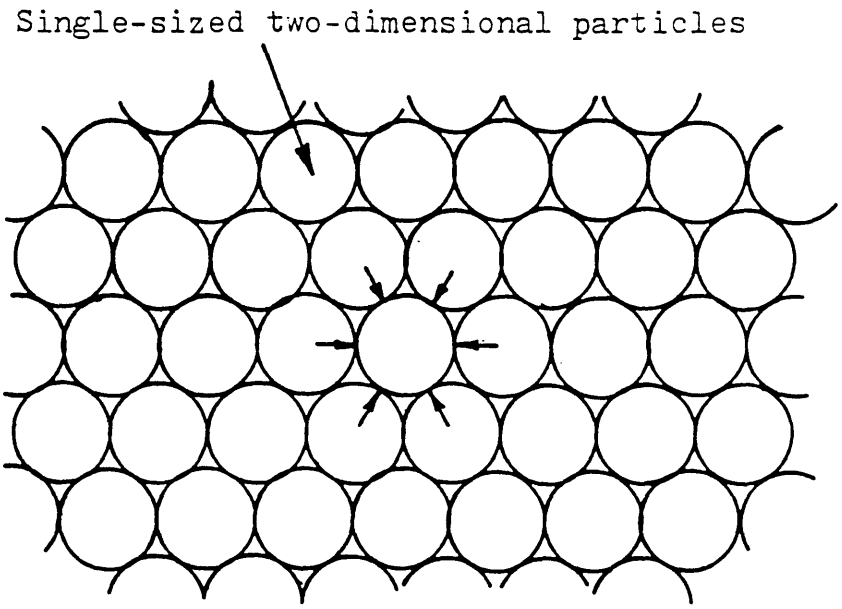

Figure 4.15 Model for Systematic Arching Theory (Trollope, 1957; Revised by Evans, 1984)

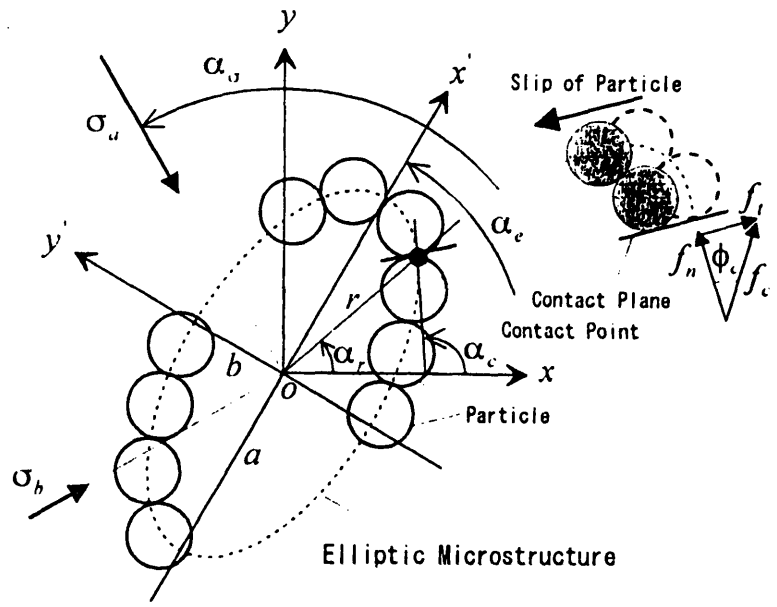

Figure 4.16 Geometrical Definition of Elliptic Structure (Maeda et. al., 1995)

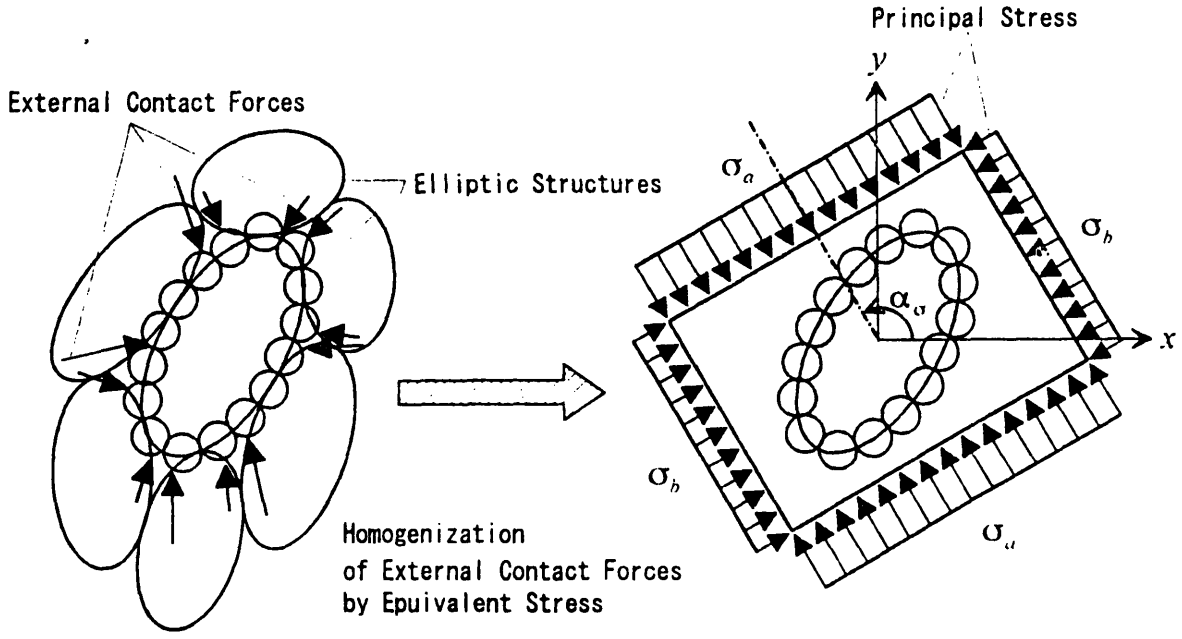

Figure 4.17 Homogenization of External Contact Forces with Stress (Maeda et. al., 1995)

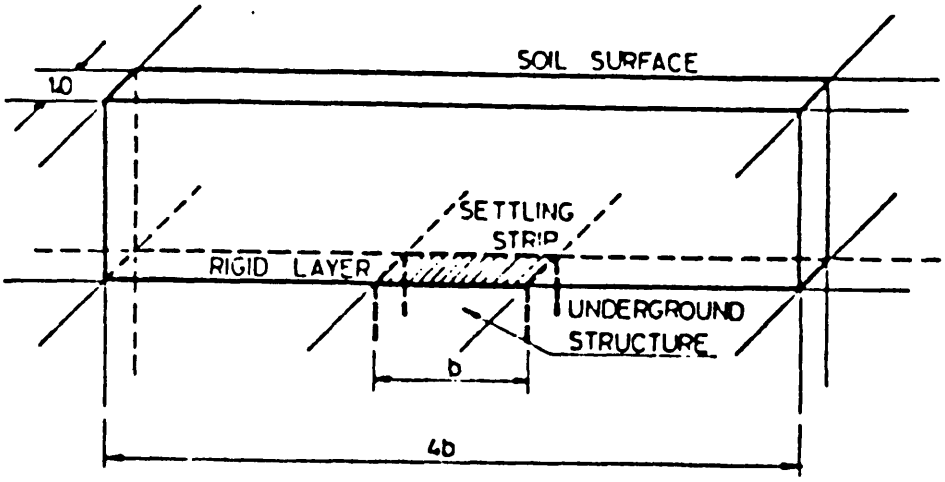

Figure 4.18 Computational Model of the Finite Difference Analysis (Getzler, et. al., 1970)

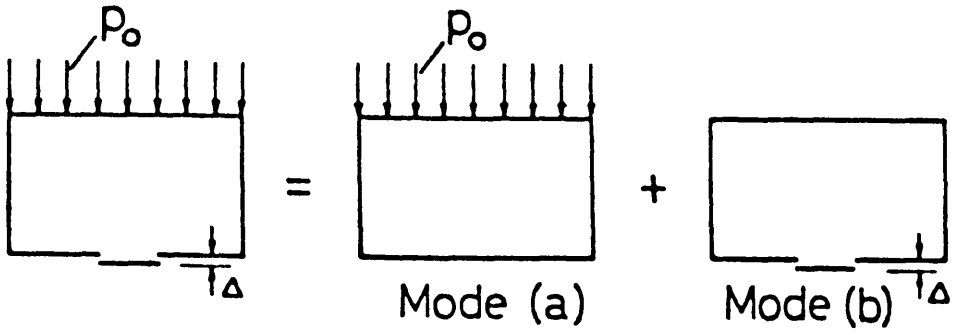

Figure 4.19 Superposition of Two Different Modes (Getzler, et. al., 1970)

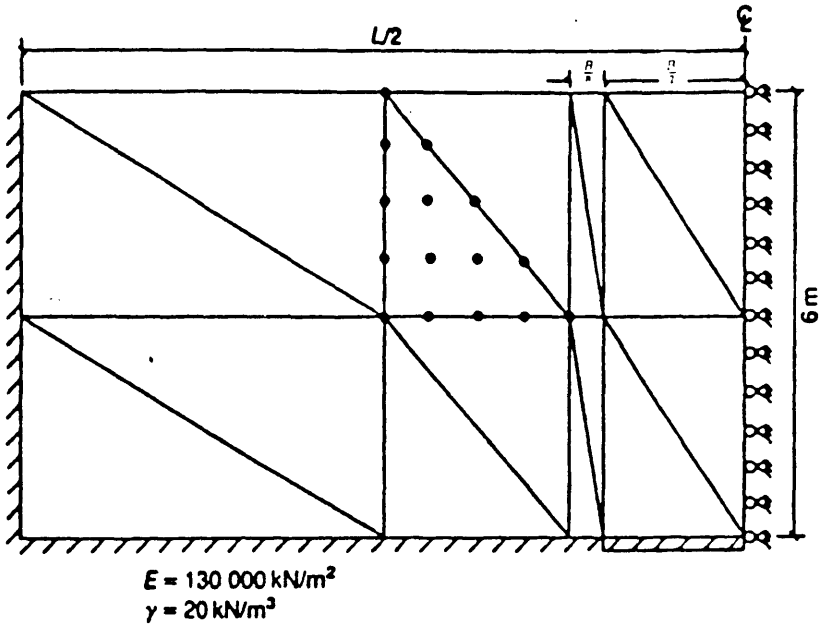

(a) $L/B = 5$

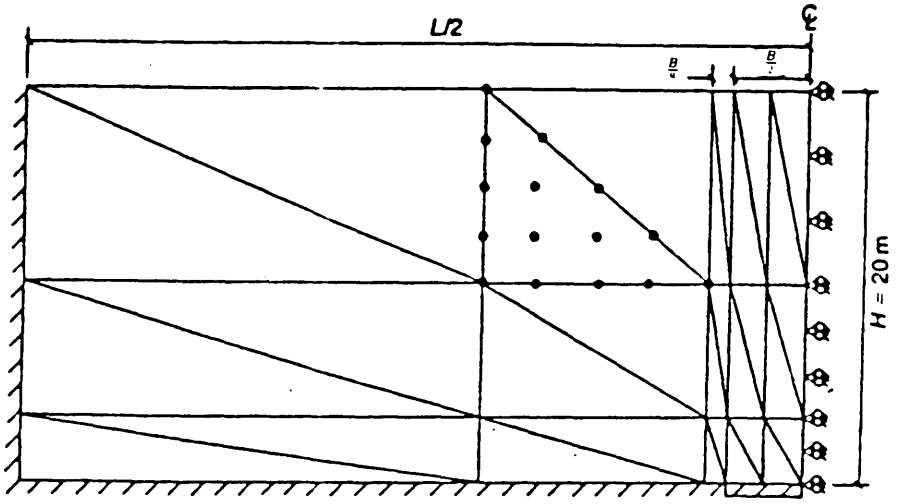

(b) $L/B = 10$

Figure 4.20 Finite Element Discretization of the Trap Door Problem (Koutsabeloulis and Griffiths, 1989)

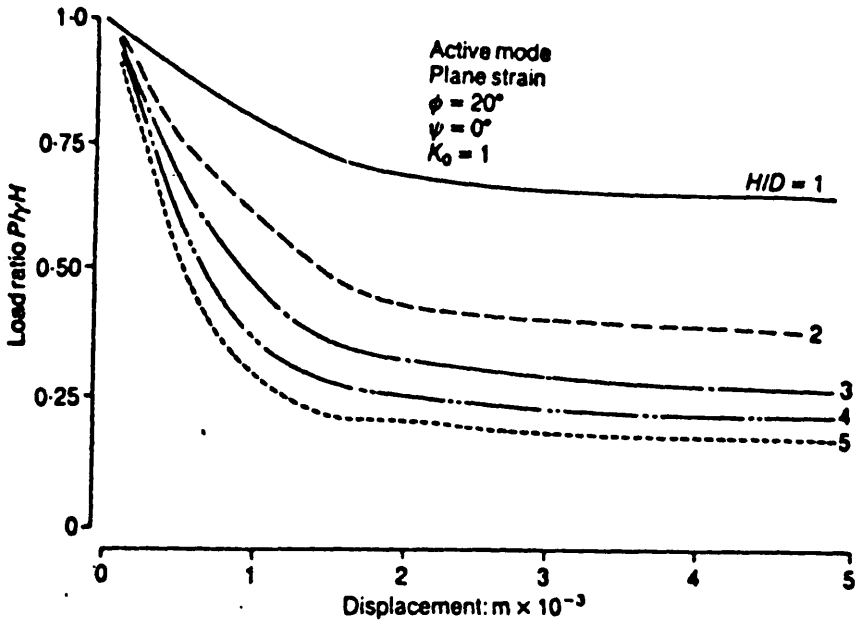

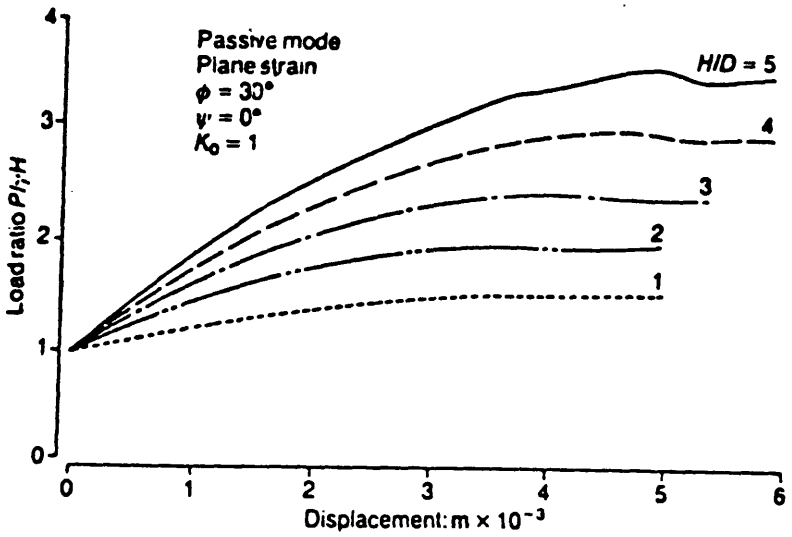

Figure 4.21 Numerical Analysis Results (Koutsabeloulis and Griffiths, 1989)

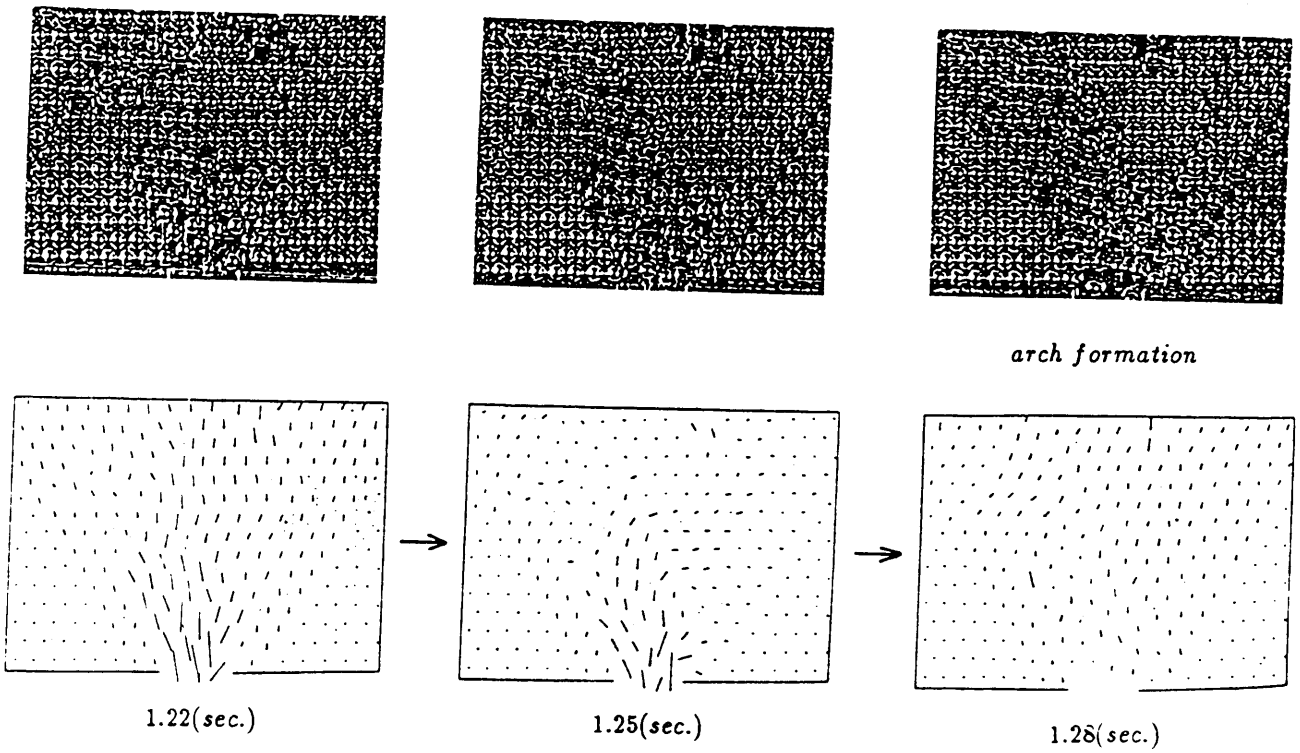

Figure 4.22 Particle Configurations and Velocity Vector Fields
(Sakaguchi and Ozaki, 1992)

Chapter FIVE
Empirical Methods

5.1 General

For the design of underground openings, there are some simplified methods which basically evolve from previous construction experience. Most of these empirical and semi-empirical methods indicate a value of the pressure to be applied to the support system of the underground opening. The shape of openings, after a failure on the roof has taken place, in many instances resembles an arch. This chapter will illustrate several empirically based methods and explore the concept of arching effect embedded in them. Some have been obtained from very simple static analyses and others were entirely founded on the experience of the person proposing it.

5.2 Classification of Empirical Methods

The empirical methods generally use the assumption that a zone of loosening exists above the underground structure. The loosening zone may have different shapes depending on the assumptions and derivations in a method; for instance, in Figure 5.1, the loosening zone is bounded by a parabola. In this method, the force acting on the structure is assumed to be the weight of the material within the loosening zone plus surcharges.

In general, there are two approaches when determining the loads on the supports of underground openings. One approach is to take the effect of overburden depth into account, and the other is to disregard the effect. Consideration of the overburden depth

depends on whether the stresses exceed the elastic limit of the geomaterial in the design. When the stresses do not exceed the elastic limit of the geomaterial, the development of a loosening zone is unaffected by the depth of the overburden. Hard rock is an example here. On the other hand, when stresses fall in the plastic range of geomaterials, the effect of overburden is a relevant factor, not only regarding the magnitude of pressure on the underground structure but also regarding the time required for the development of a loosening zone. Consequently, the use of methods taking the depth factor into account is necessary. Crushed rock and sand are examples for this case. Therefore, we can divide the existing empirical methods into two major groups, one considering the overburden depth and the other neglecting it.

5.3 Methods Considering the Overburden Depth

5.3.1 Bierbäumer's Theory (1913)

Bierbäumer's theory was developed during the construction of the great Alpine tunnels (Széchy, 1973). According to this theory the tunnel is acted upon by the load of rock mass bounded by a parabola of height $h = \alpha H$ (Figure 5.1) in which α is the "reduction coefficient". The rock mass in the pressure bulb of Figure 5.1 is called a "loosening zone" which produces the load acting on the tunnel.

Bierbäumer proposed the following approach to estimate the reduction coefficient α. This approach assumed that upon excavation of the tunnel, the rock material tended to slide down along rupture planes inclined at $(45^0 + \phi/2)$. The configuration is shown in

Figure 5.2. The weight of the sliding rock mass was conteracted by the friction force (S) developing along the vertical sliding planes, which can be expressed as:

$$S = fE = \tan\phi \cdot [\tan^2(45^0 - \frac{\phi}{2})]\frac{H^2\gamma}{2} = H^2\gamma \tan\phi[\tan^2(45^0 - \frac{\phi}{2})]$$

(Eq. 5.1)

in which

f = coefficient of friction = $\tan\phi$,

ϕ = friction angle of rock mass,

E = normal forces acting on the vertical sliding planes

= (area of triangle DFB' or ECA' in Figure 5.3) $\times \gamma \times K_a$

$= [\frac{1}{2} \cdot H \cdot H \tan(45^0 - \frac{\phi}{2})] \times \gamma \times \tan(45^0 - \frac{\phi}{2})$,

K_a = Rankine's active ratio = $\tan(45^0 - \phi/2)$,

γ = unit weight of rock mass,

H = depth of tunnel (from the ground surface to the crown of tunnel).

All the formulas here are considered unit length in the direction perpendicular to the underground opening face (i.e. plane strain condition). Therefore, the weight of rock mass (W) acting on the tunnel crown (using a width B instead of b, because the assumption of two vertical sliding planes in Figure 5.2) is:

$$W = \gamma \times \text{area of } CA'B'D = \gamma \times H \times B = \gamma H[b + 2m \cdot \tan(45^0 - \frac{\phi}{2})]$$

(Eq. 5.2)

in which

H = the height of rock mass above the tunnel,

B = the distance between two sliding surfaces = $b+2m\cdot\tan(45^0 - \phi/2)$,

b = the width of the underground opening,

m = the height of the underground opening.

Because of the shear forces on the sliding surfaces, the weight of rock mass above the tunnel will not fully act on the tunnel. Hence, the force acting on the tunnel (P) is the difference between W (Eq. 5.2) and 2S (Eq. 5.1):

$$P = W\text{-}2S = \gamma H[b + 2m\cdot\tan(45^0 - \frac{\phi}{2})] - H^2\gamma\tan\phi[\tan^2(45^0 - \frac{\phi}{2})]$$

(Eq. 5.3)

The pressure on the crown of the tunnel (p) is thus equal to:

$$p = \frac{P}{B} = \frac{P}{b + 2m\tan(45^0 - \frac{\phi}{2})} = H\gamma[1 - \frac{H\tan\phi\tan^2(45^0 - \frac{\phi}{2})}{b + 2m\tan(45^0 - \frac{\phi}{2})}] = \alpha H\gamma$$

(Eq. 5.4)

in which

$$\alpha = \text{reduction coefficient} = [1 - \frac{H\tan\phi\tan^2(45^0 - \frac{\phi}{2})}{b + 2m\tan(45^0 - \frac{\phi}{2})}] \qquad \text{(Eq. 5.5)}$$

Therefore only the pressure $\alpha H\gamma$, instead of $H\gamma$, acts on the tunnel. In other words, $h = \alpha H$ is the effective height of rock mass above the tunnel that should be consider when designing a tunnel. This implied the geostatic pressure was reduced by friction produced by the horizontal earth pressure of the wedges ECA' and DFB' acting on the vertical sliding planes. This pressure reduction was the so call arching effect.

Bierbäumer considered the force acting on the trap door calculated force from the above method as "the maximum load". He proposed the other simplified method to calculate the possible minimum load acting on the door. This method utilizes the equilibrium of a triangular prism which has two sides making an angle ϕ with the vertical (Figure 5.3). When friction is fully mobilized along the sides, the forces on these sides have no vertical component. "The minimum load" (P_{min}) on the tunnel roof, then just balances the weight of the triangular prism:

$$P_{min} = \frac{\gamma B^2}{4 \tan \phi} \qquad \text{(Eq. 5.6)}$$

Széchy (1973) discussed the Bierbäumer's theory. He mentioned that the correctness of Bierbäumer's theory could not be completely verified in practice. The best results were obtained for openings excavated at great depths in materials displaying high internal friction (shear strength).

5.3.2 Balla's Theory (1963)

Balla (1963) assumed in his theory that the geomaterial lying above the tunnel would suffer loosening and downward movement as a consequence of tunnel excavation. This downward movement would take place along some kind of sliding surface and consequently the displacement would suffice to mobilize the shear strength of the material.

He assumed the sliding surfaces were circular and they would start from the upper corners of a rectangular tunnel (Figure 5.4). The radii of the circular curves were determined by the following procedure: (Balla, 1963)

1) Find an arbitrary point on a horizontal line at the elevation of the tunnel crown (like point O_1 in Figure 5.4).

2) Use the distance between O_1 and the distant upper corner of the rectangular tunnel as a radius to plot a circular curve (such as radius R in Figure 5.4).

3) Find the intersection of this circular curve and the axis of symmetry of the tunnel (point O in Figure 5.4).

4) Plot a straight line through the intersection point found in step 3) and tangent to the circular curve made in step 2) (line OA in Figure 5.4).

5) Find the inclination angle (to the horizontal) of line OA (i.e. angle θ in Figure 5.4) and the friction angle of rock mass (ϕ).

6) If the inclination angle (θ) is equal to ($45^0 - \phi/2$) which corresponds to that of the sliding planes of passive earth pressure, then the radius R obtained in step 2) is the radius for the circular sliding surface. Figure 5.4 shows the case of $\theta = (45^0-\phi/2)$. Use the same radius and point O_2 to plot the other sliding surface. The area between these two sliding surfaces and the crown of the tunnel (OO_1O_2) is the loosening zone in rock mass.

7) If the value of the inclination angle is not ($45^0 - \phi/2$), repeat step 1) to step 5) until the angle is equal to ($45^0 - \phi/2$).

The rock pressure on the tunnel is obtained from the equilibrium of all forces acting vertically in and on the loosening zone (OO_1O_2):

$$G + 2Q_v + 2K_v + P = 0 \qquad \text{(Eq. 5.7)}$$

in which

G = the weight of the loosening zone (or the sliding rock mass) enclosed within the circular sliding surfaces,

Q_v & K_v = the resultants of shear stresses acting along each sliding surface,

P = the resultant rock pressure acting on the roof (crown) of the tunnel.

The decrease of load on the tunnel supports due to arching is taken into account in the variables Q_v and K_v. Balla determined the distribution of stresses along the sliding surfaces (i.e. Q_v and K_v in Eq. 5.7) by Kötter's differential equation. He found that the variables in Eq. 5.6 were functions of the dimensions, locations and depth of the tunnel and a function of the strength characteristics of the overlying rock. By assuming a uniform distribution of the crown pressure, he obtained:

$$p_a = H\gamma\left(F_H + \frac{b}{H}F_b - \frac{c}{H\gamma}F_c\right) \qquad \text{(Eq. 5.8)}$$

in which

p_a = the pressure on the roof (crown) of the tunnel,

H = the depth of the tunnel (from the ground surface to the crown of the tunnel),

γ = unit weight of rock mass,

b = the width of the tunnel,

c = cohesion in rock mass,

F_H = factor representing the depth effect on p_a,

F_b = factor representing the width effect on p_a,

F_c = factor representing the cohesion effect on p_a.

F_H, F_b, and F_c are functions of the friction angle of rock mass (ϕ). The values for these factors can be found in Figure 5.5 provided by Balla. Some factor values are also listed in a table in that figure. According to these numerical values, one can see that the effect of cover depth (F_H factor) is predominant.

In Balla's theory, many assumptions based on his experience were made. The defect in this theory is the fact that both the loosening and pressures of the lateral rock mass beside the tunnel are neglected as the sliding surfaces start from the corner points.

5.3.3 Terzaghi's Recommendations for Load on Tunnel Supports (1946)

As discussed in Chapter 3, Terzaghi conducted the most widely known experimental and theoretical investigations of arching (Terzaghi, 1936 & 1943). He also combined the knowledge and experiences obtained from many tunneling projects to produce design values for tunnel support loads under various ground conditions (Proctor and White, 1946 & 1977). Many of Terzaghi's recommendations are still in wide use today.

Terzaghi thought the load on tunnel supports was the height of geomaterial which tended to drop out of the tunnel roof (crown). This load on tunnel supports depended more or less on the state of stress in the ground prior to tunnel construction. Also the geological condition of the ground would affect the load on tunnel supports. In perfectly or almost perfectly intact rock, no support was required unless popping was encountered. In stratified or moderately jointed rock, the tunnel support served its purpose if it was capable to sustain a moderate rock load. In crushed rock, the loading conditions were similar to those to be encountered when mining through sand; and in zones of rock decom-

position, they were similar to those in tunnels through clay (Terzaghi, 1946). According to these descriptions, Terzaghi suggested different values of load on tunnel based on the ground conditions.

In this section, the focus is on the arch action that Terzaghi explored in his observations in construction and experiments, since it is the major topic of interest in this literature study. Within all of the different kinds of ground conditions, the crushed rock case and the sand case assume an arching effect. These two cases will be discussed in detail in the following paragraphs.

The term *arch action* indicates the capacity of the rock located above the roof of a tunnel to transfer the major part of the total weight of the overburden onto the rock located on both sides of the tunnel. The body of rock which transfers the load will briefly be referred to as the *ground arch* (Figure 5.5). The arch action is the consequence of the local stress loosening produced by tunnel excavation. The mechanics of the arch action is shown in Figure 5.6. The shaded area (**acdb**) in that figure is the ground arch with a width B_1, and the zone of arching is assumed to have a depth D. While the tunnel is being excavated and the support is being installed, the mass of crushed rock or cohesionless sand constituting the ground arch tends to move into the tunnel. This movement is resisted by the friction along the lateral boundaries **ac** and **bd** of this mass. The ground arch shown in Figure 5.6 presents the concept of arching. However, it is inconvenient to use this configuration in actual calculation. Terzaghi, therefore, provided a simplified model to calculate the load on tunnel supports in Figure 5.8. The friction forces transfer the major part of the weight of the overburden, with height H, onto the material located on

both sides of the tunnel. The roof support of the tunnel carries only the balance which is equivalent to a height H_p. H_p is the "equivalent overburden height" (Figure 5.8). This height is used to represent the pressure on a tunnel in this section. The actual pressure acting on the tunnel can be obtained by multiplying this height with the total unit weight of the geomaterial.

Terzaghi suggested that the thickness, D, of the ground arch was roughly equal to $1.5B_1$ while above the ground arch the pressure conditions in the rock remained practically unaffected by the tunnel operations. Within the range of D (Zone of Arching, Figure 5.6), a very small downward movement of the tunnel crown suffices to reduce the rock load on the support of the intrados of the arch to a value $H_{p\ min}$, which is much smaller than the thickness, D, of the ground arch (Terzaghi, 1946). If the crown of the ground arch is allowed to subside still more, the rock load on the roof support again increases and approaches a value $H_{p\ max}$, which is still much smaller than D (Terzaghi, 1946).

After the roof support is installed and tightly backpacked, the rock load increases at a decreasing rate by about 15% from H_p to $H_{p\ ult}$, i.e. $H_{p\ ult} = 1.15H_p$ (Figure 5.7). The load-depth relationship for a tunnel in sand or crushed rock is thus indicated by curve C in Figure 5.7. The 15% increase of H_p is the so called "time increase of the rockload". Terzaghi also suggested that H_p could be related to the width B_1, the width of the ground arch (Figure 5.6), and that B_1 was roughly equal to the width of tunnel (B) plus the height (H_t). Therefore, the load on a tunnel, H_p, is represented as follows:

$$H_p = C \times B_1 = C \times (B + H_t) \qquad \text{(Eq. 5.9)}$$

in which

C = a constant depending on the degree of compactness of the crushed rock or sand and on the distance *d* through which the crown of the ground arch subsided while the tunnel was constructed and the roof support was being installed.

The distance *d* here is not known and it can hardly be determined by practical means. Hence, the values for the constant C in Eq. 5.9 were recommended by Terzaghi from his model testing results and experience. He considered different conditions of the tunnel: (1) above water table or below water table, and (2) various geomaterials which include loose sand, dense sand, and rock. The values for H_p are shown in Table 5.1. The ultimate value in the table is equal to 1.15 times the initial value as discussed above. Terzaghi simplified the real ground arch shown in Figure 5.6 to the configuration in Figure 5.8. Only the rectangular part above the tunnel roof is carried by tunnel itself. The other parts are carried by arching effect or by the rock wedges at the sides of the tunnel.

According to Terzaghi's experience, the actual roof load on a tunnel was normally much closer to the minimum than to the maximum values (Table 5.1). This fact indicated that a slight movement of the geomaterial towards the tunnel would activate the arching effect in the entire ground arch. He suggested a quick installation of tunnel support since the load on a tunnel would increase from $H_{p\ min}$ to $H_{p\ max}$ gradually if more settlement of the ground arch was allowed.

5.4 Methods Neglecting the Overburden Depth

The methods in this group essentially determine the loosening pressure in the geomaterial which is caused by underground excavation. Any relationship between the overburden depth and the pressure on the opening is neglected. A common feature of these theories is the assumption that the temporary supports, or permanent lining of the opening will be acted upon only by the weight of the stress-free body developed as a consequence of loosening following excavation. Only one method will be introduced here.

5.4.1 Kommerell's Theory

The oldest and most widely known of these theories is that developed by Kommerell, who determined the height of the loading body from the deformations of the supporting structure in the opening (Széchy, 1973). The theory is justified by the consideration that the displacement, or deflection of the supporting structure is representative of the displacement in the disturbed mass of geomaterial. As a consequence of this displacement geomaterial is relaxed to a height *h*, which is equal to the height of the geomaterial column capable of filling this space of height *e* by loosening. Hence, if the ensuing specific strain is δ%, then:

$$e = \frac{h\delta}{100} \qquad \text{(Eq. 5.10)}$$

and thus

$$h = \frac{100 \cdot e}{\delta} \qquad \text{(Eq. 5.11)}$$

in which

δ = the loosening coefficient of the geomaterial as a percentage. Some loosening coefficients for different geomaterials are given as follows:

loose granular soil (sand)	δ (%) = 1-3 %
moderately cohesive soil (dry clay)	δ (%) = 3-5 %
cohesive soil (marl, gravely clay)	δ (%) = 5-8 %
soft rocks (sandstone, limestone)	δ (%) = 8-12 %
solid rocks	δ (%) = 10-15 %

The tunnel support is required to carry the weight of a rock mass bounded by a half ellipse of height *h*, as shown in Figure 5.9. Point O is the point of origin in the coordinate system, *x* and *y* are coordinates of the points on the ellipse, *e* is the deformation for the geomaterial, *h* is the height of the loosening zone, and *b* is the width of the tunnel. Therefore, the equation of the ellipse in Figure 5.9 will be:

$$\frac{x^2}{(b/2)^2}+\frac{y^2}{h^2}=1 \qquad \text{(Eq. 5.12)}$$

Substituting *h* in Eq. 5.12 with the *h* value in Eq. 5.11:

$$\frac{4x^2}{b^2}+\frac{y^2\delta^2}{10000e^2}=1 \qquad \text{(Eq. 5.13)}$$

The total load on the tunnel is:

$$\begin{aligned} P &= \gamma \times (\textit{Area of the half ellipse}) \\ &= \gamma \times \frac{1}{2}(\pi \cdot \frac{b}{2} \cdot h) = \gamma \times \frac{1}{2}(\pi \cdot \frac{b}{2} \cdot \frac{100e}{\delta}) \\ &= \frac{25\gamma\pi be}{\delta} \end{aligned} \qquad \text{(Eq. 5.14)}$$

Therefore, if we know the loosening coefficient (δ) from the type of the geomaterial, and assume the permissible deflection of the tunnel roof (*e*), we can obtain the height of the loosening zone (*h*) from Eq. 5.11, the shape of the loosening zone from Eq. 5.13, and also the total load on the tunnel roof (*P*) from Eq. 5.14.

Nevertheless, Kommerell's theory can only be used as a rough approximation because of the following reasons:

1) Loosening is possible in granular soils or crushed rocks as a result of the redistribution of individual particles. Loosening is impossible in bulk solid rocks, where only elastic expansion upon load release of the order of a few millimeters can occur.
2) The linear relationship assumed to exist between the deflection of the roof (e) and the height (h) of the loading mass could not be verified by measurements nor explained theoretically because it is purely an empirical relationship.

5.5 Discussion

The empirical and semi-empirical methods are often applied by engineers in conjunction with other approaches, such as numerical analyses, to the design of underground structures. Coefficients used in these methods may include the conditions (like depth) and the properties (like friction angle) of the geomaterial. Generally, these methods only present the pressure acting on the support system of a buried structure and not the displacements of the geomaterial and structure. The benefits of using the empirical methods are "quick" and "simple". If engineers choose a method which was derived from experiences with ground conditions and construction methods similar to those for the proposed structure, good results can normally be obtained.

However, there are still some uncertainties in these empirical methods. Especially some of the assumptions in these methods may not be realistic, e.g. the assumptions of the

loosening zone in aforementioned sections ,and the simplified equilibrium equations for the forces in the loosening zone. In addition, some assumptions are even incorrect under certain circumstances. For example, the theories in Section 5.4 which deal with the determination of loosening pressure in rock masses due to underground construction, neglect the effect of depth. These theories assume the development of arching action in the geomaterial, and consider that the size of the load mass on the top of a tunnel only depends on the size of the opening and the strength characteristics (such as the internal friction angle of the geomaterial). These assumptions are invalid when the opening is close to the ground surface or at a small depth. They are also invalid when the geomaterial undergoes plastic deformation or time dependent behaviors ,since the depth of the geomaterial will be an important factor under these circumstances. Comparing the empirical methods, based on the previous assumptions, with other analytical methods, suggests analytical methods are more appropriate in actual situations as they attribute a decisive role to the manner in which the stress distribution is changed in the vicinity of the opening. Hence, empirical methods should be applied in conjunction with the other analytical methods, in order to confirm their results.

Table 5.1 Overburden Load (in feet) in Sand and in Blocky and Seamy Rock (Proctor and White, 1946)

Material		Above water table		Below water table[1]	
		$H_{p\ min}$	$H_{p\ max}$	$H_{p\ min}$	$H_{p\ max}$
Dense sand[2]	Initial	$0.27\ (B + H_t)$	$0.60\ (B + H_t)$	$0.54\ (B + H_t)$	$1.20\ (B + H_t)$
	Ultimate	$0.31\ (B + H_t)$	$0.69\ (B + H_t)$	$0.62\ (B + H_t)$	$1.38\ (B + H_t)$
Loose sand[2]	Initial	$0.47\ (B + H_t)$	$0.60\ (B + H_t)$	$0.94\ (B + H_t)$	$1.20\ (B + H_t)$
	Ultimate	$0.54\ (B + H_t)$	$0.69\ (B + H_t)$	$1.08\ (B + H_t)$	$1.38\ (B + H_t)$
Moderately blocky[3]		$H_{p\ in} = 0$	increasing up to	$H_{p\ ult} = 0.35\ (B + H_t)$	
Very blocky and shattered		$H_{p\ in} = .60\ (B + H_t)$	increasing up to	$H_{p\ ult} = 1.10\ (B + H_t)$	

1. Values are roughly equal to twice those for dry sand.
2. Values computed on basis of laboratory tests.
3. Values computed on the basis of the results of observations in railroad tunnels.

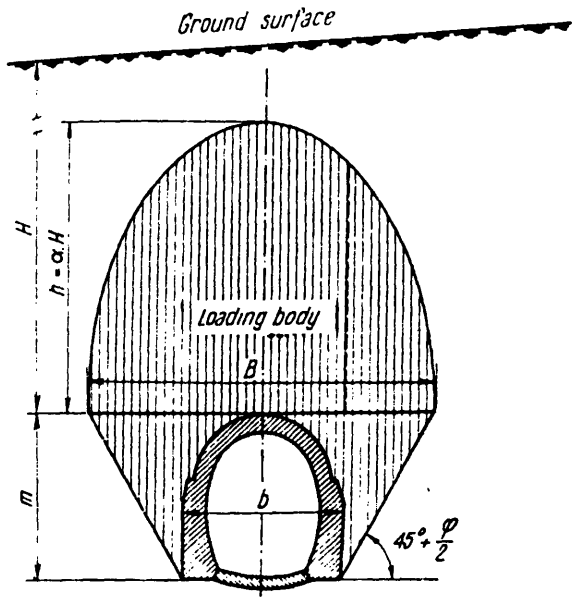

Figure 5.1 Rock Pressure Bulb after Bierbäumer (Széchy, 1973)

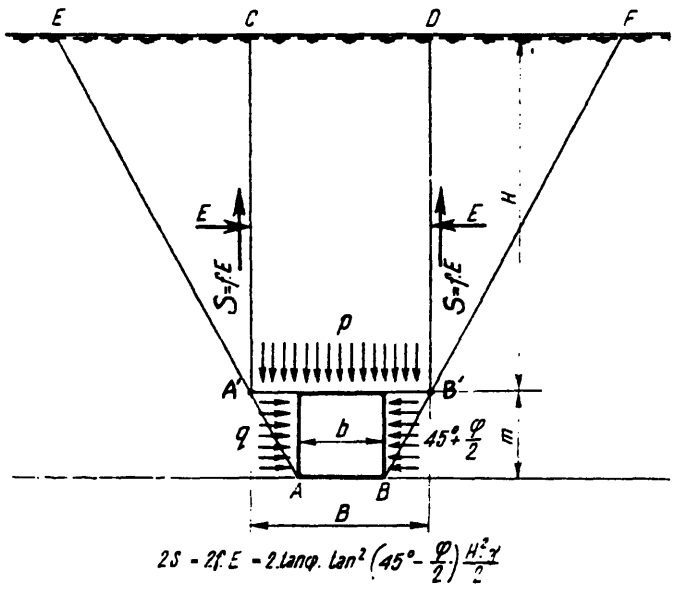

Figure 5.2 Assumption Model of Bierbäumer's Theory: Maximum Load (Széchy, 1973)

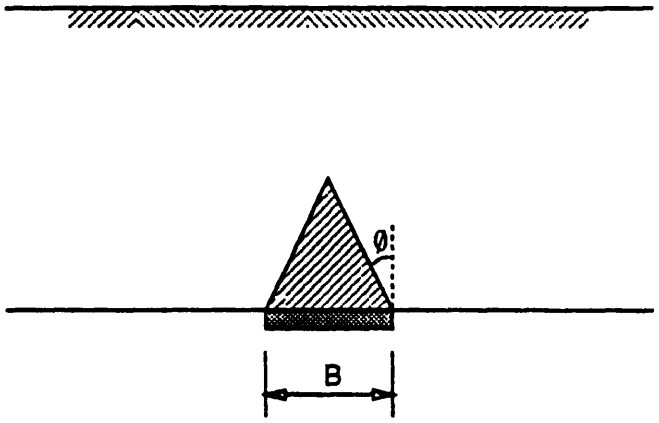

Figure 5.3 Assumption Model of Bierbäumer's Theory: Minimum Load (from Iglesia et. al., 1990)

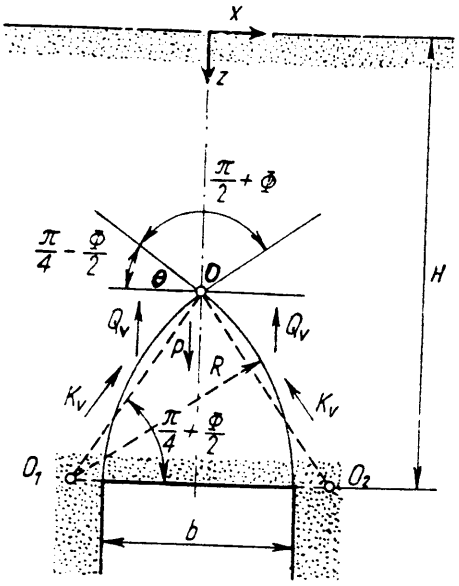

Figure 5.4 Principle of Balla's Theory (Balla, 1963)

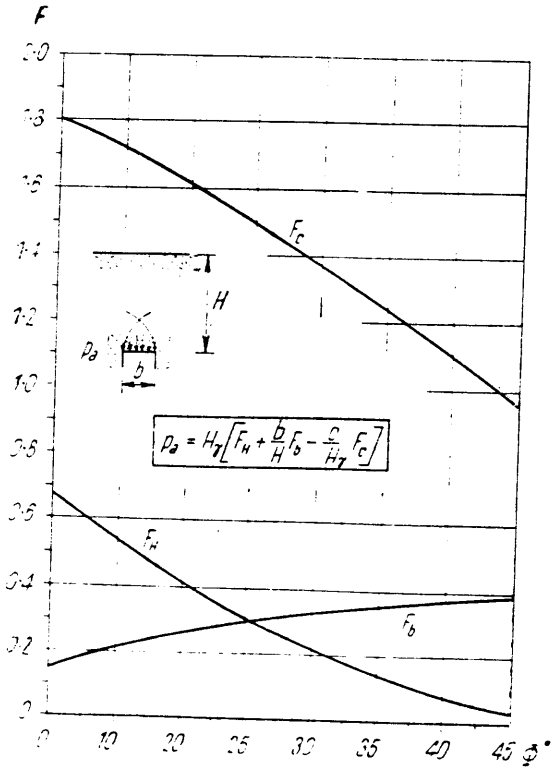

Figure 5.5 Resistance Factor Diagram and Table (Balla, 1963)

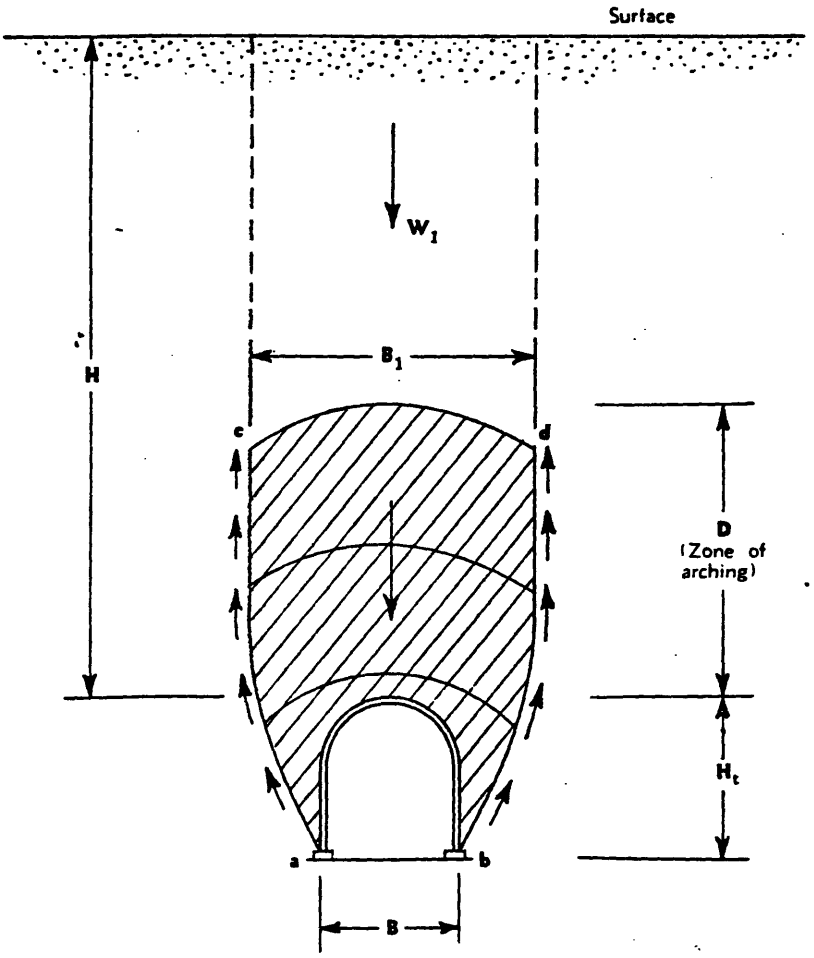

Figure 5.6 Configuration of Ground Arch (Proctor and White, 1946)

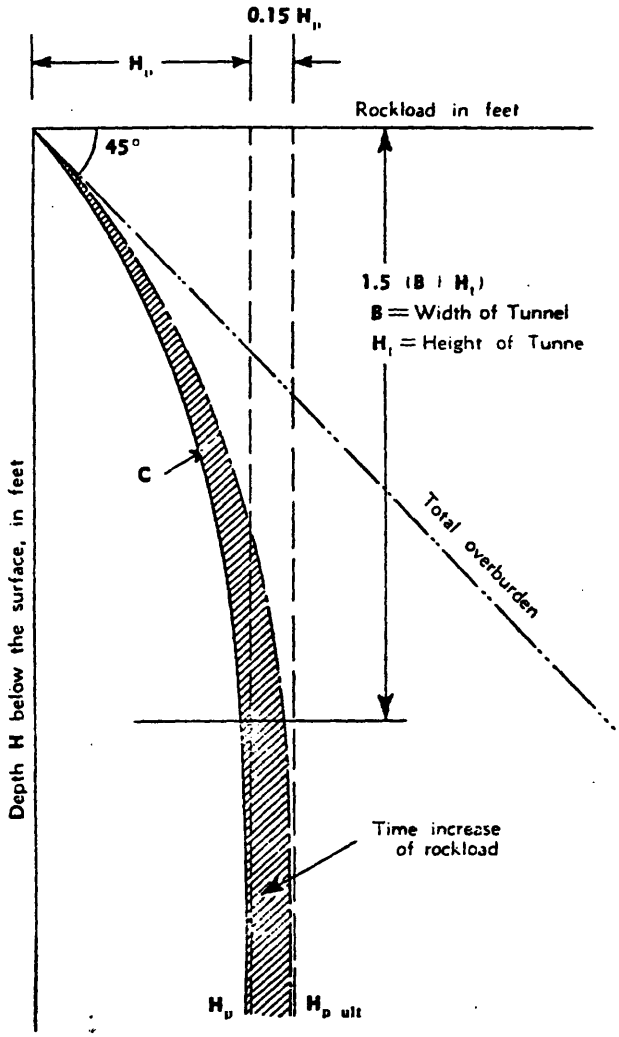

Figure 5.7 Load-Depth Relationship on a Tunnel in Sand or Crushed Rock (Proctor and White, 1946)

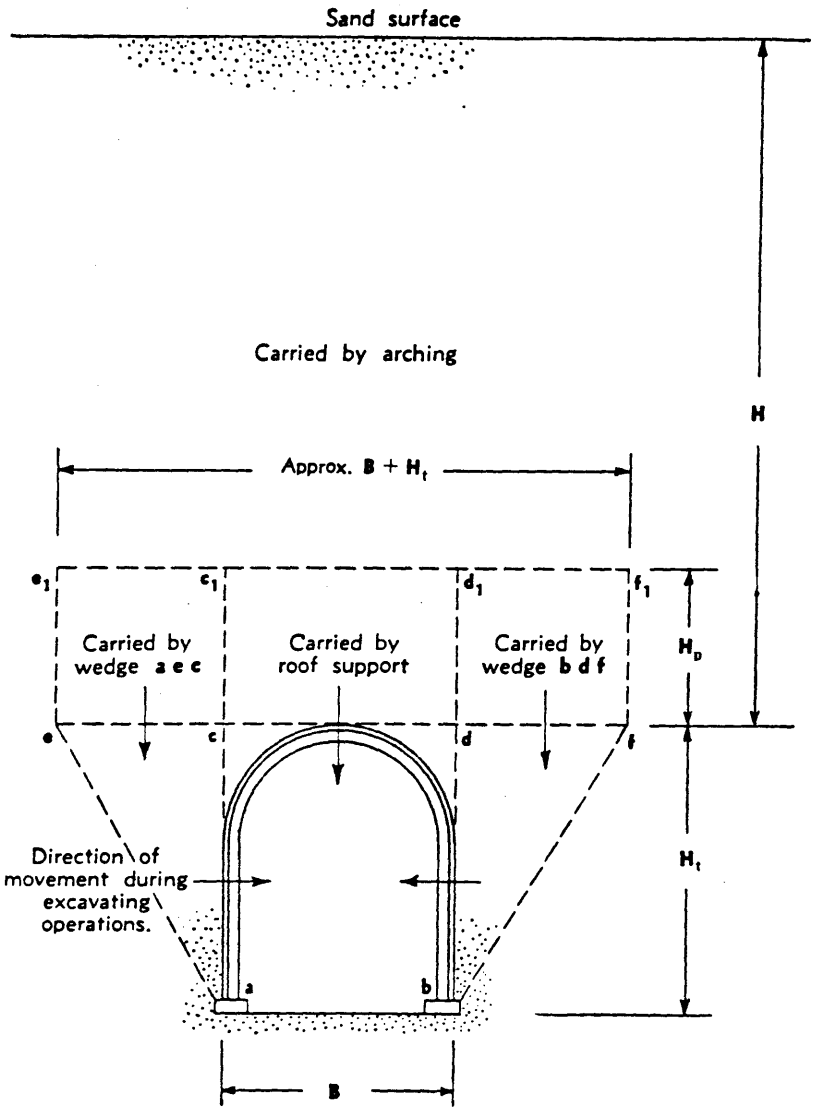

Figure 5.8 Simplified Model of Load on Tunnel Support (Proctor and White, 1946)

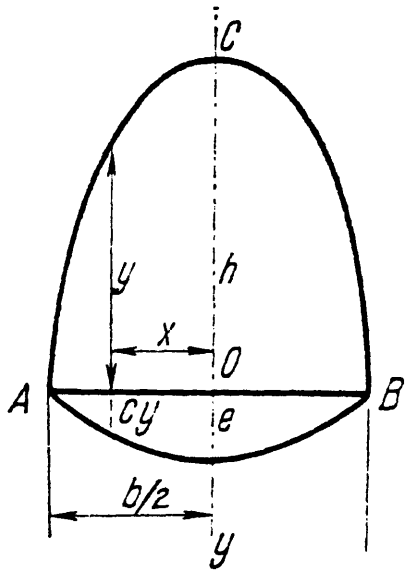

Figure 5.9 Shape of Kommerill's Pressure Diagram; Line **AB**: the Tunnel Roof (Széchy, 1973)

Chapter SIX
Experimental Investigations and Photoelasticity Methods

6.1 General

In this chapter, several experimental investigations will be reviewed. After Terzaghi's trap door experiment, several different trap door experiments were performed. They are similar to Terzaghi's experiment but with different improvements or extensions. For example, McNulty (1965) increased the pressure on the trap door to simulate the in-situ stress level. Ladanyi and Hoyaux (1969) used an ideal granular mass (aluminum rods) in plane strain in their trap door experiments to check the validity of the classic bin theory (i.e. the assumption of vertical failure planes in Terzaghi's arching theory, see Section 3.2). Harris (1974) performed experiments with several trap doors to investigate the effect of advancing face in underground construction. Evans (1984) used different shapes (circular and rectangular) of trap doors to conduct his experiments. Iglesia et. al. (1990) performed the trap door experiments with different materials (sand, wooden, and aluminum rods) in a centrifuge to explore the arching effect. Photoelastic methods used in exploration of stresses around underground structures (Riley, 1964) and interparticle contact forces (Paikowsky et. al., 1993 & 1995) will also be discussed in this chapter.

6.2 Experiments by McNulty (1965)

The trap door experiments from Terzaghi (1936) are small scale experiments. The stresses acting on the trap door are fairly small comparing to those stresses in real con-

struction sites. In order to reach stress levels commonly encountered in the field, McNulty (1965) applied air pressure at the surface of the sand in a trap door experiment which is otherwise similar to Terzaghi's 1936 experiment.

In McNulty's experiment, a cylindrical soil chamber with a circular trap door at its bottom was used (Figure 6.1). McNulty developed both active and passive arching in his study by measuring the pressure acting on the trap door (P_B) as the door displaced upward or downward by an average displacement (δ). In addition, the effects of overburden depth (H), trap door diameter (B), surface pressure (P_S), and different soil properties were also evaluated in his study. The layout of McNulty's axisymmetric tests is shown in Figure 6.1. There is a parameter called the "arching ratio" (AR) in Figure 6.1. This parameter equals the pressure on the trap door divided by the surface pressure:

$$\text{AR (arching ratio)} = \frac{P_B \text{ (pressue on the trap door)}}{P_S \text{ (surface pressue)}} \qquad \text{(Eq. 6.1)}$$

In order to investigate the influence of different soil properties, two sands were used. Sand 1 was the Reid-Bedford Model sand. It was a clean, uniform, find sand with D_{10} = 0.16 mm and average friction angle of 33^0. Sand 2 was the Cook's Bayou sand. It was a clean, uniform, medium sand with D_{10} = 0.22 mm and average friction angle of 38^0.

Typical results from McNulty's series of axisymmetric tests are shown in Figure 6.2 (sand 2 is used here). These results show that even a very small deflection (i.e. a very small value of δ/B in the figure) can cause considerable changes in the load on the trap door. This outcome is similar to the previous observations by Terzaghi (1936). However, in Terzaghi's experimental results for active arching, the pressure on the trap door would increase gradually and reach a constant ultimate value (i.e. a normalized force,

$F/F_0 \times 100\%$, which is about 12.5%) after a sudden decrease ($F/F_0 \times 100\% = 6\% \sim 9.6\%$), at the beginning (details in Figure 3.2). This phenomenon was not observed here. The load-displacement curves for active arching in Figure 6.2 do indicate that there was an apparent decrease of pressure, but the pressure on the door did not increase afterward; it (pressure) would keep decreasing until an ultimate value was attained.

The load-displacement curves in the active arching cases show that the load reduction is greater as the depth of soil overburden increases. For the passive arching (i.e. the trap door moving upward), the increase in load is greater as the overburden depth increases (e.g. the H/B =2 curve in Figure 6.2). However, McNulty found that the influence of H/B value on the passive arching curves was minimal when $H/B > 2$. This indicates that as the ratio of the soil depth to the trap door diameter (H/B) increases in the active arching case, a stronger soil arch will be developed in the soil body and transfer more load from the trap door. On the other hand, the trap door will take more pressure when the soil depth/trap door size ratio increases (i.e. H/B is greater) in the passive arching case.

McNulty also compared results of the two different types of sands he used in his experiments. Sand 2 was stronger than sand 1 since sand 2 had a higher friction angle (38^0). The results for the active arching experiments with a surface pressure of 75 psi are depicted in Figure 6.3. For the shallow soil depths (H/B = 1/3 and 2/3 in Figure 6.3), the ultimate arching ratios differ by about 10%, though the trap door moves the same for both sands to develop the ultimate arching ratio. Sand 2 has the lower value in the figure and this means it can transfer more load than sand 1. At H/B = 4, the ultimate arching ratios of these two sands are close to each other, but it takes sand 1 twice the door movement to

reach this ratio than sand 2 (see the bottom plot in Figure 6.3). The similar behavior of the two sands at small values of H/B is attributed to the immediate attainment of a state of plastic equilibrium caused by a slight door movement with shallow soil depths. The difference at greater soil depth is due to the difference in the soil strength (i.e. the friction angle).

6.3 Experiments by Ladanyi and Hoyaux (1969)

Ladanyi and Hoyaux (1969) performed an experimental program involving an ideal granular mass overlying a model trap door in plane strain conditions. Figure 6.4 shows their apparatus. The geomaterial was simulated by a stack, 40 inches high and 80 inches wide, of aluminum rods supported by a U-shaped rigid steel frame. The rods were 2.5 inches long and had circular cross sections with two different diameters, 1/8 inch and 3/16 inch. They were cut to the required length, sanded in a sand drum and then mixed in equal proportions to form the testing samples. The resulting granular medium had a unit weight $\gamma \approx 0.079$ lb/in^3 and a friction angle $\phi \approx 29^0$ at the anticipated stress levels. No surface pressure was applied. Hence, the anticipated stress levels in the experiments were very low. The trap door here was a buried structure, 3 inches wide and 2.5 inches long, represented by a rectangular rigid metallic box, which could be moved up or down like a piston inside the big testing box with aluminum rods. Figure 6.5 shows the downward (Figure a) and upward (Figure b) movements of the trap door structure.

In the tests, the pressure on the trap door was measured as a function of the vertical door movement. The rod displacement trajectories were photographically recorded.

By painting a six-inch square mesh grid on the rod sample, a photo of the overall deformation pattern of the sample was taken after the trap door was moved a certain amount. Figure 6.6 shows the results when the trap door had undergone a large downward movement (3.6 inches). It was observed that the deformation of the grid (Figure 6.6) was well limited to a narrow band above the trap door. Some lateral movement of the granular material toward the centerline was also observed during the test. This was because the granular material tended to fill the space generated by the downward movement of the trap door. The results obtained from four active arching simulations are shown in Figure 6.7. Four different overburden depths were used. They were 6 inches (H/B = 2.00), 8.5 inches (H/B = 2.84), 13 inches (H/B = 4.33), and 16 inches (H/B = 5.33). The maximum displacement of the trap door in these tests was 4 inches. The results, illustrated in Figure 6.7, were similar to the results that other researchers had observed. A rapid drop of pressure on the trap door occurred shortly after the door was lowered. In the cases shown here, the minimum pressures were obtained after the door moved downward of about 8% of the trap door width (Figure 6.7). With further door movement, the pressure on the trap door increased gradually until an ultimate value was reached. The reduction in pressure due to active arching became more significant as the soil overburden depth became greater (i.e. H/B is greater).

A theoretical approach used to estimate the pressure reduction on the trap door was derived by Ladanyi and Hoyaux. However, the major purpose of Ladanyi and Hoyaux' was to examine the appropriateness of the assumption of two limiting vertical failure planes in the traditional arching analysis (Terzaghi, 1943). A comparison of meas-

ured and calculated vertical pressures for a downward moving structure (active arching) at different depths of burial is shown in Figure 6.8. The calculated results were close to the measured results. Hence, Ladanyi and Hoyaux believed that, within the depth interval investigated, the variation of pressure acting on a vertically translating rigid horizontal trap door could be reasonably predicted by assuming the existence of two limiting vertical failure planes extending from the edges of the trap door to the free surface (see Figure 3.5 & Figure 3.6). A correct pressure prediction was, however, only possible when proper considerations were made concerning the lateral stress ratio (K) and the value of normal stresses (σ_h) acting along the assumed vertical failure plane.

6.4 Experiments by Harris (1974)

Harris (1974) performed sandbox trap door experiments aimed at simulating the stress redistribution around a long wall coal mining operation. Harris' apparatus is shown in Figure 6.9. It consisted of a series of trap doors which could be lowered independently to model the advancing face. Diaphragm pressure cells were located as shown to measure the stresses on the trap doors. By lowering the doors in succession, Harris obtained the stress distribution from beyond the influence zone ahead of the face. Typical results are shown in Figure 6.10. Areas of stress concentration (at abutments) developed ahead of and to the side of the face. A less developed abutment (the "rear abutment area" in Figure 6.10) appeared within the extracted zone (above the lowered doors). Harris' results can also be interpreted as the stress distribution around an advancing tunnel face in soft ground. We can conclude that the stress field near the face is not like that predicted by

most approaches. Instead, it is a very complicated three-dimensional pattern. A constant stress distribution does not develop until one to two face widths behind the advancing face. Similar experimental results were found in Evans' experiments (details in Section 6.5).

6.5 Arching in Granular Soil (Evans, 1984)

6.5.1 Experimental Setup

The theoretical continuum approach using plasticity theory developed by Evans (1984) was discussed in Chapter 4. This section describes several trap door tests that were performed by Evans to verify the validity of the theoretical approach and to further explore the load redistribution process in buried structures.

Evans' trap door tests included: (1) active arching above a circular trap door, (2) active and passive arching above a rectangular trap door under plane strain conditions, and (3) active arching above a row of trap doors lowered in succession so as to simulate an advancing tunnel. Figure 6.11 shows the circular trap door apparatus which was an initial test instrument. Evans constructed it for the purpose of determining whether the diaphragm type pressure transducers would give accurate results in his arching study. Figure 6.12 presents the rectangular trap door apparatus which was the primary test instrument in his study (plain strain conditions). The rectangular trap door apparatus was installed with a series of rectangular trap doors so it also can be used for the simulation of an advancing tunnel. Basically, the instruments used in Evans' experiments were similar to those used in the other trap door tests (e.g. Terzaghi's test in 1936). Evans, however, used the dia-

phragm type transducers to get more accurate pressure readings on the trap doors and on the bottom of the testing box.

In order to investigate sand type effect, four different sands were used: (i) Fine Leighton Buzzard sand, (ii) Coarse Leighton Buzzard sand, (iii) medium tan sand (Bin 23 sand), and (iv) fine white sand. The soil samples were prepared by the raining deposition technique, resulting in loose-sand samples.

6.5.2 Test Results

Figure 6.13 shows the variations of soil displacement pattern with increasing trap door displacement during an active arching test in the primary test apparatus. A triangular shaped zone expanded vertically with noticeable dilation present. This result matches Evans' analytical approach by plasticity theory which was shown in Figure 4.9 (a). When the dilation angle (ν) is larger than zero, the soil body expands and the free body diagram is triangular. The relation of normalized vertical stresses on the trap door versus its displacements is shown in Figure 6.14. This relation is, again, similar to Terzaghi's trap door testing results (Figure 3.2, Loose sand) and typifies the active arching behavior observed. Vertical stresses decreased rapidly as door movement began, until they reached a minimum value. As door motion proceeded, the stresses went up to a point where the displacement was about 10% of the trap door width, at which the stresses became quite steady afterwards.

As to the passive arching case, Figure 6.15 shows the typical patterns of soil deformation in Evans' tests. A trapezoid zone expanded in the vertical direction and showed

apparent dilation in the soil body. Evans' plastic analytical model for passive arching in plane strain condition is similar to this result when $\nu > 0$ (Figure 4.10 (a)). Figure 6.16 describes the quantitative results of Evans' passive arching tests. The stresses on the trap door increased quickly as soon as the door was moved upward and then reached a peak value. After the peak, the stresses on the door began to decrease till a fairly constant value was reached. The passive arching test results of Evans' experiments are similar to McNulty's results shown in Figure 6.2, differing by the fact that no apparent peak value was observed in McNulty's results. McNulty found that the ratio of the overburden soil depth (H) to the trap door width (B) affected the level of arching obtained. Evans' test results confirmed that observation. The percentage change in the trap door stresses increased as the H/B ratio increased (Figure 6.2 and 6.16).

The simulations of an advancing tunnel by successive lowering of a series of trap doors were performed by Evans' study as well. When the trap doors were lowered (active arching) or raised (passive arching) in consequence, the deformation of the soil body was observed (as shown in Figure 6.17 and 6.18) and the stresses on each trap door were measured. Evans found that, even at shallow depths, the "tunneling" process caused redistribution of stresses more than one diameter in advance, at least 0.5 diameter to each side and 1.5 diameters behind the face. His results clearly showed that those arching approaches which do not account for three-dimensional behavior will incorrectly model the kinematical compatibility in soil. Evans believed that instead of no volume change as assumed in the traditional two dimensional arching models, there should have been a volume increase in the soil when arching occurred.

The use of four different sands in Evans' tests resulted in similar behaviors except in the tests simulating an advancing tunnel. In these tests, smaller stress redistribution was observed for the fine white sand compared to the medium tan sand under identical test conditions. However, no further explanation was given in Evans' study.

6.5.3 Comparison of Plasticity Theory Approach and Test Results

The theoretical results presented in this section are based on the primary test apparatus in a plane strain condition (Figure 6.12). Evans compared his test results with the predicted values based on his plasticity approach (Section 4.3) and those developed others. A dimensionless "load factor" (C_c) was used for the comparison shown in this section. It was defined as:

$$C_c = \frac{F}{\gamma B^2} \qquad \text{(Eq. 6.2)}$$

in which,

F : the force per unit length of door parallel to the infinite axis, i.e. $F = B \cdot (\sigma_V)_{avg}$,

γ : the soil's unit weight,

B : the trap door width.

The value of the coefficient of lateral stress (K) needs to be decided before using Evans' theoretical approach to calculate the force acting on the trap door. Evans has actually measured the K value in some of his experiments. He noticed its variability depending on the vertical location as well as the level of trapdoor displacement. He picked out K equal to 1.2 to calculate all of the theoretical results.

(I) Plane Strain Arching/ Active Case:

Figure 6.19 and 6.20 provide comparisons between experimental results and predicted values through plots of load factor (C_c) versus H/B. Figure 6.19 presents experimental results for the maximum arching points (the peak) from Evans' tests, Terzaghi's tests (1936), and Harris' test (1974). Several theoretical predicting results are also shown in Figure 6.19. They include Széchy (1966), Vertical Slip Surfaces (Matyas & Davis, 1983a), Silo Theory (Janssen, 1895; Jakobson, 1958), Silo Theory as Modified by Terzaghi (1943), and Evans' Plasticity Theory Solution (1984). Table 6.1 has a summary of the formulas for the aforementioned theoretical methods. All the curves are drawn for the sand friction angle (ϕ) = 35^0 and K = 1.2. The plasticity theory solution is also shown for additional friction angles. Figure 6.20 shows results at the ultimate arching state (the steady value in Figure 6.14) and the predicting results from the plasticity theory solution. A comparison of these two figures suggests: (i) better predictions of load factors at maximum arching than any of the existing theories, and (ii) reasonably good predictions of load factors at ultimate arching. Since the soil body is in a plastic condition at ultimate arching, Evans' approach is the only method able to be applied.

(II) Plane Strain Arching/ Passive Case:

Figure 6.21 and 6.22 provide the comparison between experimental results and predicted values. Test data for the maximum arching state (Figure 6.21) are taken from Matyas and Davis (1983b) as well as Evans' own tests. Different theoretical approaches

were used in Figure 6.21 including US Standard for Rigid Pipe (Matyas and Davis, 1983a), Vertical Slip Surfaces (Matyas and Davis, 1983a), Ladanyi and Hoyaux (1969), Das and Seeley (1975), and Evans' Plasticity Theory Solution (1984). Table 6.2 lists the formulas of the aforementioned theoretical methods. All the curves are drawn for the sand friction angle (ϕ) = 35^0 and K = K_a (Active Rankine Ratio, $K_a = \frac{1-\sin\phi}{1+\sin\phi}$). Evans' theory once again provides the best prediction of forces at maximum arching. However, it consistently overestimates the magnitude by 10 to 15% (Figure 6.21). Evans explains that this overestimation is due to the assumption in his theory that uniform stresses across a trap door exist during passive arching. As to the ultimate arching state, there are not enough test data in Figure 6.22 to draw a strong conclusion regarding agreement with predicted values.

6.6 Centrifuge Modeling of Jointed Rock (Iglesia et. al., 1990)

6.6.1 Introduction

When a model is constructed smaller in size than the prototype but uses the same material as the prototype, the model is proportionately lighter than the prototype. This is usually not a major problem in models where the dead weight of the system can either be ignored or simply included in the external loads, for example, with applications in structural engineering. However, for geotechnical problems, the body forces can neither be neglected nor replaced with equivalent external forces that will produce the same effects. Therefore, if a geotechnical system is to be modeled physically at a small scale, both the

magnitude and the variation of geostatic stresses have to be duplicated in the model (Iglesia et. al., 1990). The best way to do this is by using a centrifuge to attain the desired geostatic stresses in the model.

Centrifuge modeling was started in the 19th century when a French engineer Phillips(1869) suggested that a centrifuge be used to simulate self-weight stresses in structural beams. Through the years, physical modeling of geotechnical systems with the centrifuge has become very popular. Centrifuge modeling for geotechnical research has been accepted widely in soil engineering. Iglesia et. al. (1990) tried to find out whether the centrifuge modeling scheme also applied to jointed rock mass. The following section illustrates their study.

6.6.2 Trap Door Experiments Using Centrifuge Modeling

The experimental setup adopted by Iglesia et. al. (1990) at MIT involved a jointed rock mass model with a trap door underneath. The trap door design was similar to several former experiments, e.g. Terzaghi (1936), McNulty (1965), Ladanyi and Hoyaux (1969), Evans (1983), etc. Figure 6.23 shows the concept of the trap door system and Figure 6.24 presents the real trap door utilized in the centrifuge modeling. The whole rock mass model system was spun up gradually to a desired gravity level, at which the trap door was lowered (i.e. active arching case), and measurements of the force on the door with the corresponding displacement were taken. Different sizes of small-scale models and of trap doors were used with various levels of pseudo-gravitational acceleration in the centrifuge at which the door was moved down. The primary objective of this research was to inves-

tigate the scaling relationships for centrifuge models of jointed media (wood rods and aluminum rods). A series of tests with granular materials (coarse sands and glass beads) was performed first to give an assessment of similitude for the designed system.

6.6.3 Experimental Results

A "modeling of models" exercise has been carried out with granular materials using various corresponding scales of particle size, door width, overburden depth, and gravity level. The test results were served as a benchmark upon which the experiments of scaling in jointed models could be based. Figure 6.25 presents the trap door test results of coarse sand with different soil depth. These curves showed similar shapes of the other active trap door test results (e.g. McNulty, 1965) and had the same trends as soil depth was increased, i.e. the deeper the soil, the greater the percent reduction in the load as the trap door displaced. Iglesia et. al. also performed different tests by changing different control factors. They found all of the results from various scaled models of the granular medium showed good agreement between the model and the prototype. In particular, the measured minimum loads on the trap door yielded the same average stress in appropriately scaled setups. They reached a conclusion that the criteria for similitude under plane strain conditions were satisfied in the centrifuge trap door models with granular media.

The centrifuge tests were then conducted with jointed media. Figure 6.26 presents an example which is the result from four sets of tests with different stack methods (direct stack and brick stack) used to determine the effects of g-level (40g and 80g). Figure 6.27 shows the final configuration of one set (GI 192) of the tests in Figure 6.26. An arch can

be seen clearly at the bottom of the picture. However, the test results (load-displacement relations) of jointed media did not completely fulfill the similarity requirements for appropriately scaled arrangements. The force value, especially with minimum loads on the trap door, approximate satisfying the similitude criteria for all the scale considered. These forces, nevertheless, occurred at about the same absolute door displacement which violated the centrifuge scaling laws. Similitude requirements in connection with the scaling of length dimensions were, thus, not met by the observed displacements. Iglesia et. al. believed that this finding did not suggest that centrifuge modeling was totally useless for situations involving jointed media, as they stated "The ability to generate body forces in the centrifuge makes it an invaluable tool in obtaining data against which analytical and numerical methods can be validated". They suggested, however, not to extrapolate results from model tests to actual prototype conditions when dealing with the jointed media.

6.7 Photoelastic Methods

6.7.1 Introduction

It is difficult to use traditional stress measurement methods to measure stress distributions around underground structures of complex geometry. However, photoelastic methods can solve this difficulty. Photoelastic methods are useful for measuring stresses and strains. They are based on a phenomenon that occurs when polarized light passes through certain homogeneous materials such as glass. Under straining, a brilliantly colored fringe pattern appears in the material. This colored fringe pattern results from

changes in the index of refraction (ratio of the velocity of propagation of light in a vacuum to its velocity in another medium) proportional to the amount of strain in a material in any given direction. Using this relationship, a proportionality constant can be developed that relates the "colored bands" to different levels of stress and strain.

In early photoelastic methods, stresses were induced in an elastic material which was subsequently set, freezing the stresses in place. The elastic material was then sliced and analyzed under polarizing filters. Because the material could be used only one time in each test, the cost of conducting a test by photoelastic methods was expensive. The new photoelastic method uses a special technique which can generate fringes in the material when the material is subject to external loads, but will not freeze fringes in the material after the external loads are removed. The fringes generated during the test are recorded by a high speed camera with a polarized filter. This new method allows one to reuse the photoelastic material and is, therefore, more economical.

6.7.2 Photoelastic Study in Embedded Structural Elements (Riley, 1964)

Riley (1964) used the new photoelastic method to conduct a series of studies to determine stresses in the free field of a two-dimensional plate and on the boundaries of embedded structural elements in the plate during passage of a stress wave. Two major parts were included in his experiment. First, was the explosive study. The model used was machined from a large sheet of low modulus urethane rubber. A 5/8 inch diameter hole was machined 4 inches from the point of load application along a radial line 30^0 from the centerline of the plate. The layout is shown in Figure 6.28. An explosive charge was

applied on the plate top at the centerline (Figure 6.28). A complete photoelastic fringe pattern record was obtained using a camera operating at 6780 frames per second through a polarized filter. Figure 6.29 shows an example of the fringe pattern around the hole at 1050 microseconds after the explosion. The stresses around the hole were then obtained by transforming these different colored fringes to the stresses they represent. Figure 6.30 shows the static and dynamic stress distributions on the hole boundary 1050 microseconds after the explosive charge was detonated. The static stress distribution was solved under a theoretical approach which assumed that a static load equal to the explosive load was applied on the plate top. The dynamic stress distribution (Figure 6.30) was transformed from the fringe pattern shown in Figure 6.29.

The second part of Riley's experiment was the air shock study. The model used for this part is shown in Figure 6.31. A 3/4 inch diameter inclusion was placed in a photoelastic plate at the point which was on the centerline and 4 inches from the top of the plate. The same material was used as in the first part. The air shock loading was applied to the top edge of the model by means of a 6 inch diameter shock tube. Several fringe patterns around the inclusion were obtained after the test.

Riley then compared the results of these dynamic test results with the static solutions (like Figure 6.30). He concluded that static solutions could be used as a first approximation for computing dynamic stress distributions on the boundaries of discontinuities in elastic materials. He suggested the photoelastic methods were useful in the study of stress distribution around underground structures under static loads and propagating stress waves.

6.7.3 Photoelastic Study in Direct Shear of Granular Material (Paikowsky, 1993 & 1995)

The same photoelastic technique was used by Paikowsky et. al. (1993) to study interparticle contact forces. In their experiment, particles were modeled two-dimensionally as circular and/or elliptical discs made from photoelastic material. This makes the measurement of contact forces (direction and magnitudes) possible, and allows particle tracking to evaluate their motion (translation and rotation). Riley's photoelastic measurement technique required detailed measurements to determine the stress field in a single plate. His method treated the whole testing system (a plate contains a hole or an inclusion) as one piece. In other words, the plate and the hole (or the inclusion) in the plate constitute a "continuum". However, if the interaction between discrete particles of a granular material (e.g. sand or rock) is desired under different loads, the use of photoelasticity for granular material modeling (Paikowsky et. al., 1993) would be more appropriate than Riley's continuum system.

Paikowsky et. al. (1995) used their granular material modeling system in a two-dimensional direct shear test. The direct shear box and samples are shown in Figure 6.32. All the circular particles in Figure 6.32 were made of photoelastic material. A vertical load was applied at the top of the whole particle system and the bottom solid surface was pulled out toward the left in Figure 6.32. The particle displacements and interparticle forces were measured when the bottom solid surface was being pulled out. Figure 6.33 shows the configuration of the particle system when the bottom solid surface was pulled

out by one particle diameter. All the particles in the second row (counting from the bottom) rotated 60^0 clockwise. An "arch" was formed at the right hand side, bottom corner, just like the soil arch observed in a sand direct shear test. This result demonstrated the possibility of using this experimental system to investigate all the interactions between particles, e.g. arching. However, not much qualitative analysis had been performed on the data collected to date. More analyses of the experimental data are necessary to prove the validity and versatility of their experiment. Further study in their experiment includes the effect of particle shape and particle size to the mechanical behaviors of the whole particle system, and a series of trap door tests to explore the arch effect in the granular material.

Table 6.1 Summary of Plane Strain Active Arching Formulae (Evans, 1984)

Széchy (1966)

$$C_c = \frac{H}{B}\left(1 - \frac{H}{B}\tan\phi\tan^2\left(45^\circ - \frac{\phi}{2}\right)\right) \qquad \text{for } \frac{H}{B} < 5$$

$$C_c = \frac{H}{B}\left(\tan^4\left(45^\circ - \frac{\phi}{2}\right)\right) \qquad \text{for } \frac{H}{B} \geq 5$$

Vertical Slip Surfaces (from Matyas and Davis, 1983a)

$$C_c = \frac{H}{B}\left(1 - K_0\frac{H}{B}\tan\phi\right) \qquad \text{with } K_0 = 1 - \sin\phi$$

Silo Theory

$$C_c = \frac{1}{2K\tan\phi}\left(1 - e^{-2K\frac{H}{B}\tan\phi}\right)$$

Silo Theory as Modified by Terzaghi (1943)

$$C_c = \frac{1}{2K\tan\phi}\left(1 - e^{-2K\frac{H}{B}\tan\phi}\right) \qquad \text{for } \frac{H}{B} \leq 2$$

$$C_c = \frac{1}{2K\tan\phi}\left(1 - e^{-4K\tan\phi}\right) + \left(\frac{H}{B} - 2\right)e^{-4K\tan\phi} \qquad \text{for } \frac{H}{B} > 2$$

Plasticity Theory Solutions:

For Maximum Arching Point

$$C_c = \frac{H}{B}\left(1 - \frac{H}{B}\tan\phi\right) \qquad \text{for } \frac{H}{B} < \frac{1}{2\tan\phi}$$

$$C_c = \frac{1}{4\tan\phi} \qquad \text{for } \frac{H}{B} \geq \frac{1}{2\tan\phi}$$

For Ultimate Arching State

$$C_c = \frac{\left(1 - e^{-2K\frac{H}{B}\sin\phi}\right)}{2K\sin\phi} \qquad \text{for } \frac{H}{B} \leq 2$$

$$C_c = \frac{\left(1 - e^{-4K\sin\phi}\right)}{2K\sin\phi} + \left(\frac{H}{B} - 2\right)e^{-4K\sin\phi} \qquad \text{for } \frac{H}{B} > 2$$

Table 6.2 Summary of Plane Strain Passive Arching Formulae (Evans, 1984)

U.S. Standard for Rigid Pipe (from Matyas and Davis, 1983a)

$$C_c = 1.961 \frac{H}{B} - 0.934$$

Vertical Slip Surfaces (from Matyas and Davis, 1983a)

$$C_c = \frac{H}{B}\left(K_o \frac{H}{B} \tan\phi + 1\right) \qquad \text{with } K_o = 1 - \sin\phi$$

Ladanyi and Hoyaux (1969)

$$C_c = \frac{H}{B}\left(1 + \frac{H \sin 2\phi}{2B}\right)$$

Das and Seeley (1975)

$$C_c = \frac{H}{B}\left(\frac{H}{B} K_a \tan\phi + 1\right)$$

Plasticity Theory Solutions --

For Maximum Arching State

$$C_c = \frac{H}{B}\left(1 + \frac{H}{B} \tan\phi\right)$$

For Ultimate Arching State

$$C_c = \frac{1}{2K_a \sin\phi}\left(e^{2K_a \frac{H}{B} \sin\phi} - 1\right) \qquad \text{for } \frac{H}{B} \leq 2$$

$$C_c = \frac{1}{2K_a \sin\phi}\left(e^{4K_a \sin\phi} - 1\right) + \left(\frac{H}{B} - 2\right) e^{4K_a \sin\phi}$$

where $K_a = \dfrac{1 - \sin\phi}{1 + \sin\phi}$ for $\frac{H}{B} > 2$

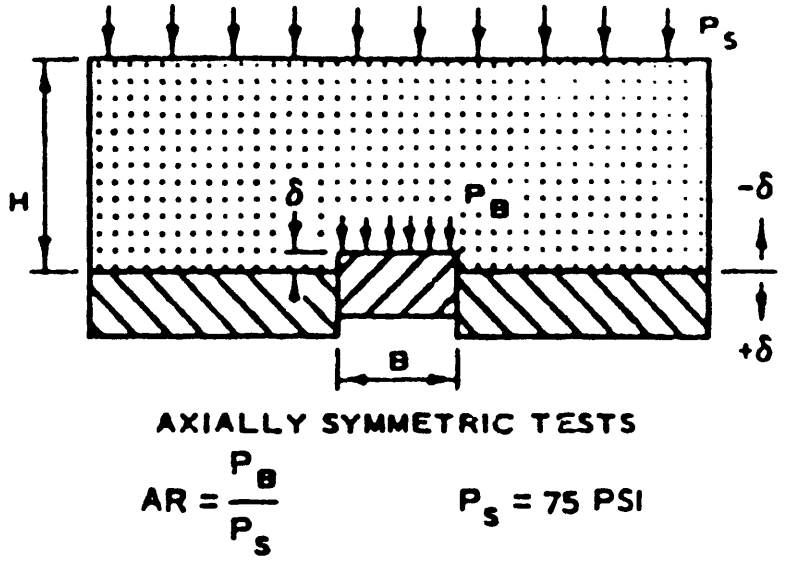

Figure 6.1 Layout of McNulty's Experiments (McNulty, 1965)

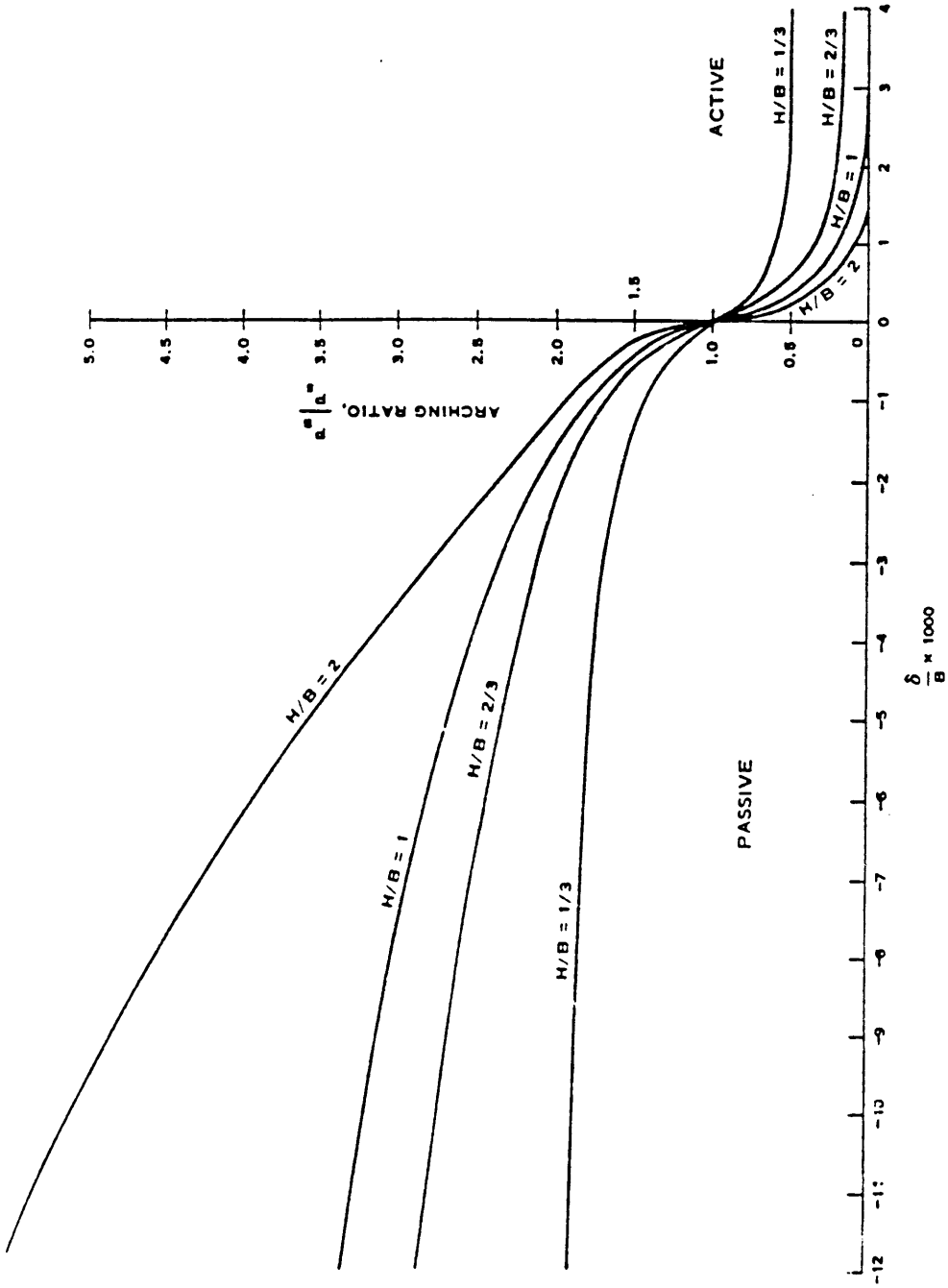

Figure 6.2 Active and Passive Arching Curves of Sand 2 (McNulty, 1965)

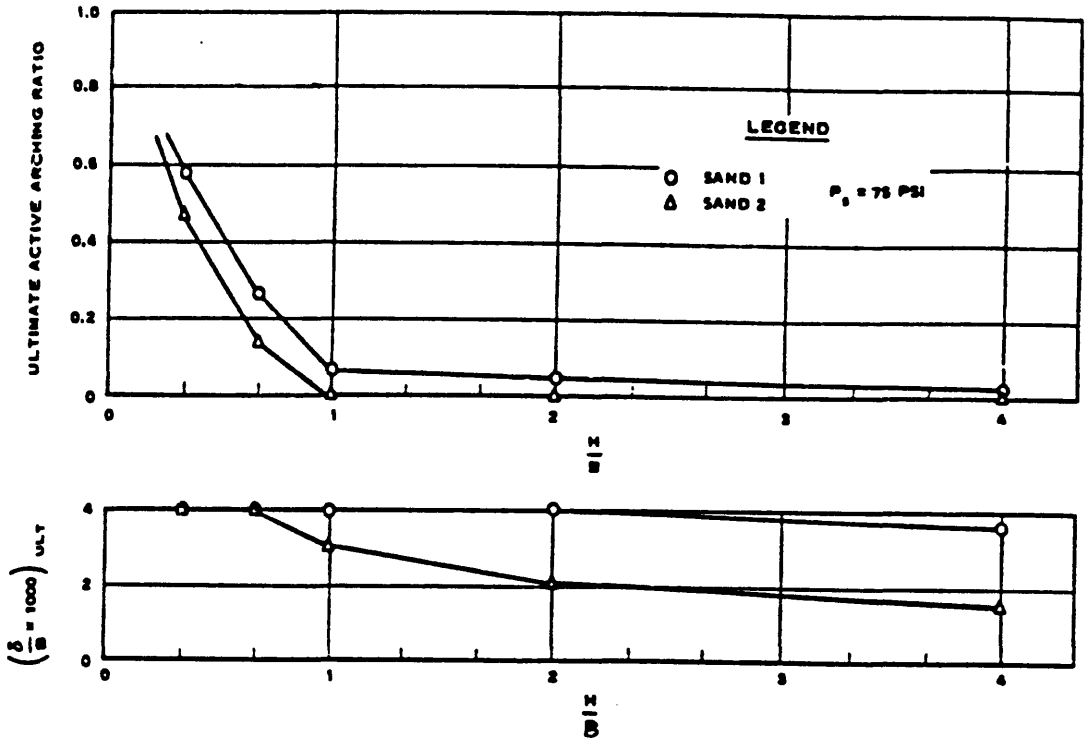

Figure 6.3 Influence of Soil Properties and Overburden Depth on Active Arching (McNulty, 1965)

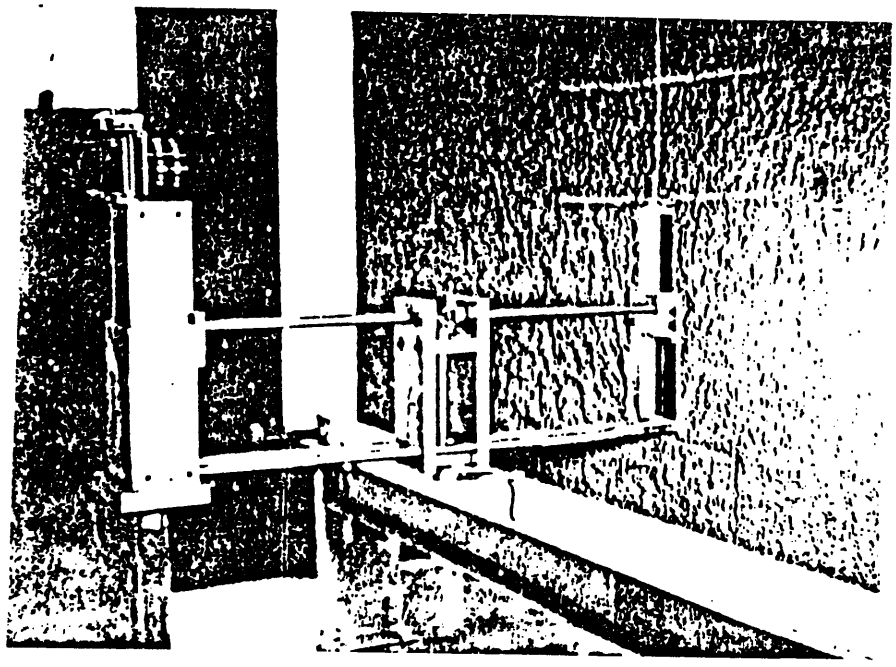

Figure 6.4 Ladanyi and Hoyaux's Experimental Setup (Ladanyi and Hoyaux, 1969)

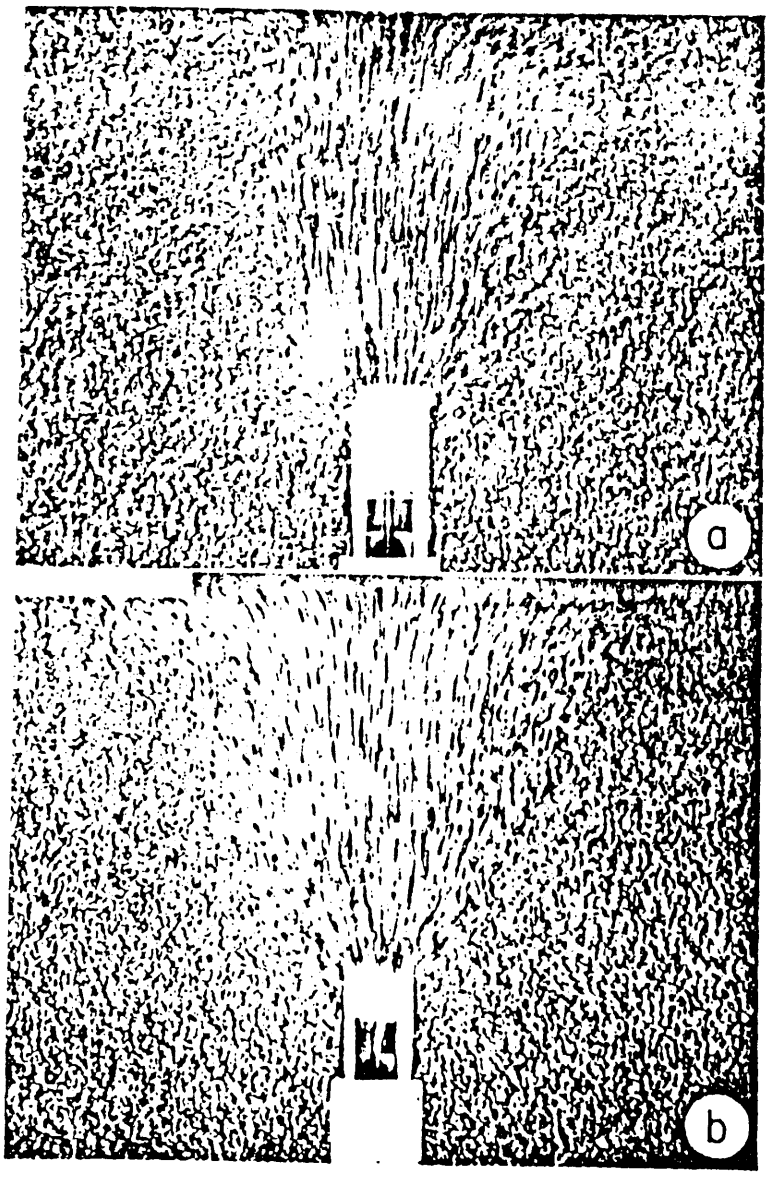

Figure 6.5 View of the displacement trajectories for (a) downward, and (b) upward movement of the structure (Ladanyi and Hoyaux, 1969)

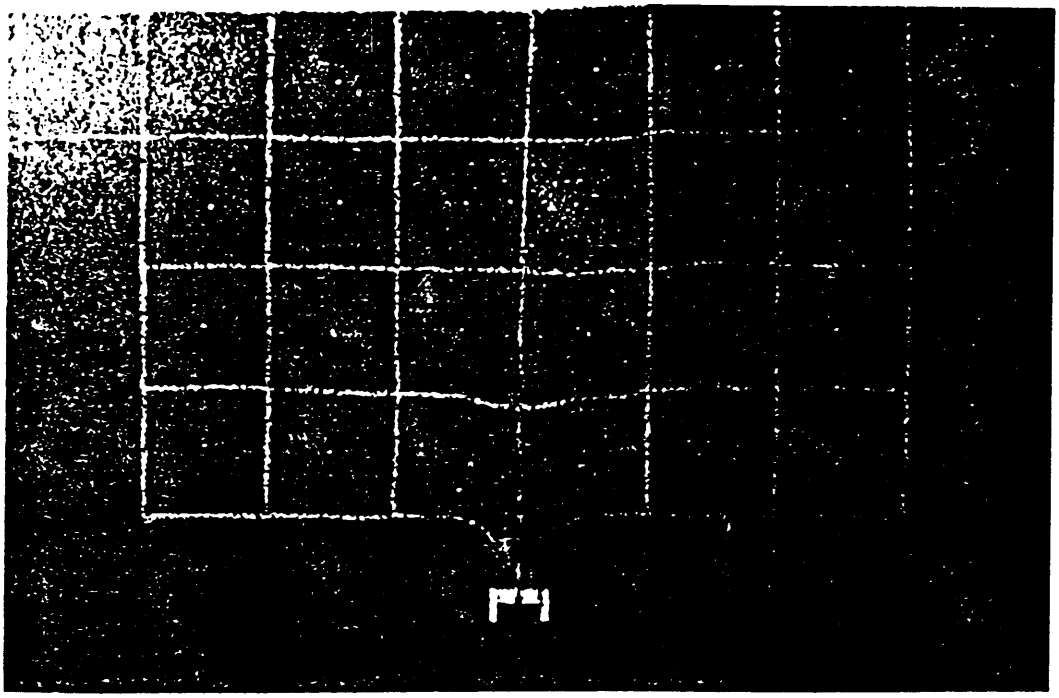

Figure 6.6 Deformed Square Grid after a Large Downward Movement of the Trap Door (Ladanyi and Hoyaux, 1969)

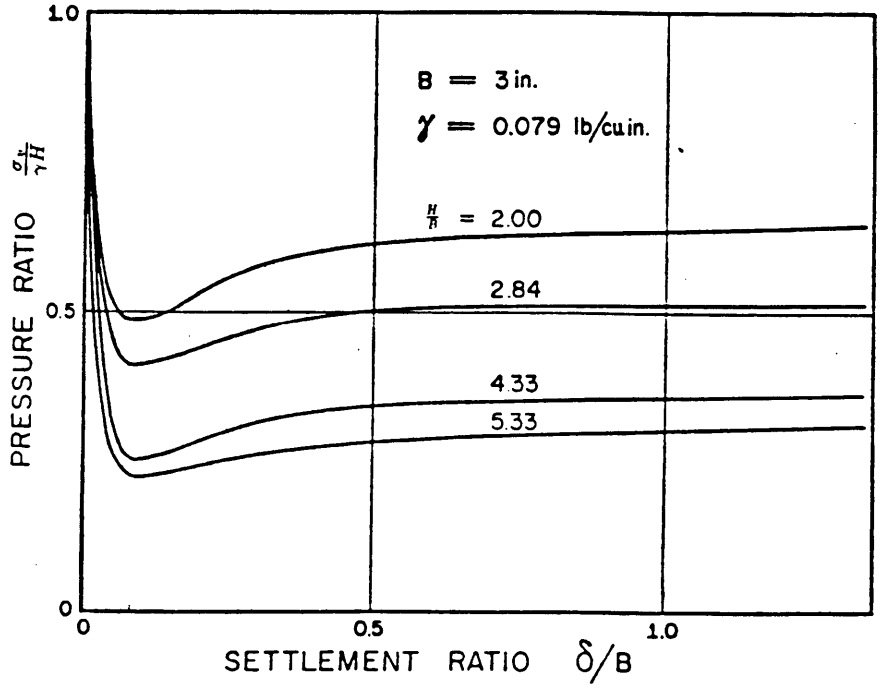

Figure 6.7 Normalized Pressure ($\sigma_v/\gamma H$) versus Settlement Curves of Active Arching (Ladanyi and Hoyaux, 1969)

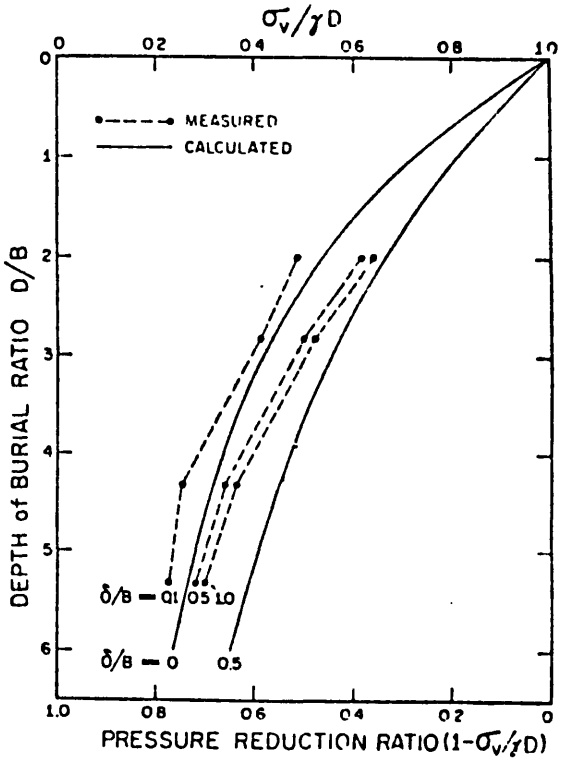

Figure 6.8 Comparison of Measured and Calculated Vertical Pressures for a downward moving trap door at different depths of burial (Ladanyi and Hoyaux, 1969)

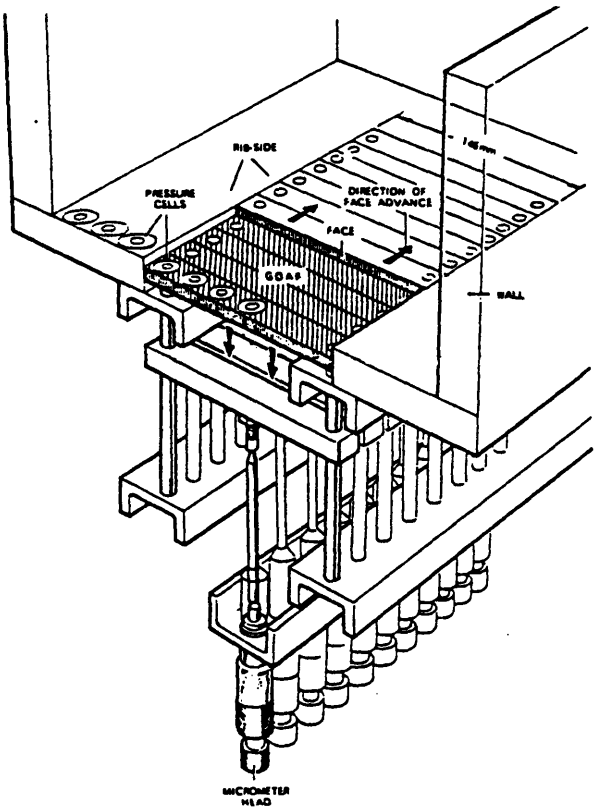

Figure 6.9 Apparatus Used in Harris' Experiments (Harris, 1974)

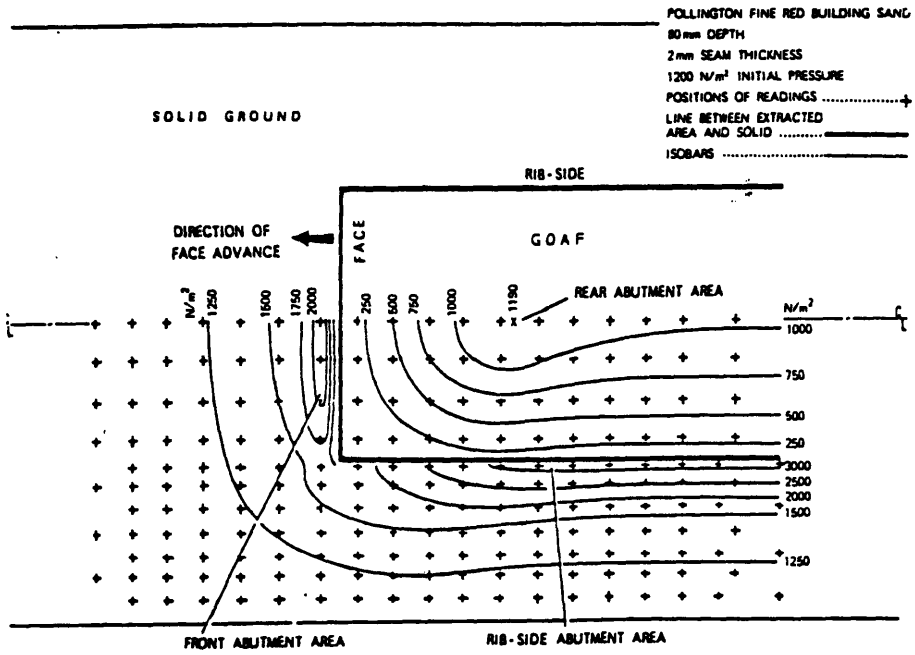

Figure 6.10 Vertical Stress Distribution from Harris' Experimental Investigation (Harris, 1974)

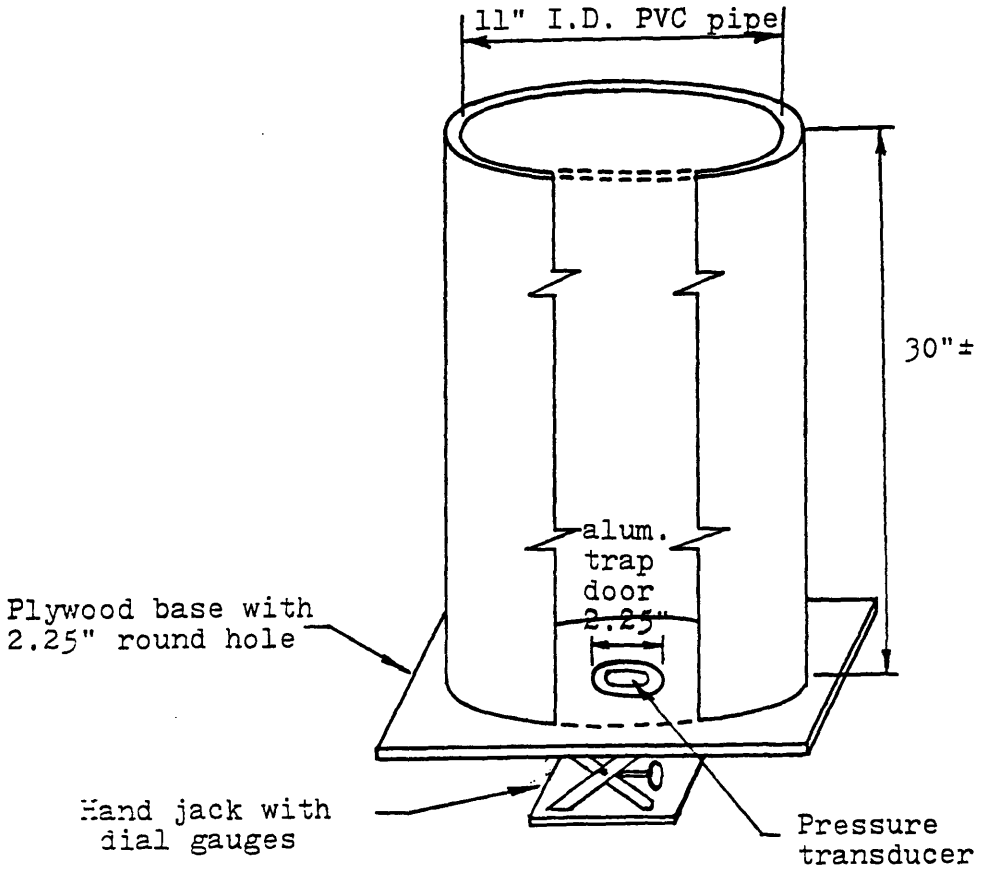

Figure 6.11 Test Apparatus with a Circular Trap Door (Evans, 1984)

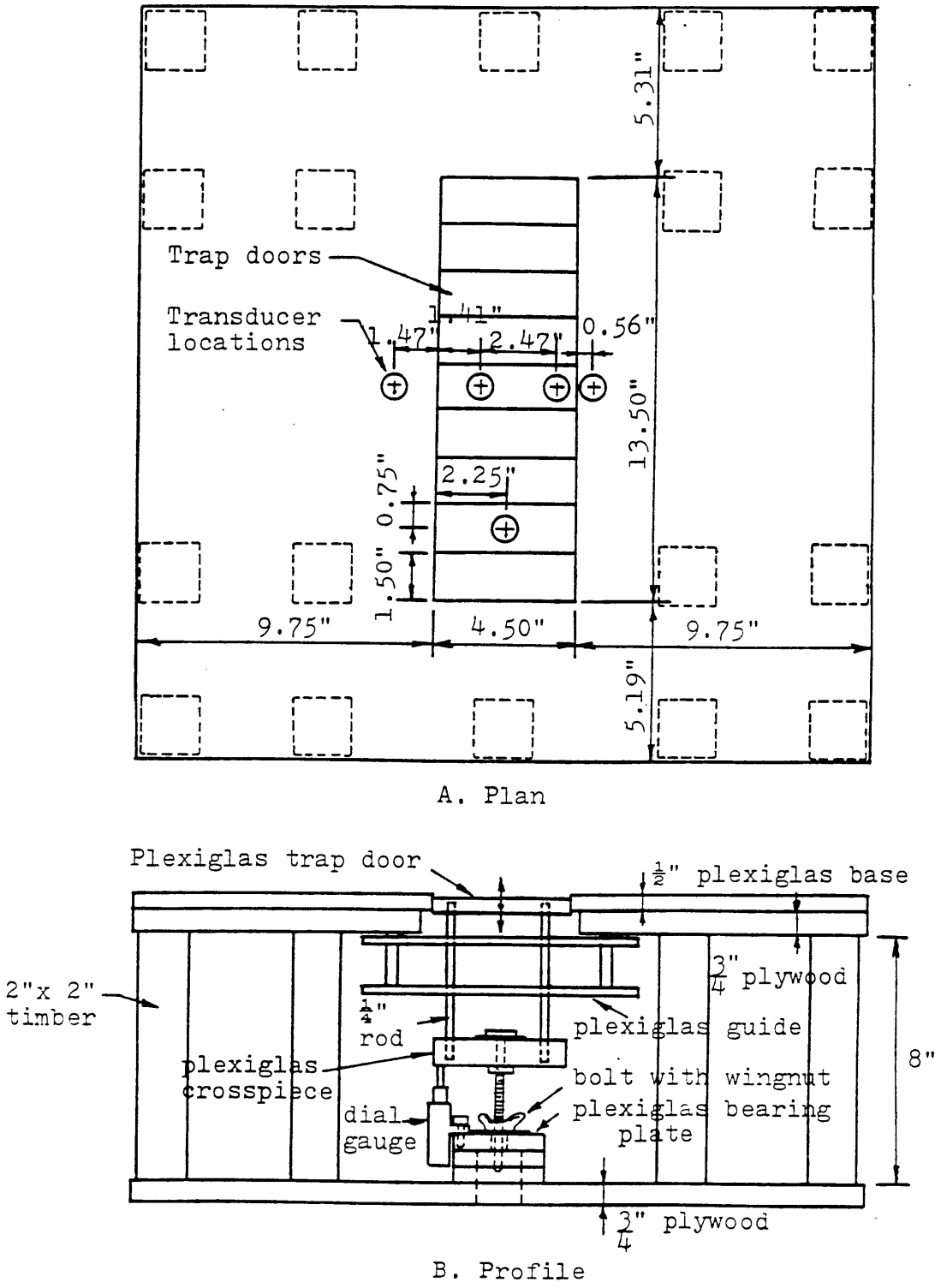

Figure 6.12 Test Apparatus with Rectangular Trap Doors (Evans, 1984)

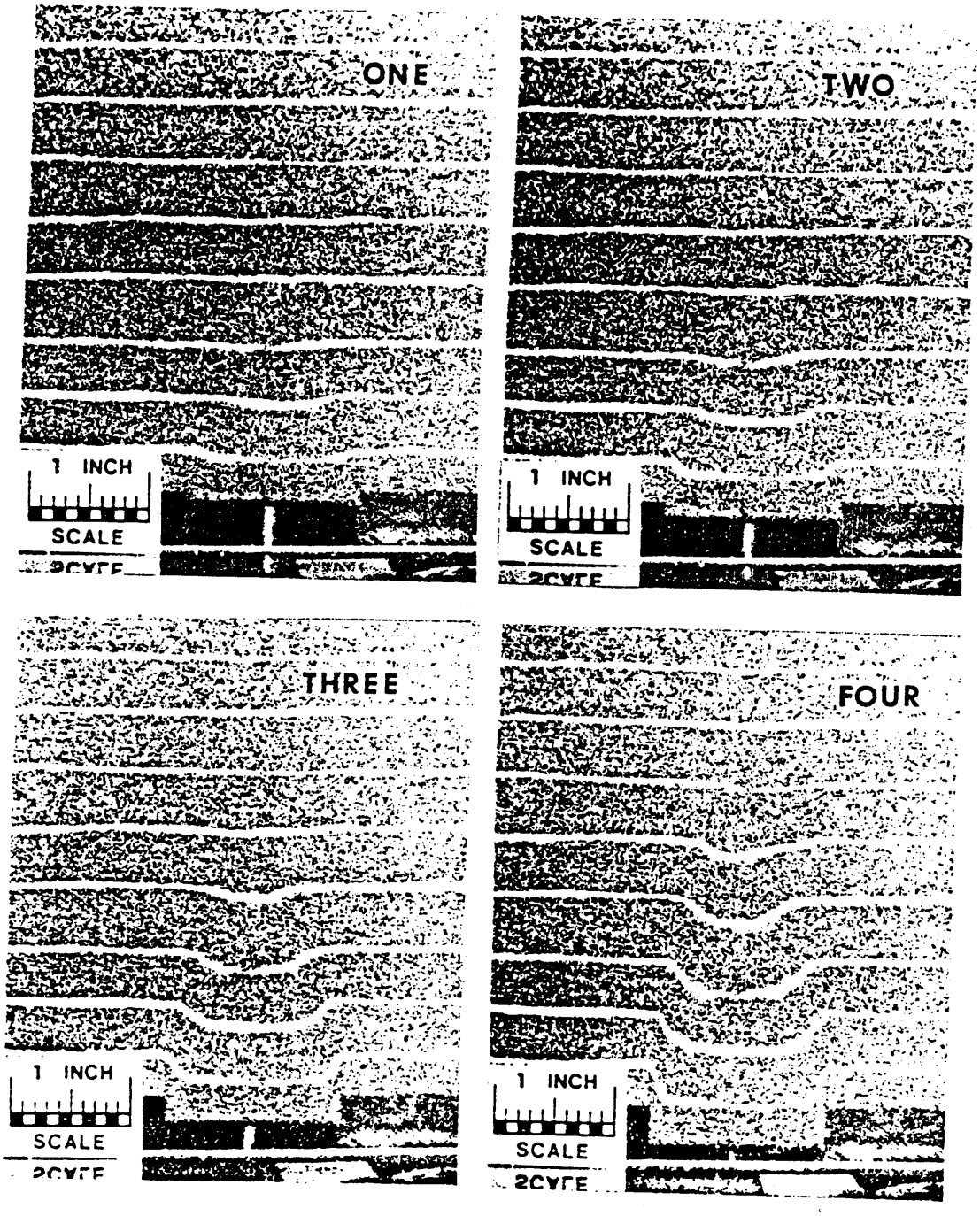

Figure 6.13 Variations of Soil Displacement Pattern with Increasing Trap Door Displacement during an Active Arching Test (Evans, 1984)

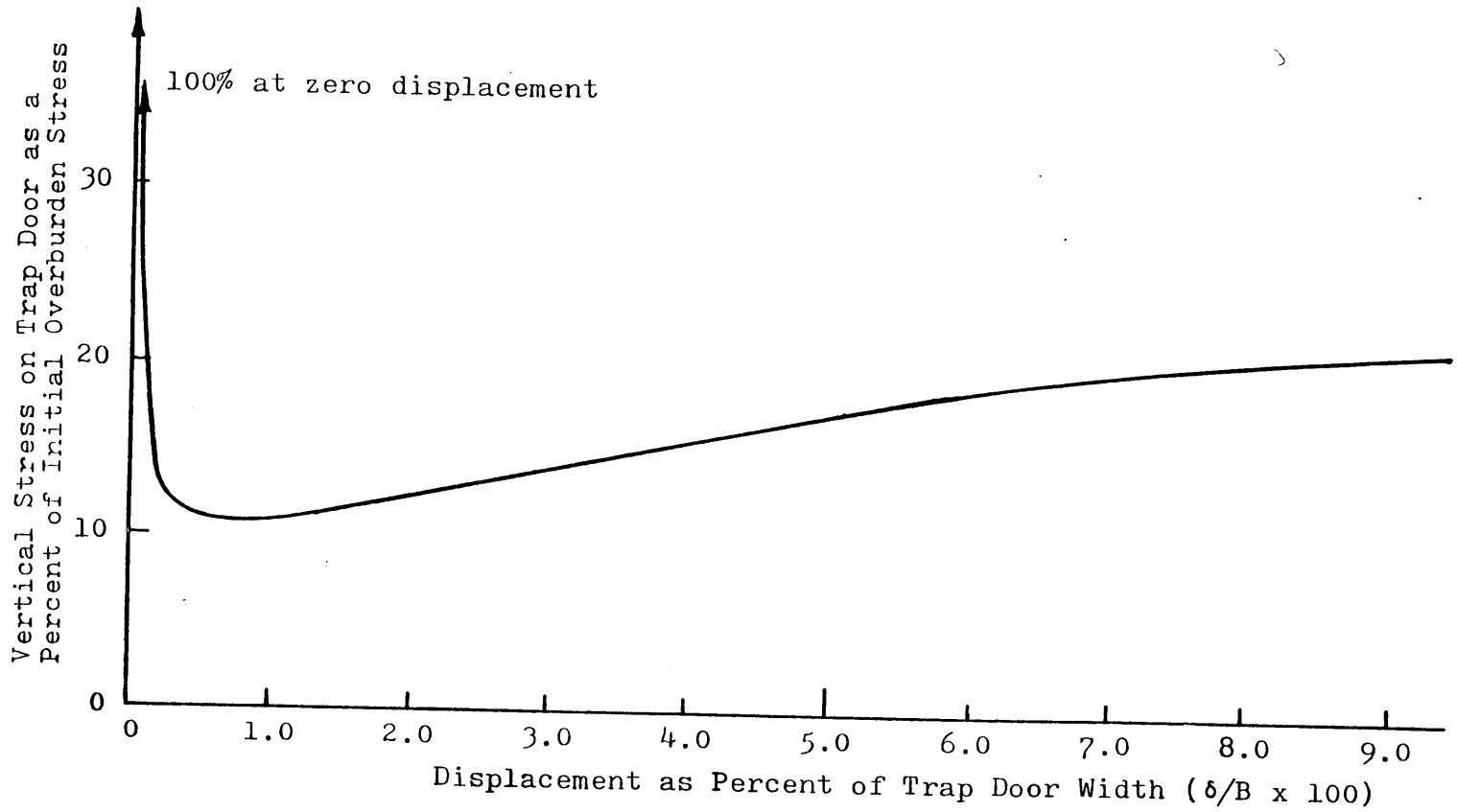

Figure 6.14 Active Arching Test Results (Evans, 1984)

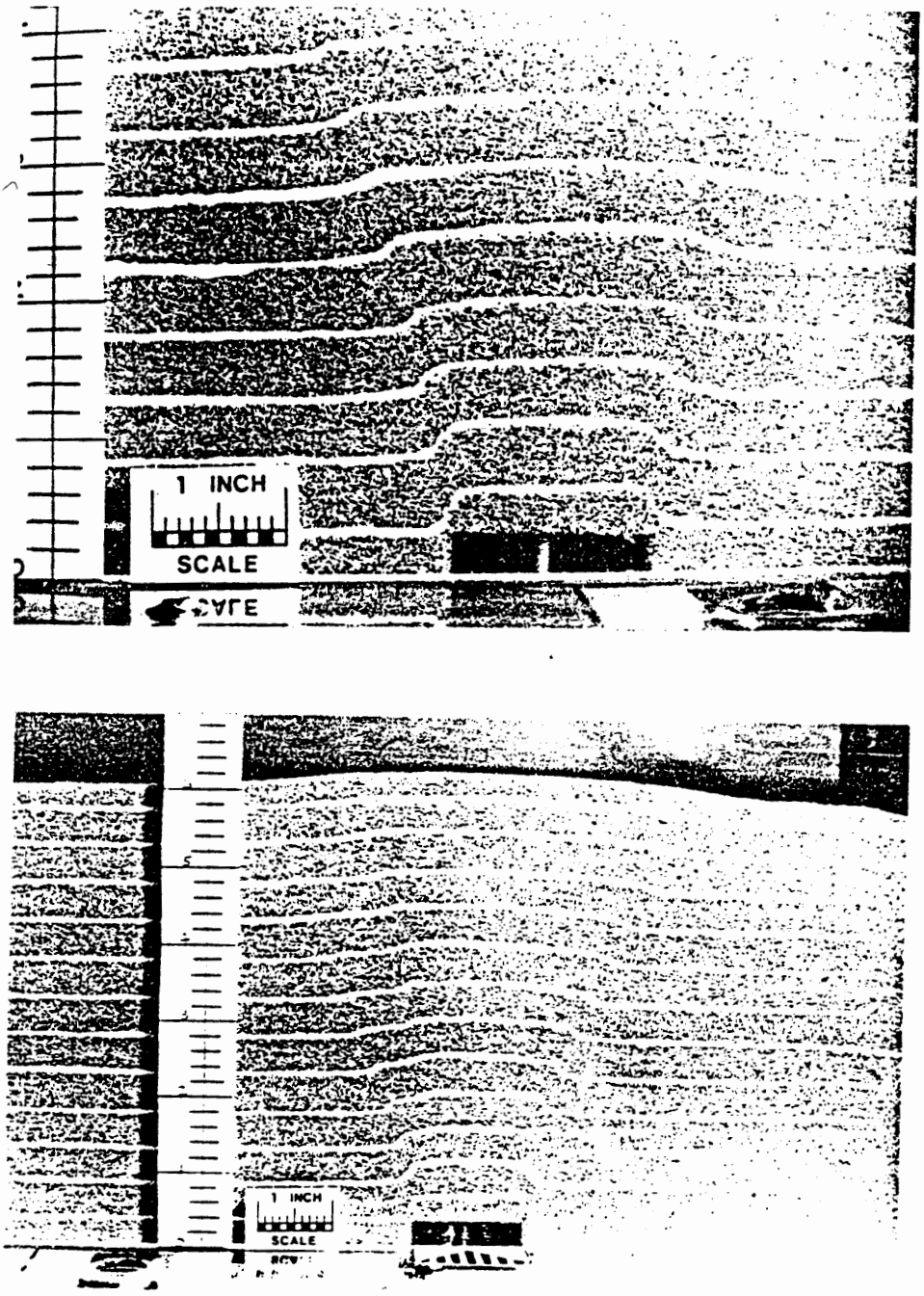

Figure 6.15 Typical Patterns of Soil Deformation During Passive Arching Tests (Evans, 1984)

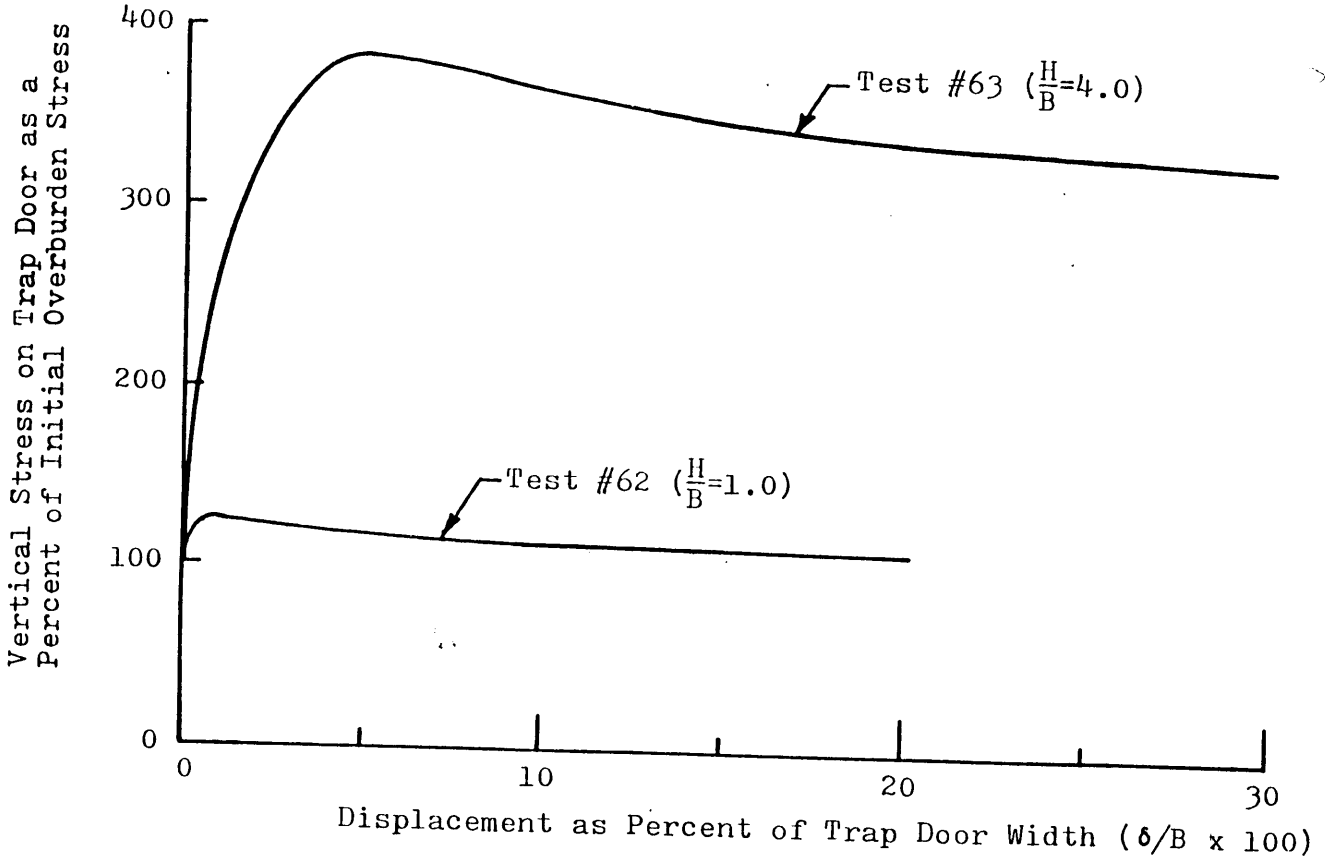

Figure 6.16 Passive Arching Test Results (Evans, 1984)

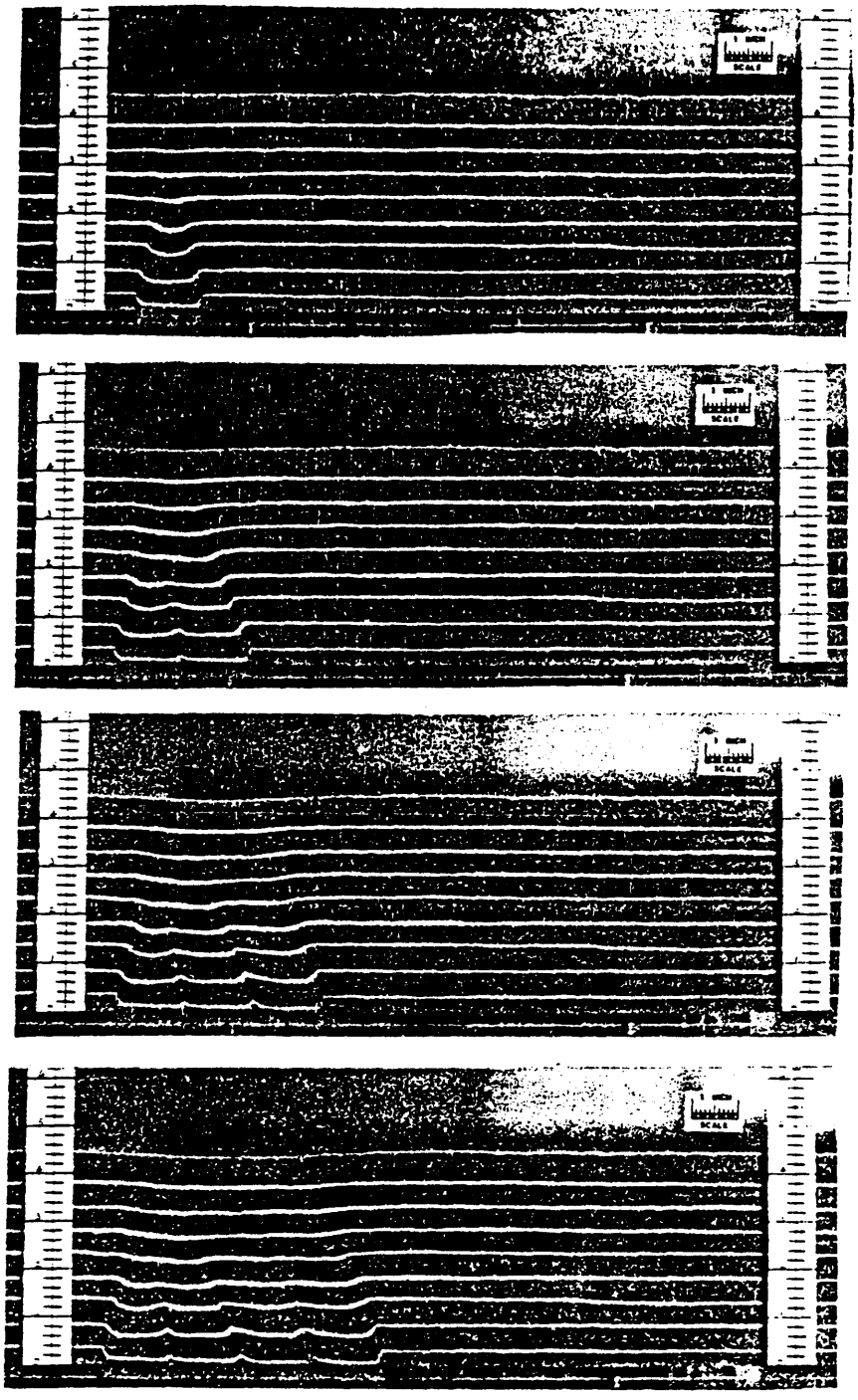

Figure 6.17 Soil Deformations Above Trap Doors Lowered in Sequence, Active Arching Case (Evans, 1984)

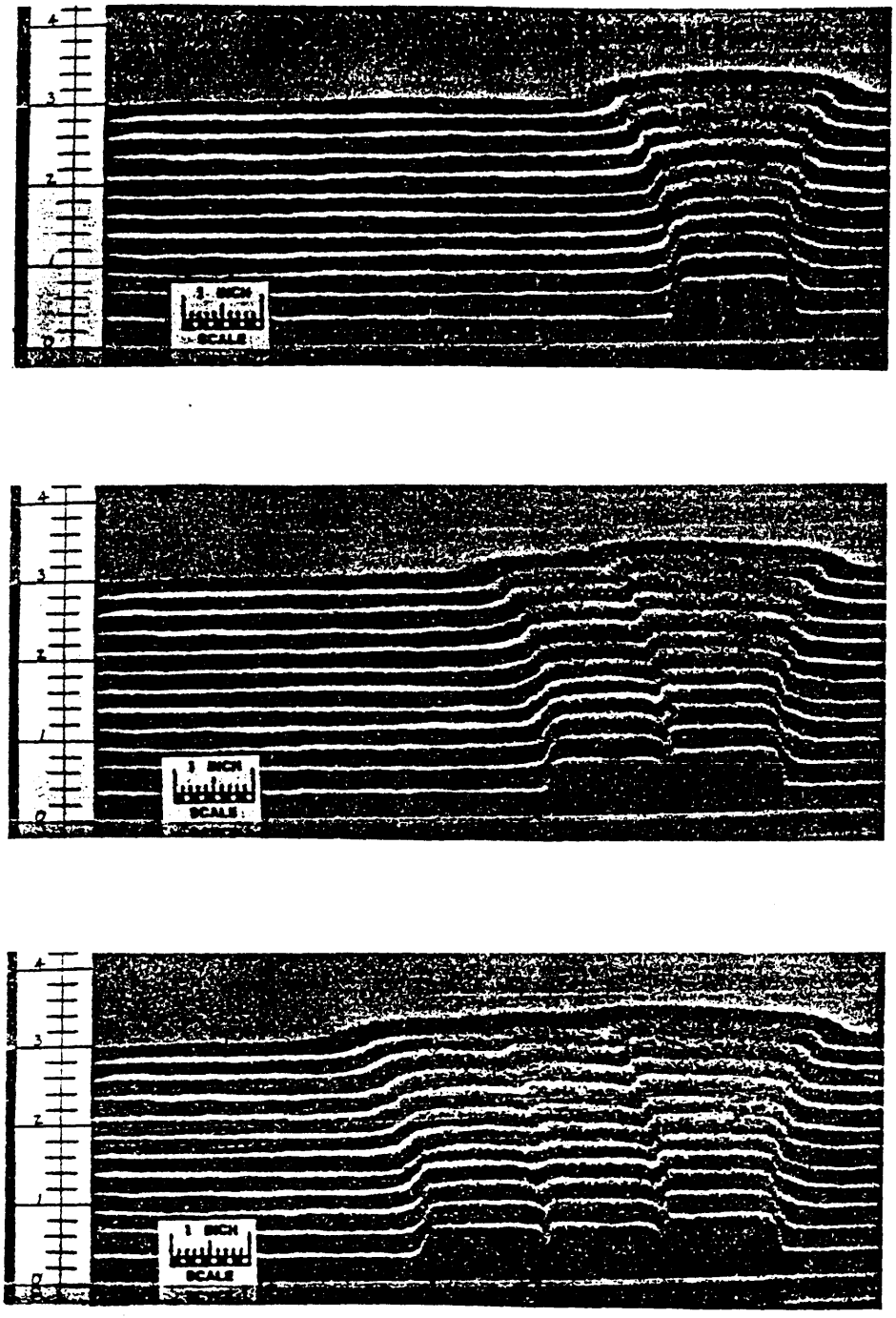

Figure 6.18 Soil Deformations Above Trap Doors Raised in Sequence, Passive Arching Case (Evans, 1984)

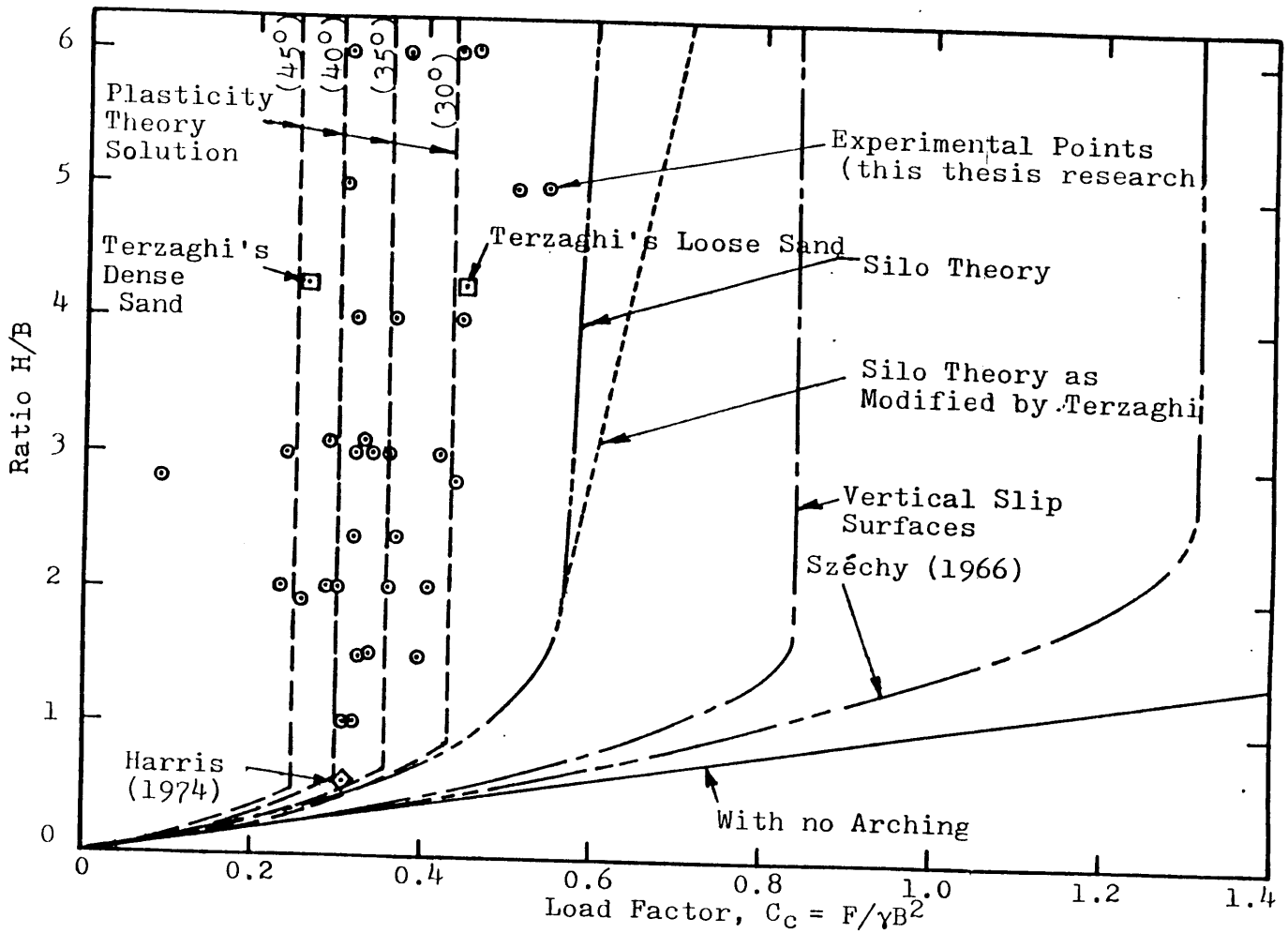

Figure 6.19 Comparison of Experimental Results with Those Predicted for Plane Strain Active Arching at the Maximum Arching State (Evans, 1984)

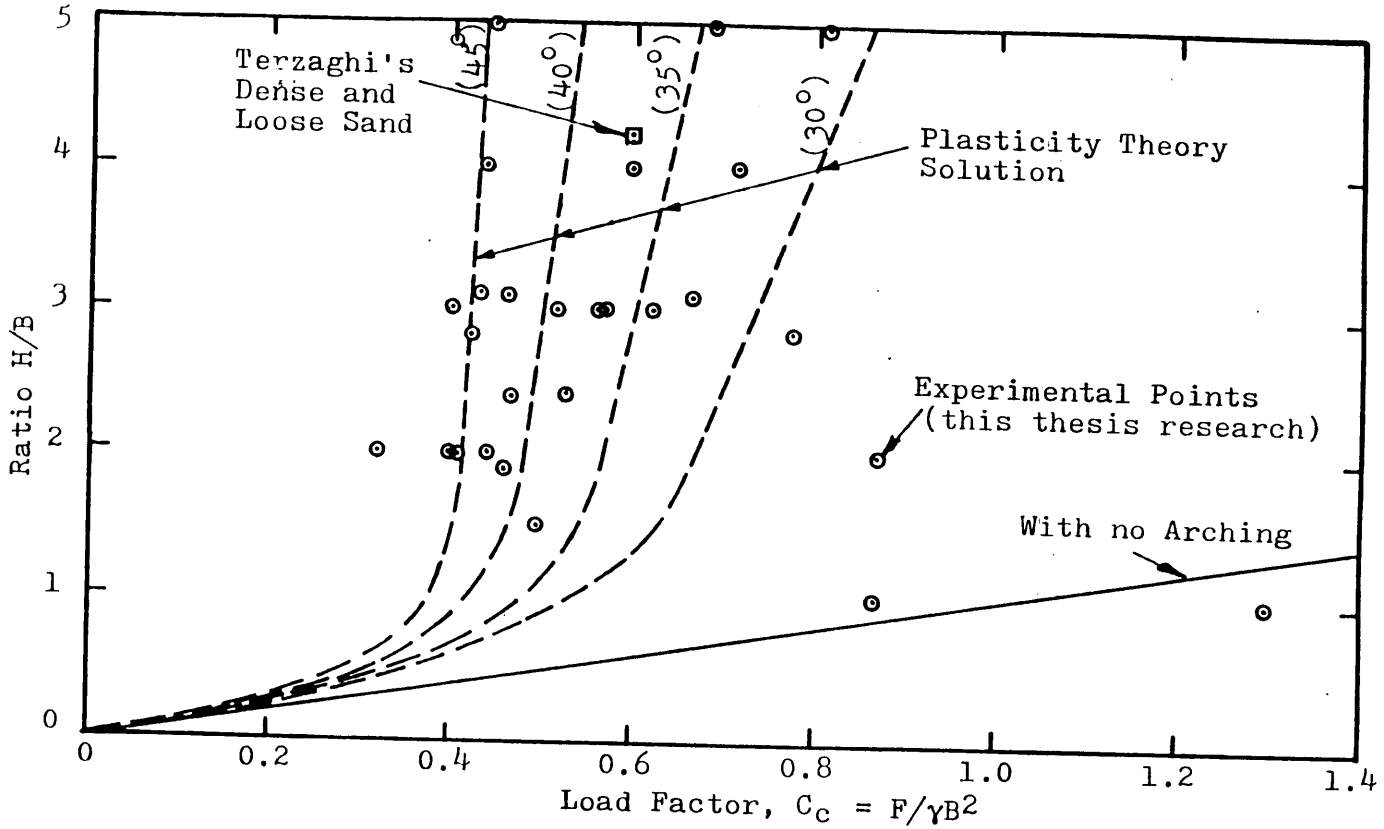

Figure 6.20 Comparison of Experimental Results with Those Predicted for Plane Strain Active Arching at the Ultimate Arching State (Evans, 1984)

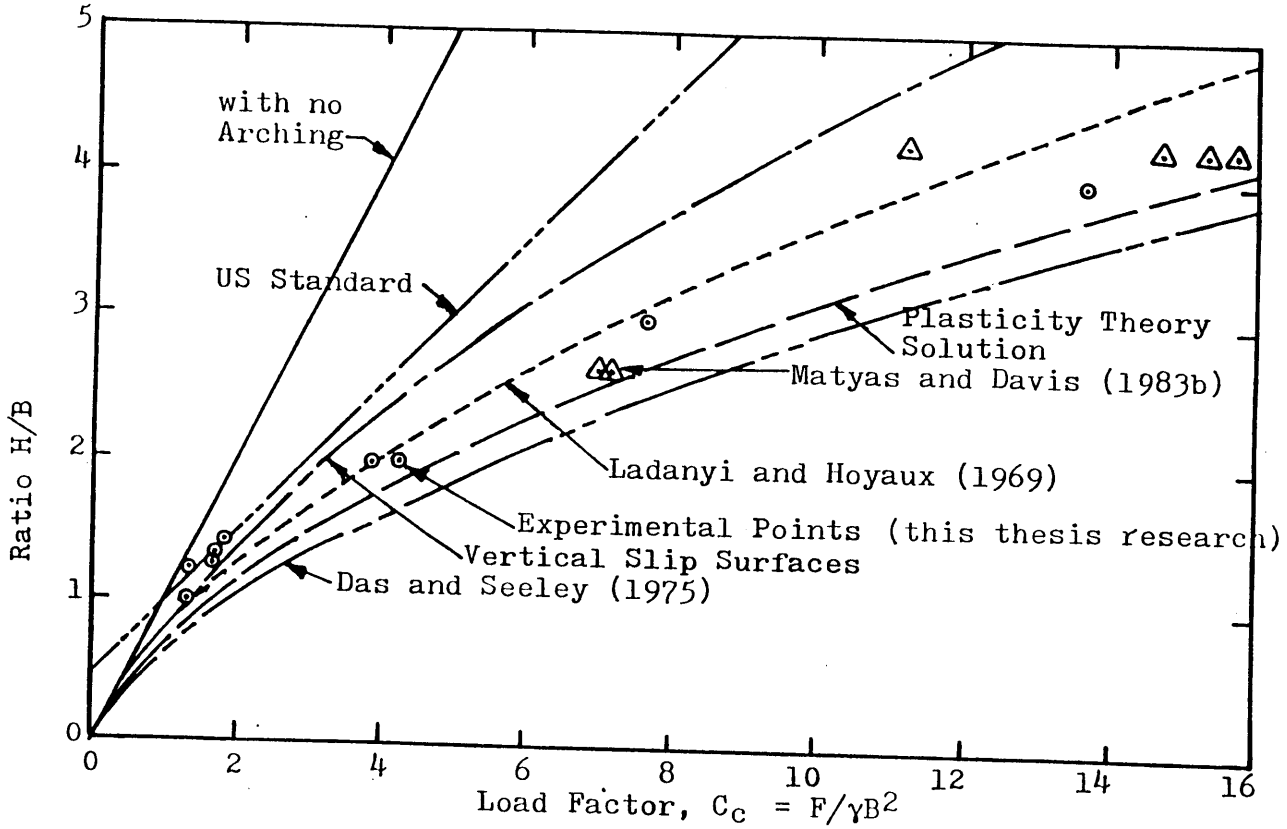

Figure 6.21 Comparison of Experimental Results with Those Predicted for Plane Strain Passive Arching at the Maximum Arching State (Evans, 1984)

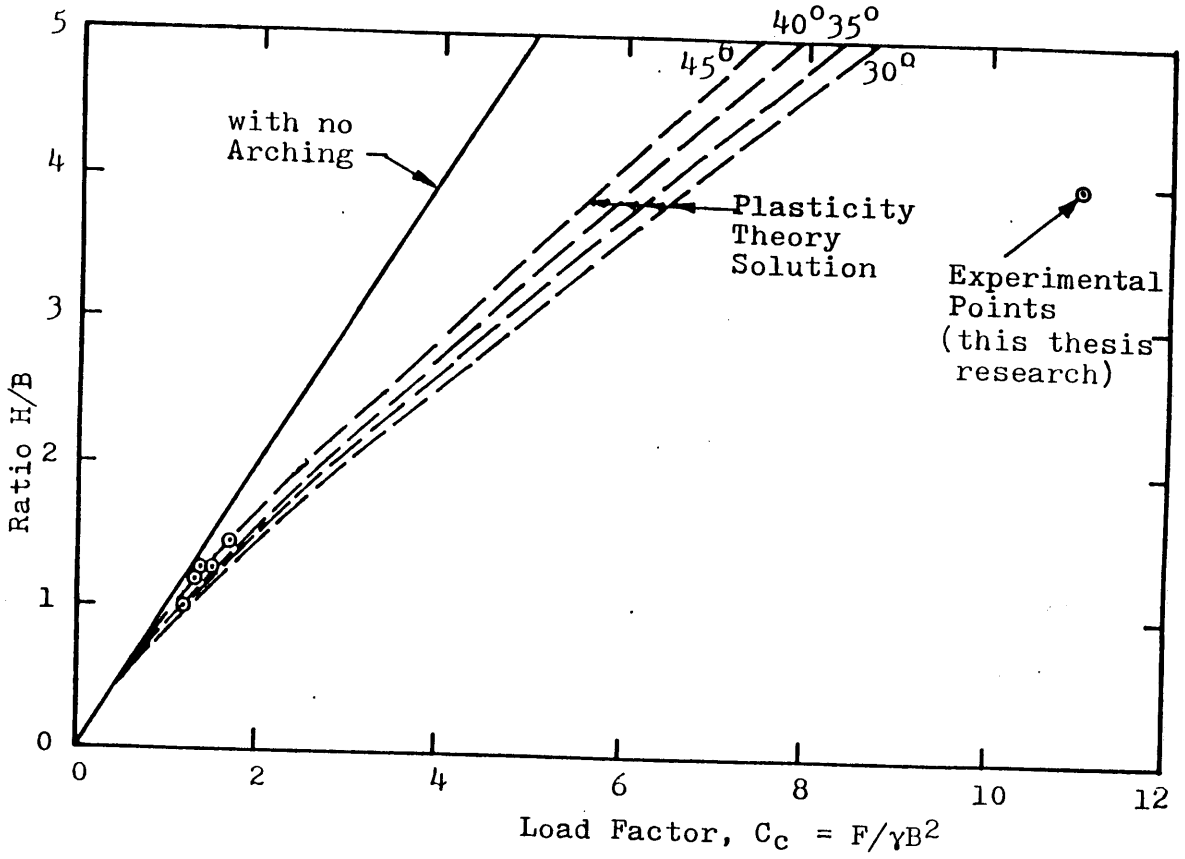

Figure 6.22 Comparison of Experimental Results with Those Predicted for Plane Strain Passive Arching at the Ultimate Arching State (Evans, 1984)

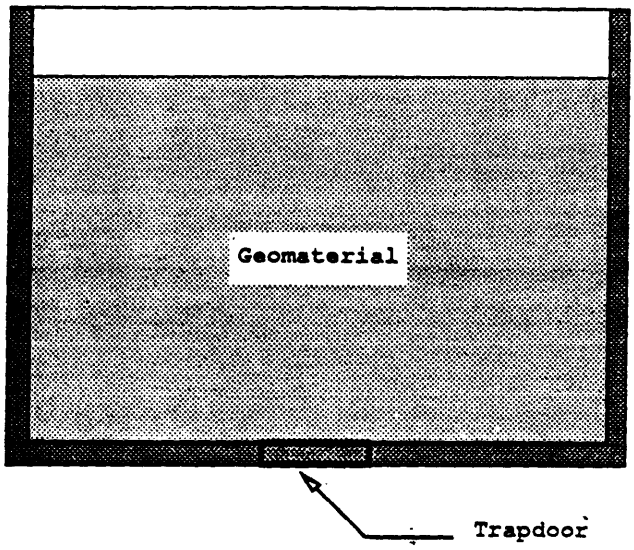

Figure 6.23 The Trap Door Concept (Iglesia et. al., 1990)

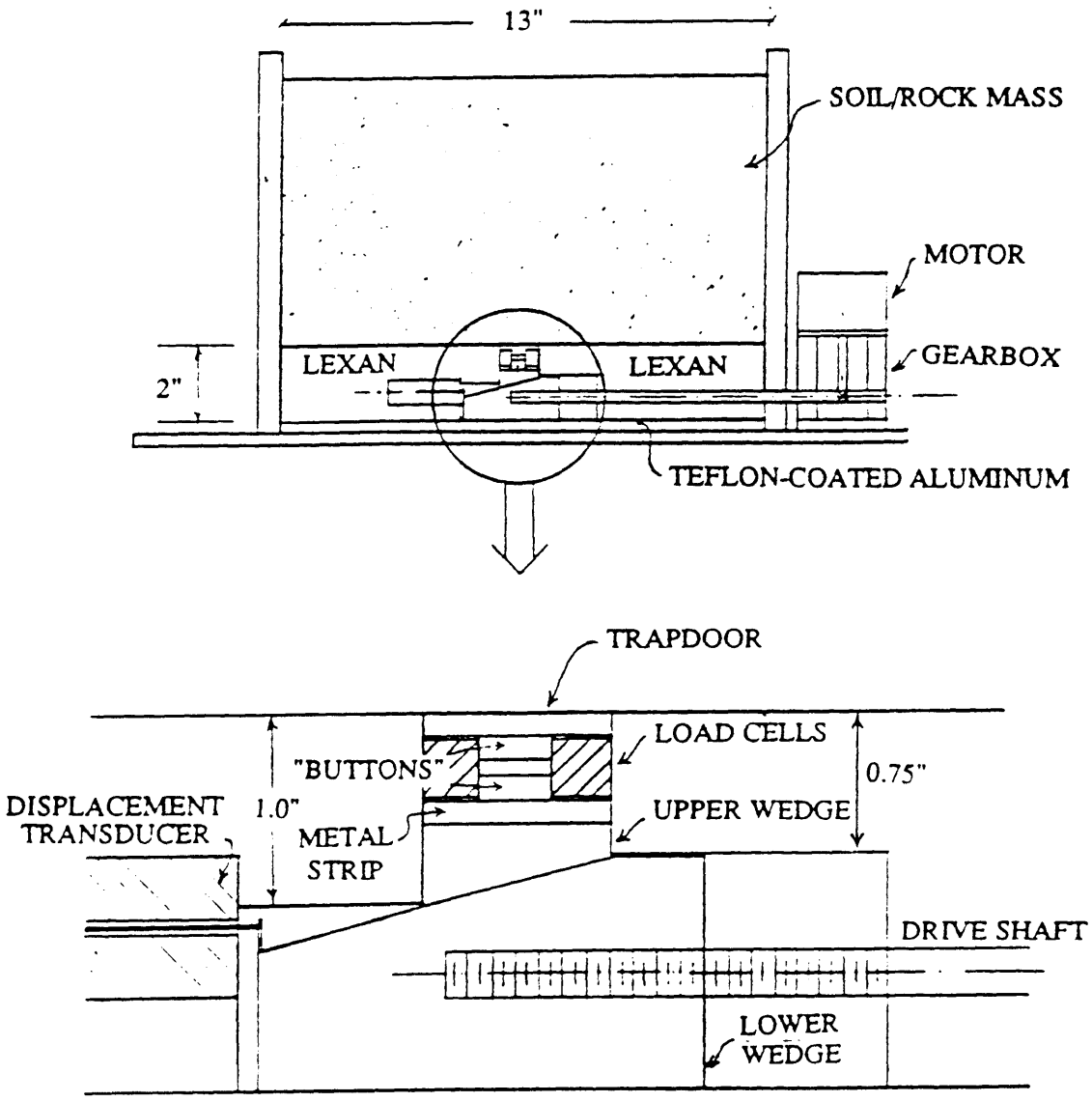

Figure 6.24 Centrifuge Trap Door Apparatus (Iglesia et. al., 1990)

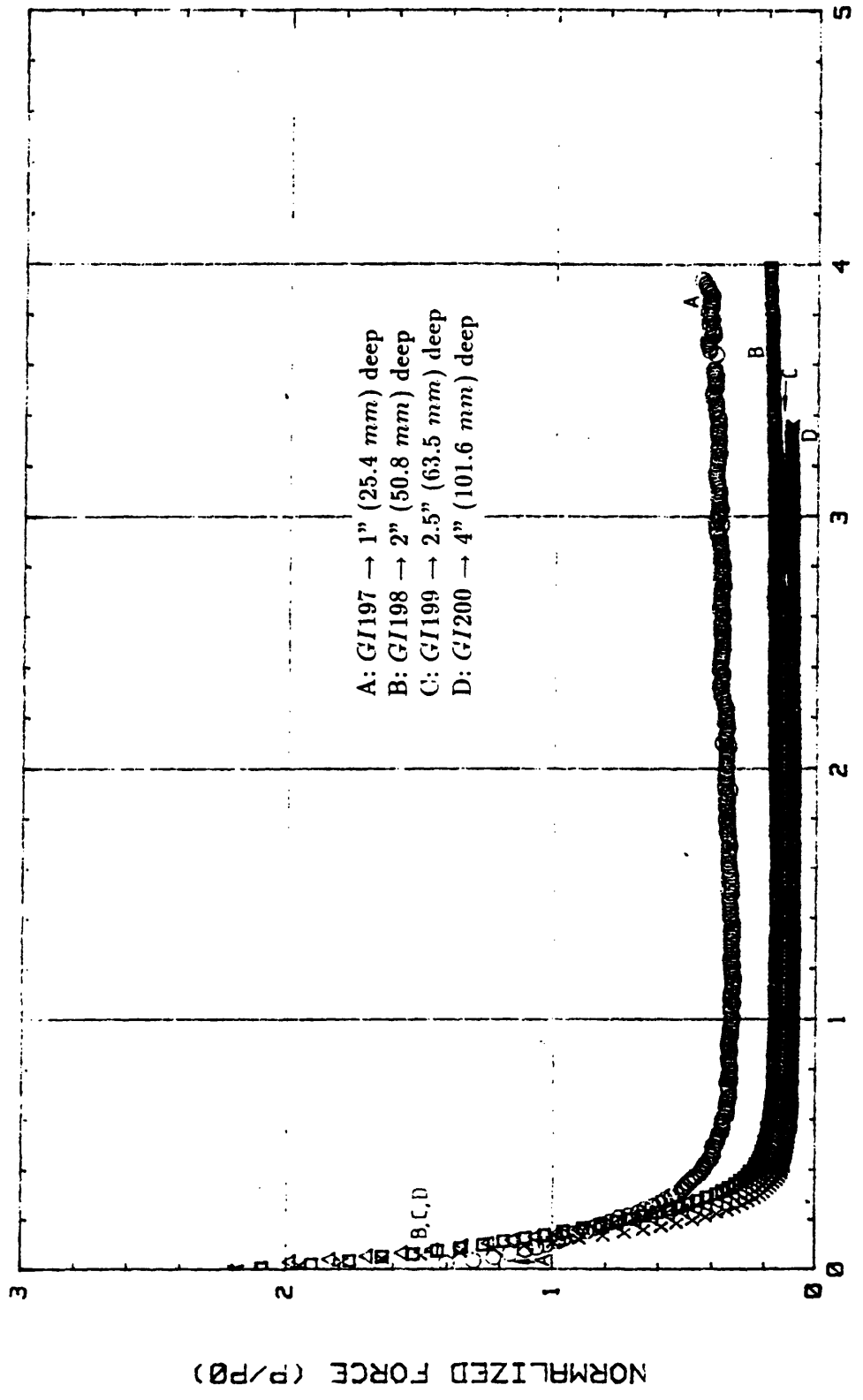

Figure 6.25 Test Results Using Coarse Sand of Varying Depths on 1" Door , Acceleration = 80 g (Iglesia et. al., 1990)

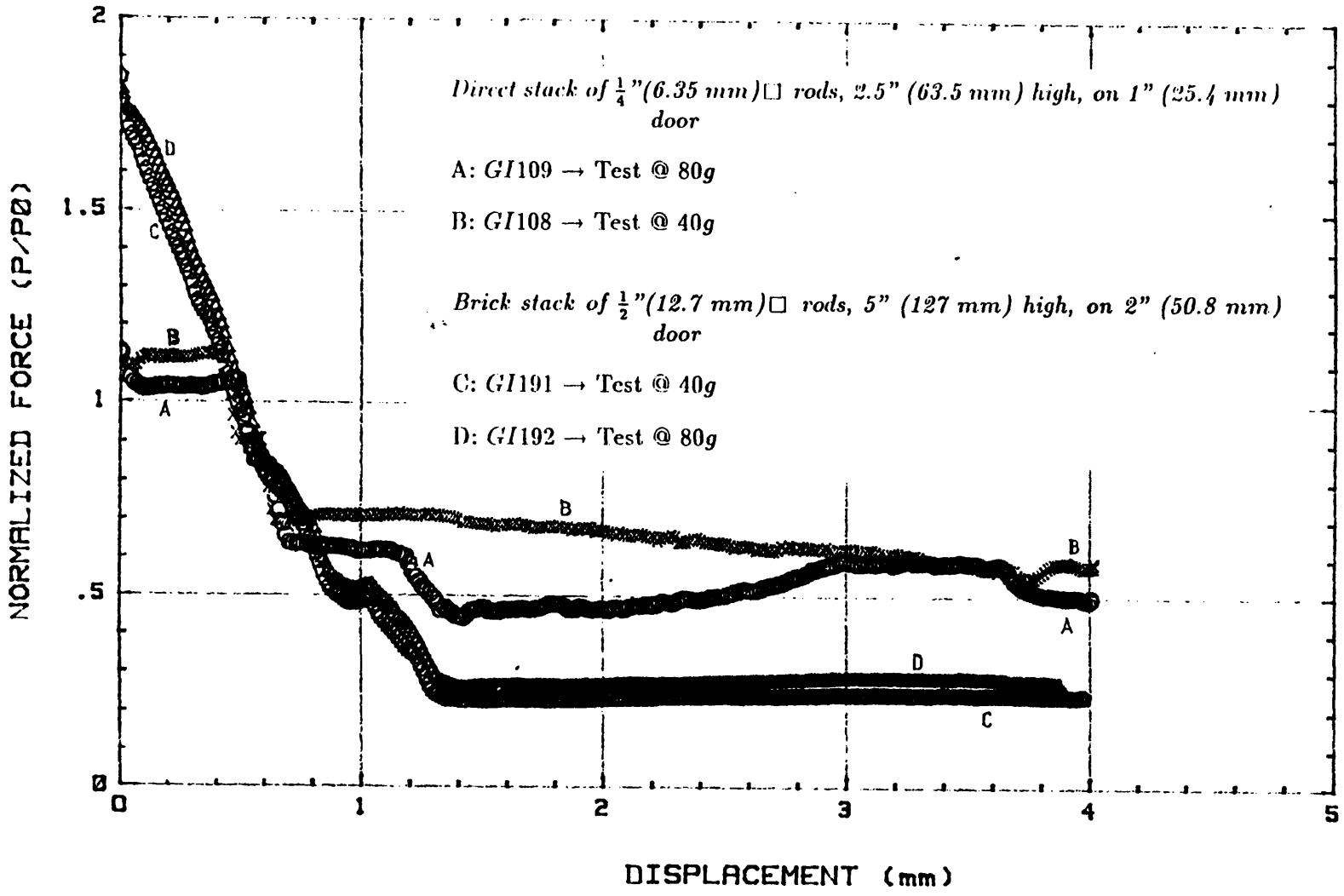

Figure 6.26 Test Results to Determine Effects of g-Level (Iglesia et. al., 1990)

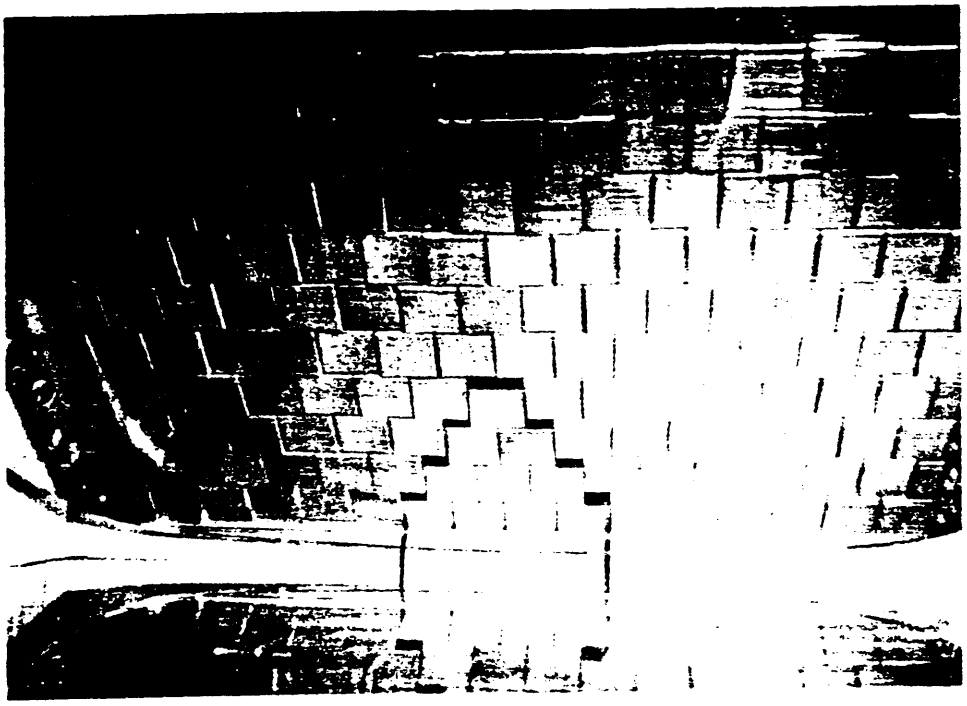

Test *GI*192 - Brick stack

Figure 6.27 Final Configuration of Direct Stack 1/2" Aluminum Rods on 2" Door (Iglesia et. al., 1990)

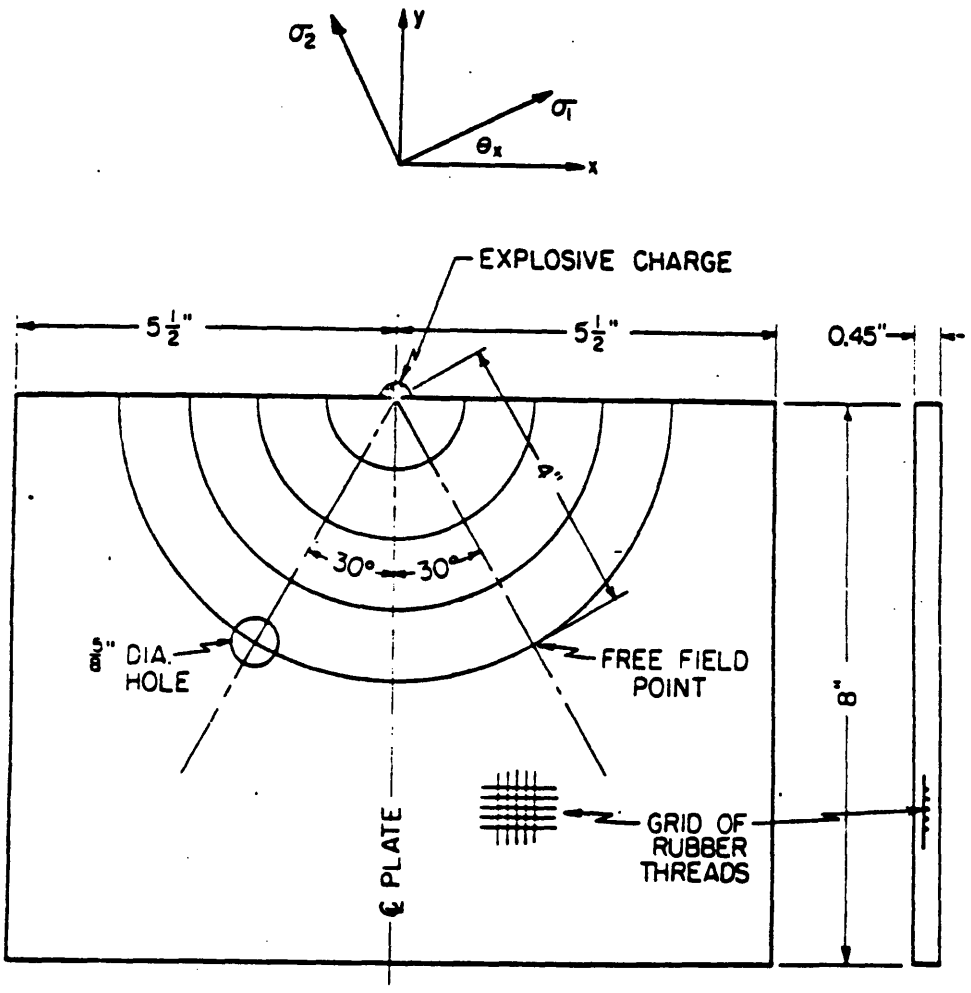

Figure 6.28 Sketch of Riley's Model Showing the Location of the Hole, and the Symmetric Free Field Point (Riley, 1964)

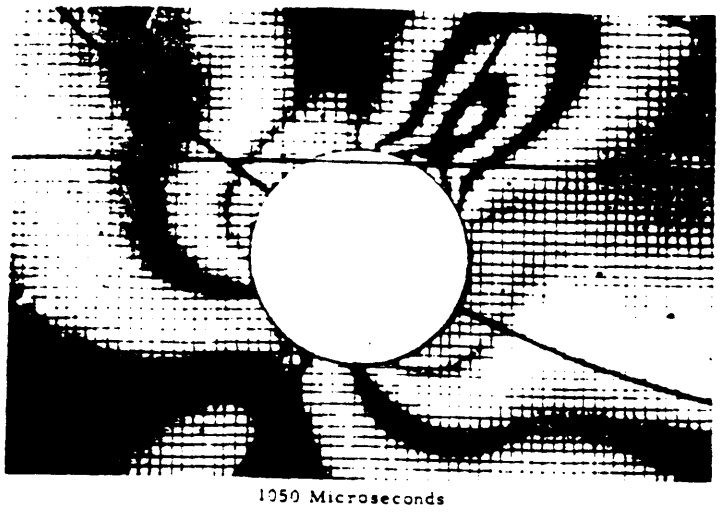

Figure 6.29 Microflash Photographs Showing the Fringe Order Distribution around the Boundary of the Hole at 1050 Microseconds after Detonation of the Explosive Charge (Riley, 1964)

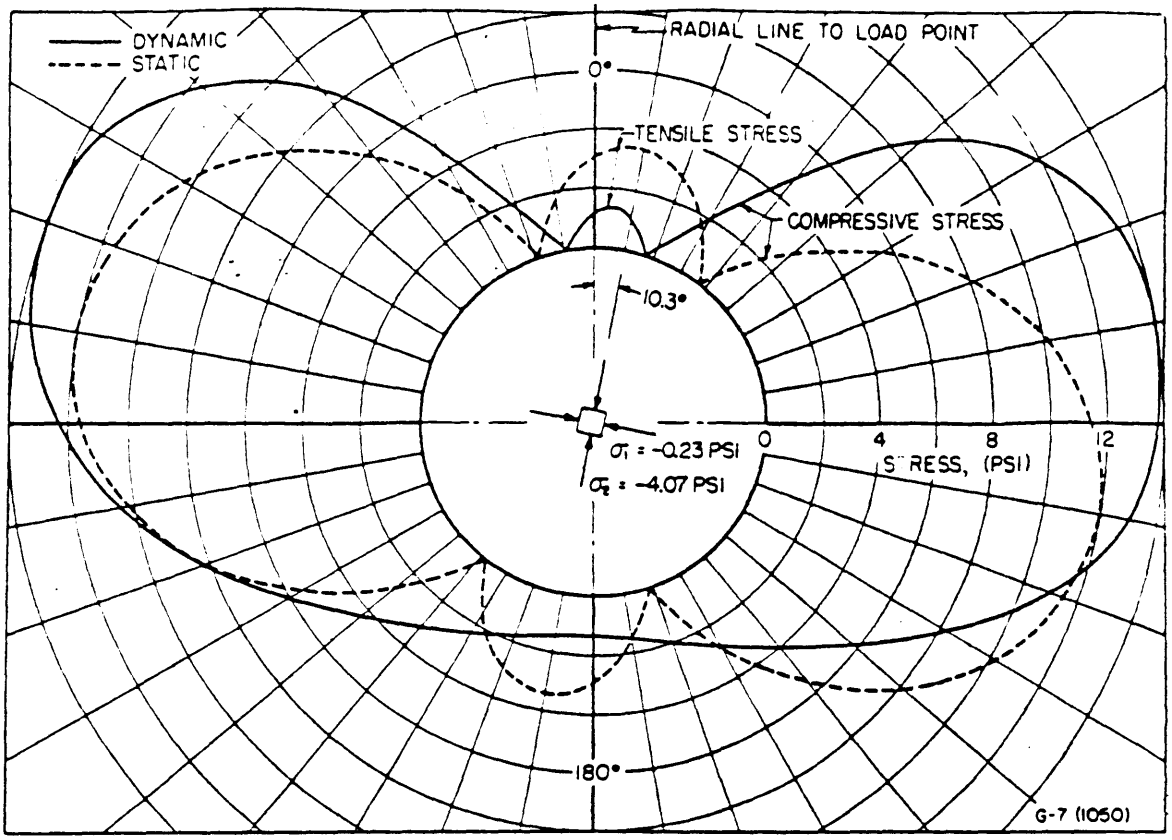

Figure 6.30 Static and Dynamic Stress Distributions on the Hole Boundary 1050 Microseconds after the Explosion (Riley, 1964)

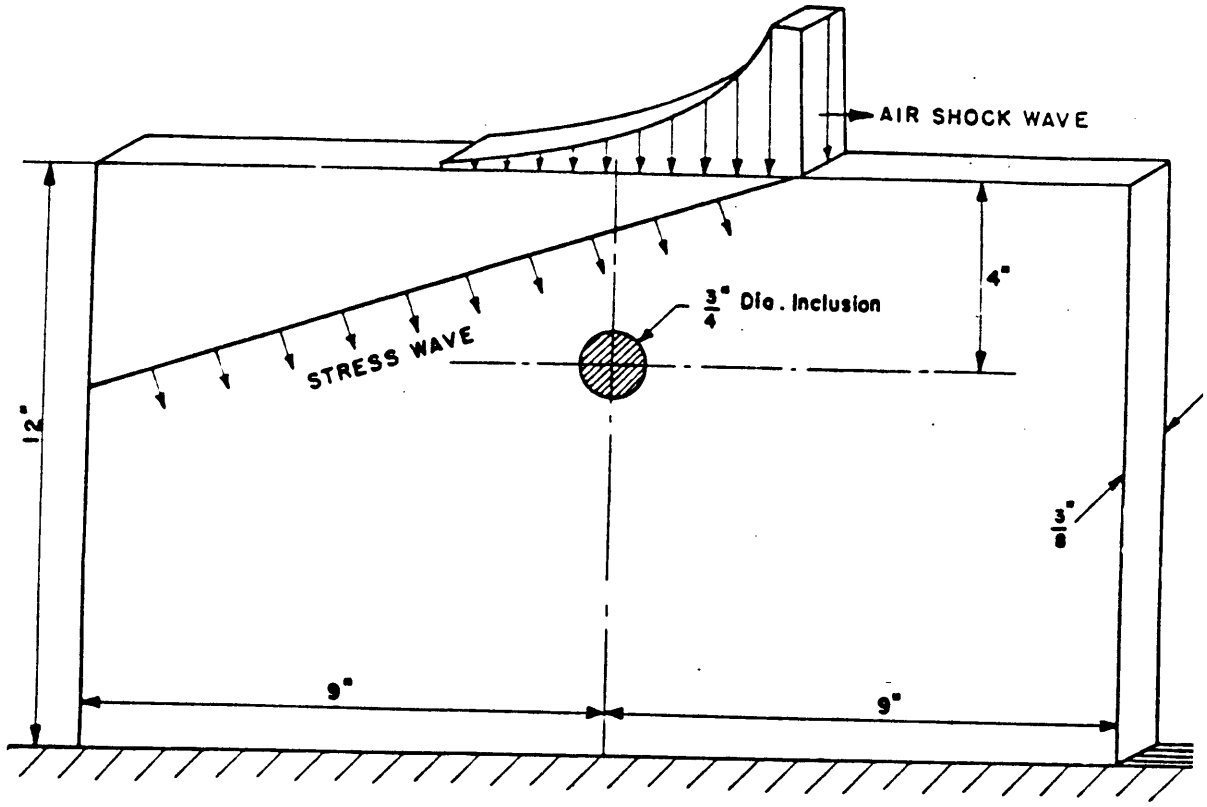

Figure 6.31 Plot of Riley's Model Showing the Location of the Hole or Inclusion and the Loaded Edge of the Plate (Riley, 1964)

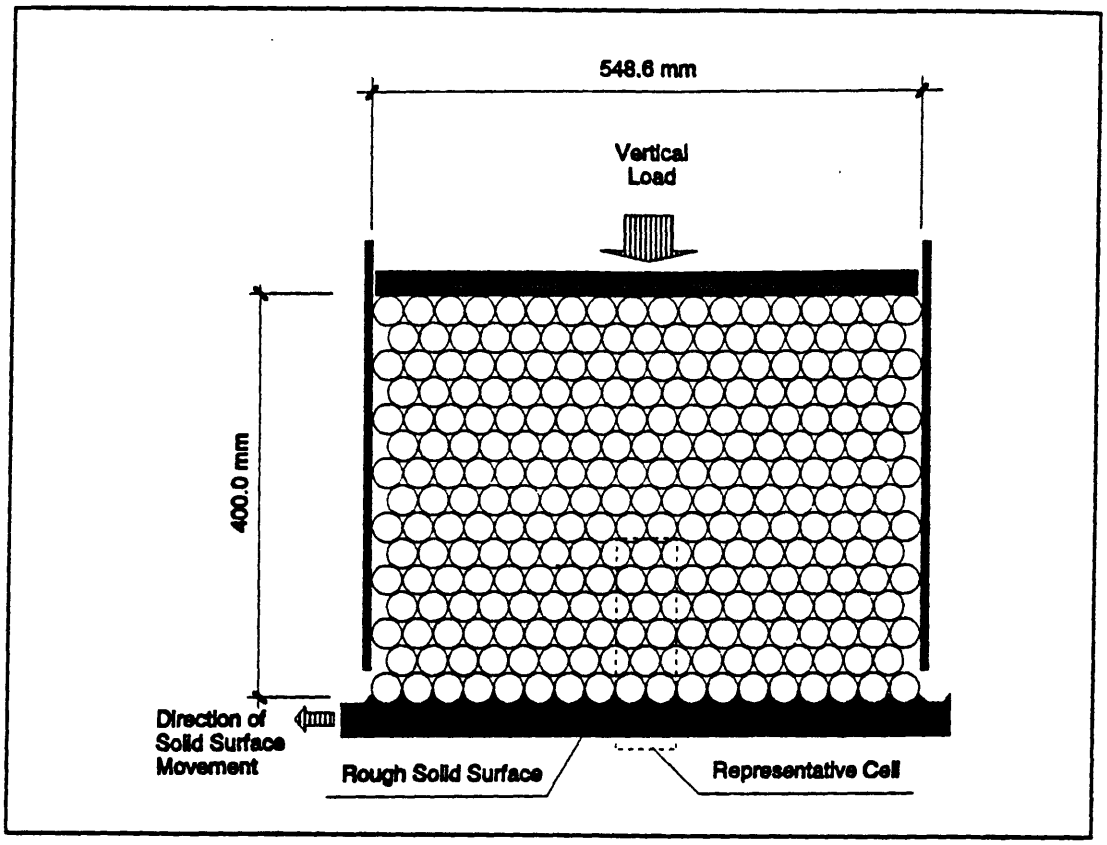

Figure 6.32 Layout of the Shear Box and Sample (Paikowsky et. al., 1995)

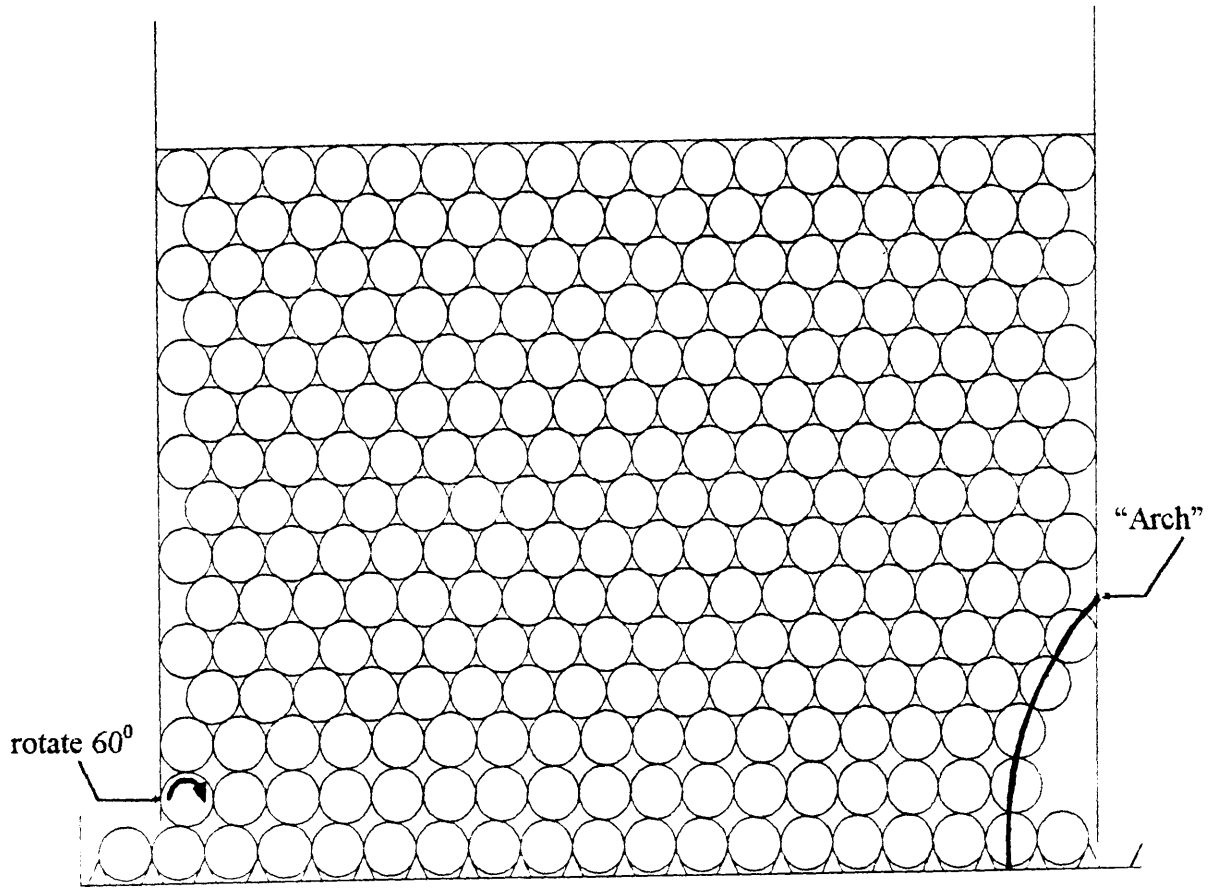

Figure 6.33 Plot of the Shear Box and Sample after One Particle Diameter Shear at the Bottom (Paikowsky et. al., 1995)

Chapter SEVEN
Summary, Conclusions and Recommendations

7.1 Summary and Conclusions

- General:

(1) Arching is a phenomenon existing widely in nature and man-made construction. It is an important issue for geotechnical engineers and researchers to comprehend and recognize in their studies and design.

(2) The arching effect can be defined as follows: "If a portion of an otherwise rigid support of a geomaterial mass yields, the adjoining soil moves with respect to the remainder of the soil mass. This movement is resisted by shearing stresses which reduce the pressure on the yielding portion of the support while increasing the pressure on the adjacent rigid portions." Arching can also occur when one portion of a yielding support moves more than adjoining parts. Generally speaking, arching is stress redistribution occurring in a geomaterial mass.

(3) Arching phenomena can be found in the cavity structures of karst terrain. The collapse of these cavity structures develop sinkholes.

- Classical Arching Theory:

(4) Silo theory (Janssen, 1895) is the first problem related to arching effect dealt by engineers. In this theory, shear forces between the granular material and the side wall of the silo played an important part in reducing the vertical stresses on the base of a silo.

The vertical normal pressure inside a silo was found to be distributed nonuniformly across the base.

(5) The first systematic study of the arching mechanism was performed by Terzaghi in 1936 using the trap door tests. Based on these tests, Terzaghi proposed his arching theory in 1943 where he defined arching as "the transfer of pressure from a yielding mass of soil onto adjoining stationary parts" (Terzaghi, 1943). He believed that soil was "arching over" the yielding part of the support. There are several limitations, however, to Terzaghi's theory: *a)* the vertical stresses on the horizontal yielding surface are assumed uniform, *b)* the trap door or yielding strip is assumed rigid, and *c)* the sliding surfaces assumed to be vertical in the theory are actually not so.

- Analytical Approaches:

(6) Theoretical solutions from continuum approaches using the theory of elasticity can describe good mechanical behavior of soil only when the soil body has very small deformations (Finn, 1963). If one wants to study the arching effect, which means the geomaterial has a plastic deformation, the continuum approaches by the plasticity theory can predict better mechanical behaviors of soil. Evans (1984) has proven this point of view in his study.

(7) Theoretical approaches based on discontinuum analysis allow one to study the mechanical behavior of granular materials with different particle sizes and shapes (e.g. Maeda et. al., 1995). However, because of the simplified assumptions and the complexity in the derivation of such theories, their application to discontinuum is still limited.

- Empirical Methods:

(8) Empirical methods for the design of underground openings are either based on very simple static analyses, or entirely founded on the experience of the proposing person. In these methods, arching effect is assumed to be the consequence of the local stress relaxation produced by tunnel excavation. A "ground arch" will transfer most of the overburden load to the adjacent geomaterials, while only a load from the weight of a "loosening zone" above the tunnel will act on the tunnel supports.

(9) Due to the uncertainties in empirical methods (e.g. Limited to local experience), these methods are suggested to be applied in conjunction with analytical methods (e.g. numerical analyses) to confirm their results.

- Experimental Investigations:

(10) Following Terzaghi's original trap door experiment, additional trap door experiments were performed by others as well. They are similar in principle to Terzaghi's experiment but contain different improvements or extensions. No real advances have been obtained in these research projects compared to Terzaghi's approach.

(11) The trap door tests of the different researchers show similar results. In active arching, the trap door is moved away from the soil. The stresses on the trap door decrease as soon as the trap door is moved, then increase until a steady value is reached. After the trap is moved, only a small amount of the overburden stresses will act on the trap door (about 10%). Most of the overburden stresses are carried by the arching. In

passive arching, the trap door is moved against the soil body. The stresses on the trap door increase to a peak value and then decrease slightly to a constant value.

(12) Based on these experiments, three major factors were identified affecting the trap door test results. They were the overburden depth (H), the ratio of the overburden depth to the trap door width (H/B), and the relative density of the tested granular soil (Dr).

(13) Photoelastic methods can be used to explore the interaction and mechanical behavior of particles in arching.

7.2 Recommendations for Future Research

(1) Various researchers have performed the trap door tests following Terzaghi (1936), modifying the original trap door tests for different purposes. For example, Harris (1974) and Evans (1984) installed several trap doors in their tests to study the effects of an advancing tunnel. Iglesia et. al. (1990) used a centrifuge to study arching effect in small scale model tests. However, the stress distribution across the yielding surface and the correct shape of the sliding surfaces are still not known well. For future research, one can try new techniques to measure the distribution of stresses within a soil body, such as the "Photogrametric method" from Yoshida et. al. (1993). The photogrametric method not only can give measurements of the stresses in soil, but also presents the configuration of soil mass after soil yields. This allows for more detailed arching mechanism to be explored.

(2) The coefficient of lateral stress (K) was discussed in many trap door studies. Besides the theoretical method used to predict the force on the trap door from Iglesia et. al.

(1990), most of the theoretical approaches and numerical analyses require an appropriate estimation of the K value to obtain good results. Hence, more studies about the coefficient of lateral stress are necessary. Improvement of the measuring techniques for the horizontal and vertical stresses in soil when yielding takes place, is also required.

(3) Arching effect is most obvious in granular materials. However, the effects of different characteristics of individual particles (e.g. particle size, particle shape, etc.) to the arching formation and stress redistribution in granular materials are still unknown. In addition, the change of contact forces and displacements of particles within a granular material are also of great importance. Studies of the interactions between particles are therefore suggested for future research.

References:

Abbott, P.A. (1967)
"Arching for Vertically Buried Prismatic Structures", Journal of the Soil Mechanics and Foundations Division, ASCE, Vol. 93, No. SM5, pp. 233-255.

Balla, A. (1963)
"Rock Pressure Determined from Shearing Resistance", Proc. Int. Conf. Soil Mechanics, Budapest, pp. 461.

Beck, B.F. (1984)
"Sinkholes: Their Geology, Engineering and Environmental Impact", Proceedings of the First Multidisciplinary Conference on Sinkholes, Florida Sinkhole Research Institute, University of Central Florida, Florida, Orlando, 1984.

Bello, A. A. (1978)
"Simplified Method for Stability Analysis of Underground Openings", Proceedings, First International Symposium on Storage in Excavated Rock Caverns, Rockstore '77, Stockholm, Sweden, Vol. 2, pp. 289-294.

Benson, R.C. and L.J. LaFountain (1984)
"Evaluation of Subsidence or Collapse Potentials Due to Subsurface Cavities", Proceedings of the First Multidisciplinary Conference on Sinkholes, Florida Sinkhole Research Institute, University of Central Florida, Orlando, Florida, pp. 201-216.

Bierbäumer, A. (1913)
Die Dimensionerung des Tunnelmauerwerks, Engelmann, Leipzig.

Bjerrum, L., C.J. Frimann Clausen, and J.M. Duncan (1972)
"Earth Pressures on Flexible Structures -- A State-of-the-Art Report", Proceedings, Fifth European Conference on Soil Mechanics and Foundation Engineering, Madrid, Spain, pp. 169-196.

Burghignoli, A. (1981)
"Soil Interaction in Buried Structures", Proceedings, Tenth International Conference on Soil Mechanics and Foundation Engineering, Stockholm, Sweden, Vol. 2, pp. 69-74.

Butterfield, R. (1969)
"A Theoretical Study of the Pressures Developed in a Silo Containing single-Sized Particles in a Regular Packing", International Journal of Rock Mechanics and Mining Sciences, Pergamon Press, Vol. 6, pp. 227-247.

Chelapati, C.V. (1964)
"Arching in Soil Due to the Deflection of a Rigid Horizontal Strip", Proceedings of the Symposium on Soil-Structure Interaction, University of Arizona, Tucson, Arizona, pp. 356-377.

Connors, P. (1995)
Examination of Boundary Effects in Interfacial Testing, M.S. Thesis, UMASS, Lowell.

Davis, R.E. and A.E. Bacher (1968)
"California's Culvert Research Program -- Description, Current Status, and Observed Peripheral Pressures", Highway Research Record, No. 249, pp. 14-23.

Douglas, I. (1965)
"Calcium and Magnesium in Karst Waters", Helictite, Vol. 3, pp. 23-36.

Einstein, H.H., C.W. Schwartz, W. Steiner, M.M. Baligh, and R.E. Levitt (1980)
"Improved Design for Tunnel Supports: Analysis Method and Ground Structure Behavior: A Review -- Vol. II", MIT, DOT-05-60136.

Evans, C. H. (1983)
An Examination of Arching in Granular Soils, M.S. Thesis, MIT.

Feld, J. (1948)
"Early History and Bibliography of Soil Mechanics", Proceedings, Second International Conference on Soil Mechanics and Foundation Engineering, Rotterdam, Vol. 1, pp. 1-7.

Finn, W.D.L. (1963)
"Boundary Value Problems of Soil Mechanics", Journal of the Soil Mechanics and Foundation Division, ASCE, Vol. 89, No. SM5, pp. 39-72.

Getzler, Z., M. Gellert, and R. Eitan (1970)
"Analysis of Arching Pressures in Ideal Elastic Soil", Journal of the Soil Mechanics and Foundations Division, ASCE, Vol. 96, No. SM4, pp. 1357-1372.

Getzler, Z., A. Komornik, and A. Mazurik (1968)
"Model Study on Arching Above Buried Structures", Journal of the Soil Mechanics and Foundations Division, ASCE, Vol. 94, No. SM5, pp. 1123-1141.

Handy, R.L. (1985)
"The Arch in Soil Arching", Journal of Geotechnical Engineering, ASCE, Vol. 3, No. 3, pp. 302-318.

Harris, G.W. (1974)

"A Sandbox Model Used to Examine the Stress Distribution Around a Simulated Longwall Coal-Face", International Journal of Rock Mechanics, Mining Sciences and Geomechanical Abstracts, Pergamon Press, Vol. 11, pp. 325-335.

Highway Research Board (1971)
"Structure Analysis and Design of Pipe Culverts", National Cooperative Highway, Research Report 116.

Iglesia, G., H.H. Einstein, and R.V. Whitman (1990)
"Stochastic and Centrifuge Modeling of Jointed Rock Vol. II - Centrifuge Modeling of Jointed Rock", US Air Force Office of Scientific Research.

Jakobson, B. (1958)
"On Pressure in Silos", Proceedings, Conference on Earth Pressure Problems, Brussels, Vol. 1, pp. 49-54.

Janssen, H.A. (1895)
"Versuche über Getreidedruck in Silozellen", Zeitschrift Verein Deutscher Ingenieure, Bd XXXIX, pp. 1045-1049.

Jennings, J.N. (1971)
Karst, the MIT Press, pp. 98-143.

Koutsabeloulis, N.C. and D.V. Griffiths (1989)
"Numerical Modeling of the Trapdoor Problem", Geotechnique, Vol. 39, No. 1, pp. 77-89.

Krynine, D.P. (1945)
"Discussion of *Stability and Stiffness of Cellular Cofferdams* by Karl Terzaghi", Transactions, ASCE, Vol. 110, pp. 1175-1178.

Ladanyi, B. and B. Hoyaux (1969)
"A Study of the Trap-Door Problem in a Granular Mass", Canadian Geotechnical Journal, Vol. 6, No. 1, pp. 1-15.

LeGrand, H.E. (1973)
"Hydrological and Ecological Problems of Karst Regions", Science, Vol. 179, pp. 859-864.

Luscher, U. and K. Höeg (1964)
"The Beneficial Action of the Surrounding Soil on the Load-Carrying Capacity of Buried Tubes", Proceedings of the Symposium on Soil-Structure Interaction, University of Arizona, Tucson, Arizona, pp. 393-402.

Luscher, U. and K. Höeg (1965)

"The Action of Soil Around Buried Tubes", Proceedings, Sixth International Conference on Soil Mechanics and Foundation Engineering, Montreal, Canada, Vol. 2, pp. 396-400.

Maeda, K., K. Miura, and S. Toki (1995)
"Mechanical Properties of Elliptic Microstructure Formed in Granular Materials", Soils and Foundations, Vol. 35, No. 2, pp. 1-13.

Marston, A. (1930)
"The Theory of External Loads on Closed Conduits in the Light of the Latest Experiments", Bulletin 96, Iowa Engineering Experiment Station, Ames, Iowa.

Matyas, E.L. and J.B. Davis (1983a)
"Prediction of Vertical Earth Loads on Rigid Pipes", Journal of Geotechnical Engineering, ASCE, Vol. 109, No. 2, pp. 190-201.

Matyas, E.L. and J.B. Davis (1983b)
"Experimental Study of Earth Loads on Rigid Pipes", Journal of Geotechnical Engineering, ASCE, Vol. 109, No. 2, pp. 202-209.

McNulty, J.W. (1965)
An Experimental Study of Arching in Sand, Ph.D. Thesis in Civil Engineering, University of Illinois.

Newton, J.G. (1976)
"Induced Sinkholes -- A Continuing Problem Along Alabama Highways", International Association of Hydrogeological Sciences Proceedings, Anaheim Symposium, No. 21, pp. 453-463.

Paikowsky, S. G. (1989)
A Static Evaluation of Soil Plug Behavior with Application to the Pile Plugging Problem, Sc.D. Thesis, MIT, pp. 163-358.

Paikowsky, S.G., K.J. DiRocco, and F. Xi (1993)
"Interparticle Contact Force Analysis and Measurements Using Photoelastic Techniques", 2nd International Conference on Discrete Element Methods, MIT, Cambridge, Massachusetts.

Paikowsky, S.G. and F. Xi (1995)
"Kinematics of 2-D Particulate Media Utilizing Image Analysis", 10th ASCE Engineering Mechanics Specialty Conference, University of Colorado at Boulder, Boulder, Colorado.

Paikowsky, S.G., J. Ting, F. Xi, and G. Mischel (1996)

"Numerical and Experimental Comparison of Shear Along Granular Material/ Solid Interface", ASME, Mechanics & Material Conference, Johns Hopkins University, Maryland.

Peck, R.B. (1975)
"Lateral Pressures Against Tunnels", Seminar on Lateral Soil Pressures Generated by Pipes, Piles, Tunnels, and Caissons, Dayton Section ASCE, pp. 14.

Proctor, R.V. and T.L. White (1946)
Rock Tunneling with Steel Supports, Commercial Shearing, Inc.

Proctor, R.V. and T.L. White (1977)
Earth Tunneling with Steel Supports, Commercial Shearing, Inc.

Ranken, R.E. and J. Ghaboussi (1975)
Tunnel Design Considerations: Analysis of Stresses and Deformations Around Advancing Tunnels, Department of Transportation, Report No. FRA-OR and D 75-84.

Riley, W.F. (1964)
"Stresses at Tunnel Intersections", Journal of the Engineering Mechanics Division, ASCE, Vol. 90, No. EM2, pp. 167-179.

Rowe, P.W. (1952)
"Anchored Sheet-Pile Walls", Proceedings, Institute of Civil Engineers, London, British England, Vol. ,pp. 27-70.

Sakaguchi, H. and E. Ozaki (1992)
"Analysis of the Formation of Arches Plugging the Flow of Granular Materials", Proceedings of the 2nd International Conference on Discrete Element Method, MIT, Cambridge, Massachusetts, pp. 153-163.

Selig, E.T. (1975)
"Stresses and Deflections Around Large Corrugated-Metal, Buried Structures", Seminar on Lateral Soil Pressures Generated by Pipes, Pipes, Tunnels and Caissons, Dayton Section, ASCE, 36 p.

Sowers, G.F. (1984)
"Correction and Protection in Limestone Terrain", Proceedings of the First Multidisciplinary Conference on Sinkholes, Florida Sinkhole Research Institute, University of Central Florida, Orlando, Florida, pp. 373-378.

Spangler, M.G. (1964)

"Protection of Underground Structures by Arch Action Associated with the Imperfect Ditch Method of Construction", Proceedings of the Symposium on Soil-Structure Interaction, University of Arizona, Tucson, Arizona, pp. 531-546.

Spangler, M.G. and R.L. Handy (1973)
"Loads on Underground Conduits", Soil Engineering, 3rd Edition, Harper Collins, New York, pp. 658-686.

Spangler, M.G. and R.L. Handy (1982)
"Loads on Underground Conduits", Soil Engineering, 4th Edition, Harper Collins, New York, pp. 727-763.

Stefanoff, G. and B. Boshinov (1977)
"Bearing Capacity of Hollow Piles Driven by Vibration", Proceedings of the 9th ICSMFE, Tokyo, pp. 753-758.

Stone, K.J.L. (1988)
Modeling of Rupture Development in Soils, Ph.D. Dissertation, Wolfson College, Cambridge University.

Széchy, K. (1966)
The Art of Tunneling, 21st Edition, Akadémiai Kiadó, Budapest.

Széchy, K. (1973)
The Art of Tunneling, 2nd Edition, Akadémiai Kiadó, Budapest, pp. 211-243.

Terzaghi, K. (1936)
"Stress Distribution in Dry and in Saturated Sand Above a Yielding Trap-Door", Proceedings, First International Conference on Soil Mechanics and Foundation Engineering, Cambridge, Massachusetts, pp. 307-311.

Terzaghi, K. (1943)
Theoretical Soil Mechanics, John Wiley and Sons, New York, pp. 66-76.

Terzaghi, K. and R.B. Peck (1968)
Soil Mechanics in Engineering Practice, 2nd Edition, John Wiley and Sons, New York, pp. 267-268.

Trollope, D.H. (1957)
"The Systematic Arching Theory Applied to the Stability Analysis of Embankments", Proceedings, Fourth International Conference on Soil Mechanics and Foundation Engineering, Vol. 2, pp. 382-388.

Trollope, D.H., M.G. Speedie, and I.K. Lee (1963)

"Pressure Measurements on Tullaroop Dam Culvert", Forth Australia-New Zealand Conference on Soil Mechanics and Foundation Engineering, pp. 81-92.

Trombe, F. (1952)
Traité de Spéléologie, Paris.

Truesdale, W.B. and E. Vey (1964)
"An Investigation of Panel-Arching Effects in Noncohesive Soil", Proceedings of the Symposium on Soil-Structure Interaction, University of Arizona, Tucson, Arizona, pp. 349-355.

Vardoulakis, I., B. Graf, and G. Gudehus (1981)
"Trap-Door Problem with Dry Sand: A Statical Approach Based Upon Model Test Kinematics", International Journal for Numerical and Analytical Methods in Geomechanics, John Wiley and Sons, LTD, Vol. 5, pp. 57-78.

Whitman, R.V., Z. Getzler, and K. Höeg (1962)
"Static Tests Upon Thin Domes Buried in Sand", MIT Research Project Report No. R62-41, December, 1962.

Whitman, R.V., Z. Getzler, and K. Höeg (1963)
"Tests Upon Thin Domes Buried in Sand", Journal of the Boston Society of Civil Engineers, January, pp. 1-22.

Yoshida, T., F. Tatsuoka, M.S.A. Siddiquee, Y. Kamegai, and C.S. Park (1993)
"Shear Banding in Sands Observed in Plane Strain", Proceedings for the Third International Workshop on Localisation and Bifurcation for Soils and Rocks, Aussois, France, September 6-9, 1993.